AMS Radiocarbon analysis of Greenhouse gases: Method development and application

Inaugural-Dissertation

zur

Erlangung des Doktorgrades

der Mathematisch-Naturwissenschaftlichen Fakultät

der Universität zu Köln

vorgelegt von

Jan Olaf Melchert

aus Dinslaken

2022

Berichterstatter:	Prof. Dr. Janet Rethemeyer
(Gutachter)	Prof. Dr. Martin Melles

Tag der mündlichen Prüfung: 20.01.2022

Erklärung zur Dissertation

Hiermit versichere ich an Eides statt, dass ich die vorliegende Dissertation selbstständig und ohne die Benutzung anderer als der angegebenen Hilfsmittel und Literatur angefertigt habe. Alle Stellen, die wörtlich oder sinngemäß aus veröffentlichten und nicht veröffentlichten Werken dem Wortlaut oder dem Sinn nach entnommen wurden, sind als solche kenntlich gemacht. Ich versichere an Eides statt, dass diese Dissertation noch keiner anderen Fakultät oder Universität zur Prüfung vorgelegen hat; dass sie - abgesehen von unten angegebenen Teilpublikationen und eingebundenen Artikeln und Manuskripten - noch nicht veröffentlicht worden ist sowie, dass ich eine Veröffentlichung der Dissertation vor Abschluss der Promotion nicht ohne Genehmigung des Promotionsausschusses vornehmen werde. Die Bestimmungen dieser Ordnung sind mir bekannt. Darüber hinaus erkläre ich hiermit, dass ich die Ordnung zur Sicherung guter wissenschaftlicher Praxis und zum Umgang mit wissenschaftlichem Fehlverhalten der Universität zu Köln gelesen und sie bei der Durchführung der Dissertation zugrundeliegenden Arbeiten und der schriftlich verfassten Dissertation beachtet habe und verpflichte mich hiermit, die dort genannten Vorgaben bei allen wissenschaftlichen Tätigkeiten zu beachten und umzusetzen. Ich versichere, dass die eingereichte elektronische Fassung der eingereichten Druckfassung vollständig entspricht.

Teilpublikationen:

Melchert, J. O., Stolz, A., Dewald, A., Gierga, M., Wischhöfer, P., and Rethemeyer, J. (2019). Exploring sample size limits of AMS gas Ion Source ^{14}C analysis at CologneAMS. *Radiocarbon* 61, 1785–1793. doi:10.1017/RDC.2019.143.

Melchert, J. O., Wischhöfer, P., Knoblauch, C., Eckhardt, T., Liebner, S., and Rethemeyer, J. (2022). Sources of CO_2 produced in freshly thawed Pleistocene-age Yedoma permafrost. *Frontiers in Earth Science, 1408*. doi: https://doi.org/10.3389/feart.2021.737237.

Datum: 21.01.2022 Unterschrift:

Jan Olaf Melchert

Abstract

The northern circumpolar permafrost regions are warming faster compared to the global mean. As a result, the duration of annual thaw seasons is increasing, so that the permafrost is subjected to increasingly deep thaw. Within the permafrost zones large amounts of carbon were buried over thousands of years and previously freeze locked due to the cold climate. These carbon sinks are affected by the consequences of global warming and become available for microbial degradation, and thereby potentially turning from carbon sinks into carbon pools. As a result of the microbial degradation of organic matter, the greenhouse gases carbon dioxide and methane are released into the atmosphere, amplifying the global warming, and forcing a positive climate feedback. Among the permafrost deposits, Pleistocene sediments, termed Yedoma, are especially vulnerable to climate change induced rapid thaw and subject to thermoerosion because of their high ice-content.

While chemical characterizations of permafrost organic matter and laboratory incubation experiments give information about the degradability of Yedoma organic matter, actual field-studies documenting the extent and exact sources of greenhouse gas release are limited. The analysis of carbon isotopes (^{13}C, ^{14}C) can be used to estimate the age of the permafrost organic matter that is being degraded into greenhouse gases and trace their sources. This is done by collecting carbon dioxide during either field expeditions or during analogue laboratory incubation experiments. Samples are handled in laboratory vacuum rigs, during which the amount of carbon dioxide is quantified and purified from other gases that have been collected along the carbon dioxide. While these methods are overall established and reliable, the analyses are, however, sensitive towards contamination from exogenous carbon sources. The sensitivity towards contamination is amplified towards increasingly smaller sample sizes, down to a few micrograms of carbon. Thus, assessments are necessary to quantify how much contamination is introduced during the preparation of carbon dioxide samples for isotopic analysis and to determine what is the smallest sample size that still delivers meaningful results.

The aims of this thesis were to evaluate the laboratory methods applied for the isotopic analysis of carbon dioxide and apply these methods and sampling devices to a field study investigating the degradability of freshly thawed Yedoma organic matter. The evaluation of our existing laboratory methods to handle carbon dioxide demonstrated that routine measurements can safely be performed on samples as small as 20 µg C. Samples as small as 2.5 µg C can also be analyzed, however the associated uncertainty is very large and prevents the analysis of ^{14}C-depleted samples. Further, new methods for the isotopic analysis of methane via accelerator mass spectrometry were established. This required the development of a workflow and pre-treatment routine to convert methane samples to carbon dioxide. After establishing a

satisfying conversion rate, first test runs of different standards and gas mixtures further allowed the identification and quantification of sources of exogenous carbon, potentially contaminating samples. During the application study, carbon dioxide emissions were collected along with Yedoma sediment samples from an active retrogressive thaw slump in the Lena River Delta in Siberia. The sediment samples were incubated in the laboratory for a 1.5-year aerobic incubation experiment, during which the amount of produced carbon dioxide was closely monitored and sampled at fixed intervals. The carbon isotopy of the carbon dioxide sampled during the field campaign was compared with the carbon dioxide produced during the incubation experiment and a mass balance approach was applied to identify carbon sources based on isotopic values.

The results show that labile organic matter pools are being degraded first and that their contribution to carbon dioxide emissions is decreasing after the initial thaw. Mostly ancient organic matter is being degraded at sites where Pleistocene-aged Yedoma is exposed, the admixture of Pleistocene Yedoma sediments with younger Holocene sediments through erosion does not favor the degradation of ancient organic matter through positive priming. Instead, younger substrates are degraded preferentially, if available. Most surprisingly, the results of the mass balance approach suggest, that a significant proportion of the carbon dioxide, that was released during the field measurement as well as during the laboratory incubation, was derived from inorganic carbon. The release of carbon dioxide from inorganic carbon is likely favored by low pH values and organic acids contained in the thaw slump sediments. The results of the carbon isotope analysis further suggest that a fraction of the carbon dioxide derived from secondary carbonates. Therefore, it is hypothesized that these secondary carbonates precipitated from microbially respired carbon dioxide and thus would not contribute to a net positive carbon emission budget.

Zusammenfassung

Der Temperaturanstieg der nördlichen zirkumpolaren Permafrost Gebiete ist stärker als der globale Durchschnitt. Das Ergebnis sind längere jährliche Tauphasen und das damit verbundene, tiefer voranschreitende, Auftauen des Permafrostbodens. Diese Permafrostböden und Sedimente enthalten große Mengen von Kohlenstoff, welche über einen Zeitraum von vielen tausend Jahren dort abgelagert und, bedingt durch ein kontinuierlich kaltes Klima, vor Zersetzung geschützt wurden. Diese Kohlenstoffsenken sind als Folge der globalen Erwärmung erhöhten Temperaturen ausgesetzt. Es besteht das Risiko, dass diese Kohlenstoffsenken dauerhaft zu Kohlenstoffquellen werden und als Folge von mikrobiellem Abbau die Treibhausgase Kohlenstoffdioxid und Methan freisetzen. Unter den Permafrost Ablagerungen werden besonders die eisreichen pleistozänen Sedimente, genannt Yedoma, von den Folgen eines wärmeren Klimas beeinflusst. Aufgrund des hohen Eisgehaltes haben diese Sedimente das Potenzial besonders schnell aufzutauen und durch Thermoerosion in kurzer Zeit viel Kohlenstoff freizusetzen.

Die chemische Analyse von organischem Material, welches in Permafrost abgelagert war, ist zwar hilfreich und liefert Informationen über die enthaltenen organischen Substrate, gibt jedoch nur wenige Informationen über das Ausmaß der möglichen Kohlenstoff Freisetzung. Feldstudien bei denen Treibhausgasemissionen gemessen und deren Quellen ermittelt werden sind entweder durch die schwierige Durchführbarkeit, aufgrund der widrigen Bedingungen in der Arktis, limitiert oder deren Ergebnisse nur schwer verallgemeinerbar. Die Analyse der Kohlenstoffisotope (^{13}C, ^{14}C) wird in diesem Zusammenhang genutzt, um das Alter der zu Treibhausgasen umgewandelten organischen Substrate und deren biologischen Ursprung zu ermitteln. Diese Analysen werden durchgeführt, indem Kohlenstoffdioxid oder Methan entweder direkt als Emission von Permafrost Ablagerungen oder aus analogen Labor Inkubationsexperimenten gesammelt werden. Die Gasproben werden vor der Analyse in Vakuumsystemen aufbereitet und von anderen, unerwünschten Gasen, getrennt und anschließend quantifiziert. Diese Methoden werden zwar routiniert angewendet, die Analysen sind jedoch anfällig gegenüber Kohlenstoff der aus externen Quellen, während der Aufbereitung und Beprobung eingetragen wird. Die Methodik zur Analyse von Kohlenstoffisotopen ist in den vergangenen Jahren stetig verbessert worden und die Möglichkeit geschaffen worden immer kleinere Mengen Kohlenstoff, bis zu wenigen Mikrogramm, zu analysieren. Mit immer kleiner werdenden Probemengen steigt auch die Anfälligkeit gegenüber Verunreinigungen durch Kohlenstoff aus externen Quellen. Um weiterhin aussagekräftige Analysen von sehr geringen Mengen Kohlenstoff zu ermöglichen, sind kritische Beurteilungen der angewendeten Methodik zur Aufbereitung nötig.

Die Ziele dieser Arbeit waren es, die Methoden zur Aufbereitung von Treibhausgasproben im Labor zu evaluieren und die Methoden und Geräte zum Beproben von Kohlenstoffdioxid zu nutzen, um Informationen über die Abbaubarkeit von organischen Substraten aus aufgetautem Yedoma zu gewinnen. Die Ergebnisse der Evaluierung zeigen, dass Messungen von Proben bis herunter auf 20 µg C zuverlässige Daten liefern. Die Evaluierung der bestehenden Aufbereitungsmethoden von Kohlenstoffdioxid zeigte weiterhin, dass Proben von etwa 2.5 µg C zwar gemessen, aber aufgrund der hohen Messunsicherheit nur gering aussagekräftig sind. Dies betrifft vor allem Proben, die nur sehr geringe Mengen ^{14}C enthalten. Weiterhin wurden neue Methoden zur Analyse von Methan mittels Beschleuniger Massenspektrometrie etabliert und anschließend getestet. Diese Tests erforderten zunächst den Bau eines Systems zur Oxidation von Methan zu Kohlenstoffdioxid und das Erreichen einer konstant hohen Oxidationsrate. Erste Tests mit verschiedenen Gasgemischen und Standards ergaben vielversprechende Daten zur Abschätzung und Identifikation von Kontaminationsquellen. Die Studie zur Anwendung wurde an Yedoma Sedimenten durchgeführt, die an einer aktiven Thermoerosionsrutschung im Lena Flussdelta in Sibirien gesammelt wurden. Ein Inkubationsexperiment wurde für 1.5 Jahre an gesammelten Sedimentproben durchgeführt und Kohlenstoffdioxid, das währenddessen produziert wurde in festen Intervallen zur Messung entnommen. Die Isotopie von Kohlenstoffdioxid aus diesem Experiment wurde mit der von im Gelände gesammelten Kohlenstoffdioxid verglichen und eine Massenbilanz auf Basis der Isotopie, errechnet, mit deren Hilfe die Quellen des freigesetzten Kohlenstoffdioxids identifiziert wurden.

Die Ergebnisse dieser Bilanzierung zeigen, dass labile organische Substrate als erstes abgebaut werden und deren Anteil an den Gesamtemissionen nach initialem Auftauen des Yedoma geringer wird. An den Orten an denen pleistozäner Yedoma durch Thermoerosion freigelegt wurde, wird zum Großteil Kohlenstoffdioxid aus alten organischen Substraten umgesetzt. Das Durchmischen von Yedoma mit jüngeren holozänen Sedimenten, welche von der über dem Hangrutsch liegenden intakten Tundra erodieren, scheint keine zusätzliche Zersetzung von alten Substraten zu begünstigen. Überraschenderweise zeigen die Ergebnisse der Massenbilanz, dass ein wesentlicher Teil des freigesetzten Kohlenstoffdioxid aus anorganischen Quellen umgesetzt wurde. Diese Freisetzung aus Karbonat wird wahrscheinlich durch geringe pH-Werte und die Ansammlung von organischen Säuren im Sediment begünstigt. Die Ergebnisse der Bilanz deuten weiterhin daraufhin, dass ein Teil dieses, aus Mineralien gebildeten Kohlenstoffdioxid aus sekundärem Karbonat freigesetzt wurde. Es wird daher angenommen, dass diese sekundären Karbonate aus mikrobiell gebildetem Kohlenstoffdioxid ausgefällt wurden und somit nicht zu einer Netto-Emission beitragen.

Table of Content

Introduction

The permafrost carbon feedback

Permafrost is defined as ground that remains permanently frozen (i.e., below 0°C) for at least two consecutive years. The definition includes any soil, rock or sediment being deposited by various mechanisms, such as aerial or alluvial transport, or being reworked as a result of cryoturbation (Ping et al., 1998; Zimov et al., 2006; Schirrmeister, 2011). Most of the global permafrost is situated in the northern circumpolar regions, where vast amounts of organic matter (OM) have been accumulated and deposited in the soils over the last thousands of years (Lindgren et al., 2016). Low temperatures that lasted over a long period of time slowed down OM decomposition rates. As a result, primarily leaf and root detritus accumulated over time and fully removed the frozen and buried OM from active carbon cycling (Harden et al., 1992; Davidson and Janssens, 2006). As a consequence of increasing global temperatures, which are most pronounced in high latitudes, permafrost and especially the ice-rich permafrost sections become subject to extensive thaw. This makes the OM that was stored for millennia in permafrost available for microbial degradation transforming organic carbon (OC) into greenhouse gases (GHGs) such as carbon dioxide (CO_2) and methane (CH_4, Schuur et al., 2008). The release of the previously stored OC as GHGs further amplifies the warming, leading to longer thaw periods during the year and consequently to thawing of deeper permafrost layers. Subsequently, even more GHGs are being produced, which forces a positive feedback (Fig. 1, Schaefer et al., 2014; Schuur et al., 2015). Rising temperatures in northern latitudes are also responsible for the decline of sea-ice and a decrease of snow cover on land, which, in turn, changes the summer albedo to further favor a warming trend (Chapin, 2005; Wu et al., 2021). Therefore, the projected temperature increase in polar regions is estimated to be about twice as fast as compared to the global mean, leading to potential losses of 10 – 65% of surface permafrost until the year 2100 (Koven et al., 2015; Box et al., 2019; Beer et al., 2020).

The northern circumpolar permafrost carbon stock

While there is consensus about the general implications of increased temperatures in polar regions such as CO_2 and CH_4 production for autotrophic and heterotrophic respiration from plants and microbes and accelerated reaction kinetics, the extent of increasing temperatures to such a highly complex and dynamic ecosystem are not fully understood (Davidson and Janssens, 2006). There is still a discourse about the mechanisms of the carbon (C) feedback. Firstly, the absolute amount of OM stored in permafrost needs to be determined. It is estimated that about 24% of the terrestrial area in the northern hemisphere (23 million km²) are covered with permafrost (Brown et al., 1997; Zhang et al., 1999). Early and limited estimates resulted in about 192 Gt of OC that is stored within the upper 100 cm of the tundra (Post et al., 1982).

In more recent years, estimates for the upper 100 cm of permafrost affected grounds were corrected to 269 Gt of OC (Tarnocai et al., 2003). During the last decades research on C stocks in permafrost continued and with increasing knowledge estimates for deeper permafrost deposits were published. These new data massively increased the estimated permafrost carbon stocks to 1024 Gt OC down to a soil depth of 300 cm and in total to 1672 Gt OC stored in the northern circumpolar region, including soils, Yedoma and deltaic deposits (Tarnocai et al., 2009). However, a revision of the methodology for the calculation of carbon stocks adjusted the estimated OC content in the permafrost region down to 1307 Gt OC, which is slightly less than about twice the amount of the total atmospheric C (Houghton, 2007). About 500 Gt OC are contained within the active layer or in taliks (unfrozen ground within permafrost areas, often associated with water bodies), while about 800 Gt of OC are perennially frozen (Hugelius et al., 2014).

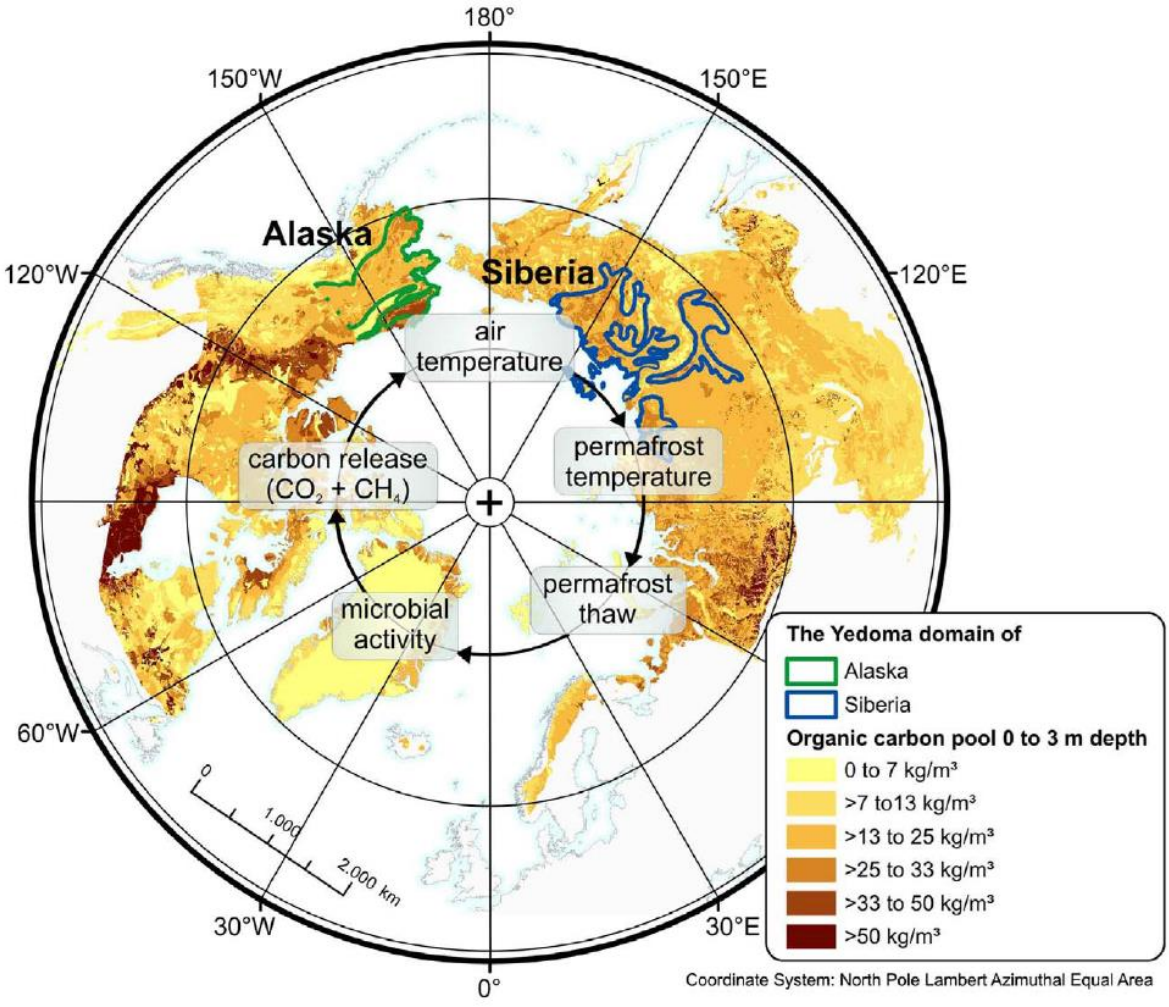

Figure 1: Concept of permafrost C feedback and map of the northern Hemisphere with estimated OC stocks of circum-Arctic permafrost down to 3 m depth and estimated extent of the Yedoma domain (adapted from Strauss et al., 2017).

Mechanisms of permafrost degradation

The active layer (AL) is defined as the uppermost layer of the permafrost that is subject to annual thaw. Here, most of the chemical and physical processes associated with permafrost degradation occur upon thaw (Hinzman et al., 1991). The top-down thawing of permafrost occurs during the warmest months of the year, in the summer. With increasing climate warming the annual thaw period is extending, so that the AL is gradually thickening (Kane et al., 1991; Åkerman and Johansson, 2008). This, in turn, enables soil drainage, and additional C mobilization pathways. C mobilization can occur by transport in watery solutions and microbial degradation, by oxygenation of previously water saturated ground layers (Guo et al., 2007; Gustafsson et al., 2011; Kittler et al., 2017). Large sections of permafrost contain extensive amounts of ice, locally exceeding the initially deposited volume of sediments. These areas are very sensitive to even small increases of the depth of the active layer (Farquharson et al., 2019). Upon thaw, meltwater from these ice-rich permafrost deposits enables rapid erosion and ground subsidence due to the collapse of the sediments above the melting ice masses (Osterkamp et al., 2009). This thermoerosional change in landscape is called thermokarst and enables different processes such as the formation of thermokarst lakes and bogs (Kuhry, 2008; Grosse et al., 2008), the formation of retrogressive thaw slumps (Alexanderson et al., 2002; Lewkowicz and Way, 2019), the downslope movement of large active layer masses (Lewkowicz, 2007), or formation of thaw gullies (Fortier et al., 2007). All of these forms of thermokarst affect deeper permafrost deposits in addition to the annually occurring top-down thaw affecting the permafrost surface (Osterkamp et al., 2000; Morgenstern et al., 2011; Kokelj et al., 2013; Turetsky et al., 2020). Therefore, the occurrence of thermokarst is discussed as a potential climate tipping element, because the thermokarst-induced changes occur rapidly and potentially mobilize large amounts of previously frozen OM rapidly into active C cycling (Czudek and Demek, 1970; Schuur et al., 2008; Grosse et al., 2011; Lenton, 2012; Strauss et al., 2017; Nitzbon et al., 2020).

Yedoma

Beringia is a geographically conceptualized region that describes the North American and Siberian Arctic from the Taymyr Peninsula to the Yukon Territory (Hultén, 1937). Large areas of this region remained unglaciated and thus an extensive sedimentary record since the Pliocene has been preserved (Schirrmeister et al., 2013). The ice-rich silt and fine sand deposits that accumulated in these unglaciated areas during the Pleistocene are termed Yedoma (Fig. 1). They can be up to 50 m thick, a result of relatively constant sedimentation rates (Schirrmeister, 2011; Schirrmeister et al., 2013; Lindgren et al., 2016). The extensive sedimentation, that started in some locations about 71 – 60 thousand years ago (Schirrmeister et al., 2011), lead to the incorporation of about 327 – 466 Gt OC, which represents a quarter

of the total OC stored in the global permafrost. The term Yedoma was historically used in the field of geomorphology, implying a term to describe hills that separate thermokarst depressions in Siberia and in the field of stratigraphy to describe the locality of Pleistocene horizons. In this thesis and other more recent Yedoma studies, it is mainly understood as silt- to sand-sized loess-like deposits across all Beringia, that contain an exceptionally high ice-content (> 80 vol%) and form local massive syngenetic ice-wedges. The sedimentary and cryo structures of Yedoma are exhibited cross-regional in addition to the occurrence of well-preserved fossilized flora and fauna (Vas'kovsky, 1963; Tomirdiaro, 1996; Kanevskiy et al., 2011; Strauss et al., 2017).

Recent studies point to a polygenetic origin of the deposits that include various sedimentation mechanisms leading to the formation of Yedoma (Strauss et al., 2017). There are regional differences in the sedimentation history that still cause debates about Yedoma genesis. Most prominent sedimentation mechanisms, in addition to cryogenic weathering and formation of syngenetic ice-wedges, were suggested to be aeolian deposition, which is stronger pronounced in eastern Beringia, and transport through water such as floodplain overbanking and alluvial runoff (Strauss et al., 2017). However, there is a consensus that excludes glacier- and shallow-marine-related sedimentation to the formation of Yedoma (Strauss et al., 2017).

Its high ice-content makes Yedoma especially vulnerable to thaw and puts it at risk for substantial GHG release through abrupt events of thermoerosion within a warming climate. Numeric models are projecting arctic warming and the release of GHGs, however, the contribution of rapid thawing from ice-rich Yedoma deposits has not yet been incorporated properly (Schneider von Deimling et al., 2015). A major data gap is the knowledge about the decomposability of Yedoma OM. Due to the constant sedimentation, it is generally assumed that OM in Yedoma deposits is rather well preserved, because it accumulated quickly and has not undergone substantial decomposition since freezing (Dutta et al., 2006; Zimov et al., 2006). So far, studies on the degradability of Yedoma OM have relied on the analysis of OM substrate quality (Strauss et al., 2015) and monitoring experiments of GHG release from Yedoma deposits in controlled laboratory environments to assess the overall degradability (Dutta et al., 2006; Lee et al., 2012; Knoblauch et al., 2013; Stapel et al., 2016; Weiss et al., 2016; Faucherre et al., 2018; Walz et al., 2018). Actual field studies are scarce, because of the remoteness from infrastructure and harsh weather conditions outside the summer months.

In numerous laboratory incubation experiments heterotrophic respiration has been monitored by the CO_2/CH_4 production to mirror in-situ GHG release from permafrost deposits (Schädel et al., 2014 and references therein). These studies suggest that the most labile components of OM are rapidly degrading upon thaw, which is reflected by high initial respiration rates just after

the start of the experiment that were declining over the course of the experiment (Dutta et al., 2006; Knoblauch et al., 2013; Schädel et al., 2014). However, lower respiration rates do not necessarily imply a higher degree of OM decomposition (Kuhry et al., 2020). The amount and composition of OM in Yedoma may vary, both spatial and temporal, besides the overarching similarities in depositional features (Strauss et al., 2015; Weiss et al., 2016; Walz et al., 2018). The analysis of OM substrates and CO_2 respiration rates gives hints towards the overall degradability of OM in permafrost deposits. However, it is unclear whether the released CO_2 and CH_4 have derived from recently thawed Pleistocene Yedoma or rather from fresh plant detritus. Assessments of the sources of OM contributing to GHG emission have been established by analyzing the isotopic composition of OM substrates and the emitted CO_2 and CH_4 (Schuur and Trumbore, 2006; Czimczik and Welker, 2010; Estop-Aragonés et al., 2018). By analyzing the radiocarbon (^{14}C) content of the released gases it is possible to determine the average time that has passed since the incorporation of the C containing parent material into the permafrost. Implications about the overall degradability can be deduced by comparing the amount of GHG emissions from old and young carbon sources. In addition to ^{14}C analysis, the stable carbon isotope ^{13}C can be used in combined mass-balance approaches to differentiate between individual sources of the GHG release, i.e., autotrophic, heterotrophic, or abiotic origin (Dorsett et al., 2011; Tamir et al., 2011; Griffith et al., 2012; Ramnarine et al., 2012; Pries et al., 2016). Efforts over the last years have been made to establish reliable methods to collect CO_2 using molecular sieve cartridges (MSCs), in addition to sediments from in-situ thawing permafrost deposits and analyze its respective ^{14}C content via accelerator mass spectrometry (AMS, Hardie et al., 2005; Garnett and Murray, 2013; Palonen and Oinonen, 2013; Wotte et al., 2017a, 2017b).

Aim and Outline of the Thesis

The projected temperature increase in the Arctic is twice the global average, this exposes the OM stored for millennia in permafrost deposits to the risk of decomposing and become a source for the release of GHGs such as CO_2 and CH_4. A rapid GHG release from ice-rich Yedoma deposits from Siberia to Canada through thermoerosion threatens to quickly tip the scales and force a positive climate feedback. Due to the scarceness of data that are assessing the sources of released GHGs there is a need for further studies. With the analysis of ^{14}C and ^{13}C from respired soil gases we gain insights about their age and origin. Methods associated with the collection and analysis of CO_2 have evolved over the last years and the establishment of these techniques as routine procedures, however, still requires evaluation. Moreover, the established methodology at our accelerator mass spectrometry facility, CologneAMS, only allows for analysis of CO_2. Assessments on the potential of CH_4 release from permafrost are nonetheless required for accurate predictions of Arctic carbon cycling. In order to improve and evolve the capability in GHG analysis the following objectives for this thesis were formulated:

a) Evaluation of the contamination with exogenous carbon that is introduced during pre-treatment procedures required for ^{14}C measurements via accelerator mass spectrometry (Manuscript I).
b) Identification of carbon sources that are contributing to CO_2 emissions from thawing deep Yedoma deposits located in the Lena River Delta (Manuscript II).
c) The development and establishment of a reliable laboratory setup to routinely prepare permafrost derived CH_4 gas for ^{14}C analysis at CologneAMS (Manuscript III).

The following chapter gives information about the methodological background of carbon isotopic analysis and about the main study area, the Lena River Delta, Siberia. Chapters 3 to 5 are independent manuscripts that were published (Manuscript I, Manuscript II) and in preparation for future submission (Manuscript III). A synthesis chapter, discussing the different manuscripts, their main findings as well as a summary with an outlook on future research perspectives will be included at the end of this thesis.

Manuscript I:

Melchert, J. O., Stolz, A., Dewald, A., Gierga, M., Wischhöfer, P., and Rethemeyer, J. (2019). Exploring sample size limits of AMS gas Ion Source ^{14}C analysis at CologneAMS. Radiocarbon 61, 1785–1793. doi:10.1017/RDC.2019.143.

The direct injection of CO_2 into an accelerated mass spectrometer allows the measurement of much smaller sample sizes compared to manual graphitization. While the requirements regarding the sample size improved, the downside of the measurement of smaller samples is

that the analysis is more prone to contamination from exogenous C. Therefore, the pre-treatment methods for the ^{14}C analysis of very small samples were critically evaluated. Different series of standards were prepared and the amount of exogenous carbon that is introduced during sample handling and processing was quantified. The determined amount of carbon contamination is relatively small, and the results indicated that the measurement of micro-scale CO_2 samples is possible and reliable for sample sizes down to about 20 µg C. This finding was essential as the ^{14}C analysis of CO_2 does require only about 10% of the amount of C that is needed for graphitization to perform a meaningful analysis.

The study was designed according to counsel given by the co-authors. Laboratory work including pre-treatment and preparation of CO_2 samples was done by me. The interpretation of the data was done in collaboration with Merle Gierga. I wrote the manuscript myself under guidance of Janet Rethemeyer.

Overall contribution of Jan Olaf Melchert: 90%.

Manuscript II:

Melchert, J. O., Wischhöfer, P., Knoblauch, C., Eckhardt, T., Liebner, S., and Rethemeyer, J. (2022). Sources of CO_2 produced in freshly thawed Pleistocene-age Yedoma permafrost. Frontiers in Earth Science, 1408. doi: https://doi.org/10.3389/feart.2021.737237.

After the successful establishment of routine procedures for the ^{14}C analysis of CO_2, a source assessment of CO_2 released from an active retrogressive thaw slump in the Lena River Delta was conducted. Applying a dual carbon isotope mass balance approach indicated that a significant amount of CO_2 was released from inorganic sources, likely favored through the mobilization of organic acids released from the microbial degradation of OM. While ancient Pleistocene-aged OM as well as recent OM are being degraded to CO_2, the mixture of both suggested that recent OM is preferred by decomposing microorganisms.

The sampling in Siberia was performed by Philipp Wischhöfer. The preparation for ^{14}C and ^{13}C analysis as well as calculations from data were done by me. The interpretation of the data was done in close collaboration with Philipp Wischhöfer. The manuscript was written by me under the guidance of Janet Rethemeyer.

Overall contribution of Jan Olaf Melchert: 70%

Manuscript III:

A new setup for ^{14}C analysis of CH_4 at CologneAMS by Jan Olaf Melchert, Merle Gierga and Janet Rethemeyer

Further studies of GHG emissions from thawing permafrost in the Lena River Delta required the establishment of methods to perform ^{14}C analysis of CH_4 emissions. A new laboratory setup was built, enabling to separate CO_2 from CH_4 and subsequently oxidize it at high temperatures to CO_2 for ^{14}C analysis. First tests of different series of standards and a biogas mixture were run on the new system to evaluate the CH_4 to CO_2 conversion efficiency, and to estimate the contamination associated with sample handling and pre-treatment.

The CH_4 oxidation vacuum system was built myself and I designed the overall study. The laboratory work including pre-treatment and preparation of CO_2 samples was done by me. Calculations and interpretation of the data were done by me, the manuscript was written by me under guidance of Merle Gierga and Janet Rethemeyer.

Overall contribution of Jan Olaf Melchert: 95%

.

Study Area

The study sites are located on Kurungnakh, which is one of the larger islands in the Lena River Delta in Northeast Siberia (Fig. 2, Boike et al., 2013). It is part of the Siberian zone with continuous permafrost, which extents between 400 and 600 m below the surface (Boike et al., 2013). The Lena Delta covers an area of about 32,000 km² (Gordeev and Shevchenko, 1995; Walker, 1998). The Lena River itself comprises a catchment area of 2.43 million km². Geomorphologically, the Lena River Delta consists of three terraces (Grigoriev, 1993): The active floodplains, mainly covering the eastern delta, are considered to be the first terrace. Between two of the main channels that are feeding the river in the western part, sandy deposits are forming small islands that belong to the second terrace, while the sand deposits covered by the Late Pleistocene Yedoma form the third terrace in the southern part of the delta (Grigoriev, 1993; Schwamborn et al., 2012). The third terrace, to which Kurungnakh belongs, is covered by an intact tundra vegetation that has formed during the Holocene. It lies beneath the Olenyeksky, one of the four main channels feeding the river. Our study site is located on the eastern side of the island, which is easily accessible from the nearby research station on Samoylov island (Boike et al., 2013). Across the eastern shore of Kurungnakh, a large active retrogressive thaw slump has formed (Fig. 3), on which large ice-wedges and the Late Pleistocene sediments are exposed, overlain by the Holocene tundra, that is annually retreating by about 7 m as a result of erosion (Stettner et al., 2018).

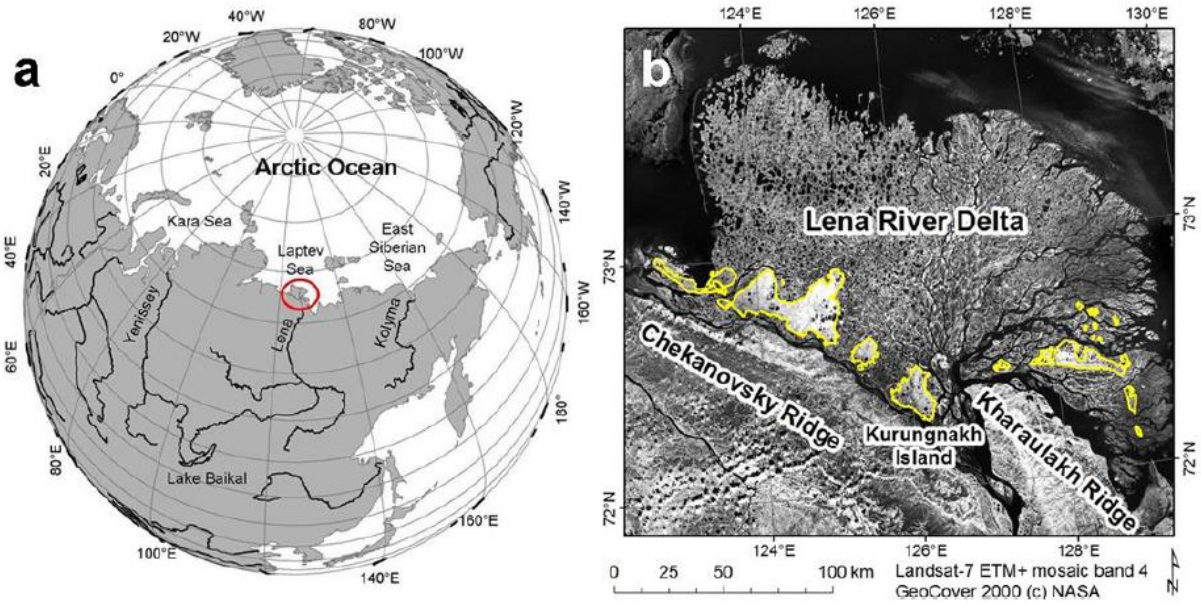

Figure 2: a) Location of the Lena River Delta in northeast Siberia and b) location of Kurungnakh island and deposits of the third river terrace (yellow) within the river delta (adapted from Morgenstern et al., 2011).

With the continuous retreat of the cliff due to erosion an ideal study site featuring conical thaw mounds is being exposed on the slopes of the thaw slump (Fig. 3A). These thaw mounds are

termed Baidzherakhs (Vasil’chuk et al., 2019). They are the remains of former Pleistocene polygonal centers. During the Pleistocene OM has accumulated in these polygonal centers (Stettner et al., 2018) that are now easily accessible after erosion.

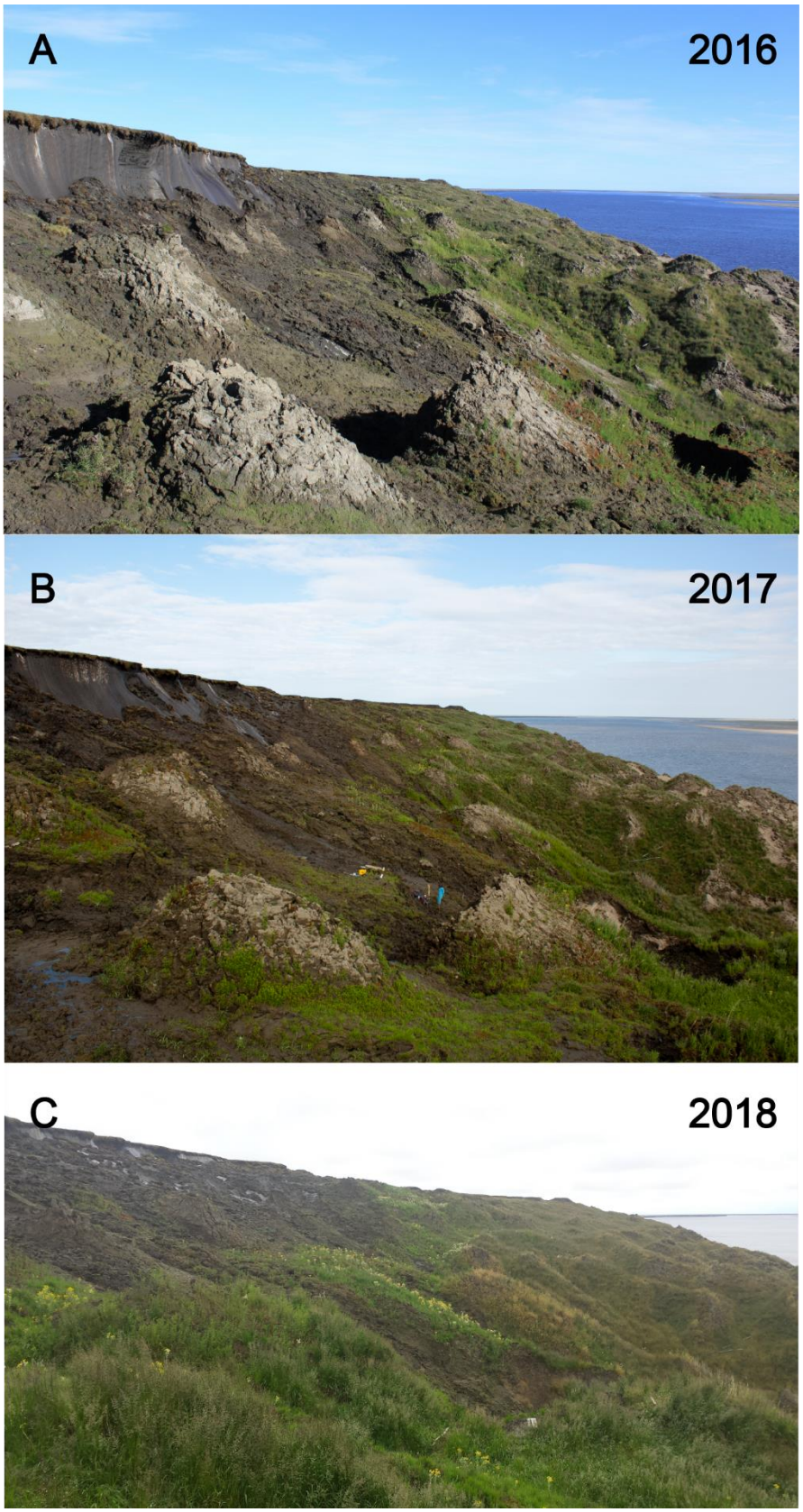

Figure 3: Exposed Yedoma sediments on the active thaw slump located on Kurungnakh island from 2016 – 2018. Pictures A to C highlight the continuing erosion clearly visible by the retreating Holocene terrace and the increasing vegetation cover of the exposed thaw mounds.

Methodological Background

Carbon Isotopes

Carbon has three naturally occurring isotopes (atoms with the same proton- but different neutron-counts). ^{12}C is the most abundant C isotope (98.89%) while ^{13}C only represents 1.11% (Hoefs, 2015). ^{12}C and ^{13}C are both stable isotopes and their quantity on Earth is constant. The third isotope (^{14}C) is created through nuclear spallation: Cosmic rays collide with gas atoms in the upper Earth's atmosphere which eject nucleons. The neutrons, ejected through the collision, collide afterwards with ^{14}N isotopes, which take up the neutron and release a proton, forming ^{14}C as a result (Libby, 1946). In contrast to ^{12}C and ^{13}C, ^{14}C is unstable and subjected to radioactive decay that occurs spontaneously. Thereby, ^{14}C is converted to ^{14}N through β^- decay, emitting an electron.

The Radiocarbon Method

The upper atmosphere is in constant interaction with cosmic rays and therefore ^{14}C is constantly being created. Through interaction with oxygen, ^{14}C forms $^{14}CO_2$, and subsequently enters the global carbon cycle. Formation and decay of ^{14}C are thus in balance leading to a natural abundance of about 10^{-10}% in the preindustrial atmosphere (Schuur et al., 2016). The $^{14}CO_2$ molecules enter the carbon cycle through photosynthesis of plants or by exchange with ocean waters. It is further distributed in carbonate bearing sediments or by animals that consume ^{14}C-containing plant material and from there into the food chain to other animals and humans. Living organisms therefore contain ^{14}C in a concentration similar to the atmosphere. After death of an organism, ^{14}C is not taken up actively anymore and over time the organisms ^{14}C concentration decreases through radioactive decay. The time that it would take 1 g of pure ^{14}C to lose 0.5 g to radioactive decay, termed half-life, is constant and has been determined to 5,730 years (Godwin, 1962). Because the half-life of ^{14}C is known, it is possible to determine the time since the organism died. This time is called radiocarbon age and is quantified by measuring the ^{14}C content relative to the amount of the ^{12}C isotopes (1).

$$R = \frac{rare}{abundant} = \frac{^{14}C}{^{12}C} \quad (1)$$

Historically, the ^{14}C content of a sample was determined by counting the radioactive decay occurring over time and thereby calculating the samples activity (Stuiver and Polach, 1977). More recent studies relying on ^{14}C analysis use accelerator mass spectrometry (AMS) as method of choice. AMS uses the slight differences in mass between the carbon isotopes, caused by the different neutron-counts, and selectively counts the heavier isotopes with regards to the lighter isotope ^{12}C.

To account for systematic errors occurring during AMS measurement, confirmation of results by measuring a standard in parallel is required. Historically, oxalic acid I (Ox-I) was used as a modern reference and the reporting of ^{14}C data still relies on this practice (Stuiver & Polach, 1977). Data in this thesis are reported as fraction modern ($F^{14}C$), which is corrected for mass dependent fractionation and is relative to 95% of the Ox-I (Stuiver & Polach, 1977). This corresponds to a decay rate which is equal to the activity of the Ox-I in the year 1950. Furthermore, this corresponds to the activity of 1890 wood, decay corrected to the year 1950, which has been chosen to represent the ^{14}C content of a pre-industrial atmosphere (Schuur et al., 2016). For this calculation, the Ox-I is not corrected for this mass dependent discrimination against heavy isotopes. The fraction modern is thus defined by equation (2):

$$F^{14}C = \frac{\frac{^{14}C}{^{12}C}_{sample}}{(0.95 * \frac{^{14}C}{^{12}C}_{Ox-I})} \quad (2)$$

The radiocarbon content of a sample ($F^{14}C$) can be converted into a specific radiocarbon age. The conversion into radiocarbon age is based on the early studies by Libby, who calculated the half-life of ^{14}C to be 5,568 years. At the time, only a limited number of measurements were performed and the half-life of ^{14}C was refined since then to 5,730 years (Godwin, 1962). By convention, the Libby half-life is, however, still used to convert the $F^{14}C$ values into a radiocarbon or ^{14}C age:

$$^{14}C\ age = -8033 \ln (F^{14}C) \quad (3)$$

As the half-life determined by Libby in 1949 is used for the calculation of the ^{14}C age, the resulting age before present (BP) is referenced to before 1950. The interaction of cosmic rays with the upper atmosphere is dependent on the sun's activity and fluctuations in Earth's magnetic field and thus the production of ^{14}C has been slightly fluctuating through time as well (Bronk Ramsey, 2008). Furthermore, the extensive nuclear-weapons tests performed during the Cold War era doubled the amount of ^{14}C in the atmosphere (De Vries, 1958). To compensate these effects calibrations are used to convert ^{14}C ages into calendar ages (cal BP, AD/BC, Reimer et al., 2020). In this thesis, however, data will be reported in $F^{14}C$ or uncalibrated ^{14}C ages.

Stable Carbon Isotope Analysis

The extra neutrons contained in ^{14}C and ^{13}C increase the atoms weight relative to ^{12}C. This slight increase in molecular weight affects the atom's kinetics and isotopic fractionations occur as a result. The distribution of heavy and rarer isotopes towards the lighter, more abundant isotope in an ecosystem is measurable by the stable ^{13}C content relative to ^{12}C. The naturally

occurring differences in this isotopic ratio (R) are small and therefore usually expressed in parts per thousand (‰) using the delta (δ) notation (Schuur et al., 2016):

$$\delta^{13}C = \left[\frac{\left(\frac{^{13}C}{^{12}C}\right)_{sample}}{\left(\frac{^{13}C}{^{12}C}\right)_{standard}} - 1 \right] 1000 \quad (4)$$

A referencing system was introduced that defined the $\delta^{13}C$ value of a belemnite fossil taken from the Pee Dee formation (PDB) in the USA to be 0‰ (Urey et al., 1951). However, since its introduction, the material of the original PDB standard was used up and instead the Vienna PDB (VPDB) was introduced, which is relatable to the original PDB (Coplen et al., 2006; Schuur et al., 2016). With the introduction of the PDB scale, it was possible to determine from where a carbon containing substance originated, enabled through the different mechanisms by which mass dependent fractionation occurred (Mook et al., 1974; Schirrmeister et al., 2011; Mauritz et al., 2019).

Isotopes preferably distribute towards a lower energetic state in a chemical equilibrium. In case of C isotopes, this occurs during inorganic C cycling i.e., precipitation of calcium carbonates (Mook et al., 1974; Schuur et al., 2016). ^{13}C therefore preferentially accumulates towards stronger, more stable chemical bonds or in a less entropic system (Schuur et al., 2016). As a result, calcium carbonate contains more ^{13}C than CO_2 in the atmosphere does, or a plant leaf, for example. Simultaneously, kinetic fractionation is another process that causes C isotope fractionation in non-equilibrium conditions (e.g., photosynthesis). During the reaction, the lighter ^{12}C isotopes react and diffuse faster and therefore are preferentially incorporated into glucose. This fractionation occurs because plants (and other organisms) consume nutrients in the most energy conserving manner possible, and therefore preferably split up weaker molecule bonds between lighter isotopes and discriminate against the heavier isotopes (Schuur et al., 2016).

By measuring and comparing $\delta^{13}C$ values of different samples, it is therefore possible to distinguish between the principal C sources from which the samples originated, for example between a plant and calcium carbonate (*ca.* -28‰ vs. 1.95‰ on the PDB scale, Schuur et al., 2016). This method is, however, only meaningful as a reference towards constant ratios calculated from stable isotopes.

Calculating Carbon Sources

The combination of the radiocarbon method with stable carbon isotope analysis can give useful information about the principal C pools that are contributing to CO_2 and CH_4 release. The ^{14}C content of the respired CO_2 and CH_4 reflects the residence time of the C-bearing material in

the ecosystem (Schuur and Trumbore, 2006). Here, we assume that most of the OM from the active layer is relatively young in comparison to OM from the permafrost layer that has been buried and frozen for up to thousands of years. The $\delta^{13}C$ values of CO_2 and CH_4, on the other hand, give evidence about organic or inorganic origin.

By applying a mass balance calculation to the data retrieved from ^{14}C and ^{13}C analysis, it is possible to determine the fraction of specific C pools that are contributing to GHG emissions (Pries et al., 2016). The constraining of the contributing C pools, the endmembers for the mass balance calculation, often relies on the analysis of additional material. This is done by ^{14}C and ^{13}C analysis of the soil or sediment from which the CO_2 emission derived. The equations used for the mass balance calculation are expressed in the following (Schuur and Trumbore, 2006; Pries et al., 2016):

$$^{14}C_{source} = \sum_1^n (f_n * {}^{14}C_n) \quad (5)$$

$$^{13}C_{source} = \sum_1^n (f_n * {}^{13}C_n) \quad (6)$$

$$1 = \sum_1^n f_n \quad (7)$$

where f_n is the fraction of one C pool that is contributing to the isotopic composition of the sampled gas. With this approach, it is possible to distinguish between old and young, as well as organic and inorganic C sources, provided enough data are available to constrain the individual C sources. While the calculation of the contribution of each individual C pool is easy for a two-pool model (two unknowns and two equations), more complex models using three or more sources, depend on software support, which solves the equations iteratively (Phillips and Gregg, 2003).

^{14}C Analysis at CologneAMS

The CO_2 collection from remote permafrost areas and the transport of the gas samples back to the laboratory for isotopic analysis without contamination or sample losses required the development of a sturdy and easy to handle container. Molecular sieve cartridges (MSCs) were built and improved that allow storage of CO_2 up to an equivalent of 2 mg C. Development and validation of the sampling setup and the MSC is explained in detail in Wotte et al. (2017a, 2017b). Briefly summarized, type 13X zeolite, contained in a stainless-steel cartridge and sealed by quick couplings, is used in a portable gas analyzer and respiration chamber setup that allows storage of in-situ emitted CO_2. The CO_2 collected in the respiration chamber is pumped through the attached MSC and subsequently adsorbs onto the surface of the zeolite. In the laboratory, the MSC is heated up to 500°C, releasing the adsorbed CO_2 into a gas phase, which is consequently flushed in a gas stream into a vacuum purification setup, where the

sample is quantified and sealed for AMS analysis, while the MSC can be reused once it has been heated and flushed thoroughly.

Until recently, CO_2 samples prepared from MSCs for radiocarbon analysis with AMS, have been converted into solid graphite targets containing 500 to 1000 µg C (Wotte et al., 2017b) using an automatic graphitization equipment (AGE, Wacker et al., 2010). However, if there is less C from a sample available, it is difficult to produce enough graphite for a meaningful analysis (Rethemeyer et al., 2013). Nevertheless, the demand for refined measurement and preparation techniques to perform compound-specific analysis has increased during the last decades. As a result, systems such as the gas ion source were developed that allow microscale AMS analysis of ^{14}C (Ruff et al., 2007; Santos et al., 2007; Fahrni et al., 2013). Improvements in AMS measurement at CologneAMS allow the measurement of samples as small as 20 µg C via the recently installed gas injection system (GIS) for the SO-110 B type ion source coupled to the HVE 6 MV Tandetron accelerator (High Voltage Engineering Europa B.V., The Netherlands, Dewald et al., 2013; Stolz et al., 2017, 2019). The installation of the GIS (Ionplus AG, Switzerland) enabled a faster handling and preparation of CO_2 samples collected from arctic permafrost on an MSC. The down scaling of sample size from initially 500 to 1000 µg C to 20 µg C required further assessment of our setups to maintain a high level of measurement quality (Santos et al., 2010; Welte et al., 2018). For sample sizes as low as 20 µg C it is important to minimize the introduction of exogenous C. During handling of the sample material, as well as during the measurement, a sample is subjected to contamination that needs be quantified as precisely as possible. The quantification of contamination allows the correction of the measured ^{14}C values and the refinement of the workflow to prevent as much contamination as possible in the future.

References

Åkerman, H. J., and Johansson, M. (2008). Thawing permafrost and thicker active layers in sub-arctic Sweden. *Permafr. Periglac. Process.* 19, 279–292. doi:10.1002/ppp.626.

Alexanderson, H., Adrielsson, L., Hjort, C., Möller, P., Antonov, O., Eriksson, S., et al. (2002). Depositional history of the North Taymyr ice-marginal zone, Siberia—a landsystem approach. *J. Quat. Sci.* 17, 361–382. doi:10.1002/jqs.677.

Beer, C., Zimov, N., Olofsson, J., Porada, P., and Zimov, S. (2020). Protection of Permafrost Soils from Thawing by Increasing Herbivore Density. *Sci. Rep.* 10, 4170. doi:10.1038/s41598-020-60938-y.

Boike, J., Kattenstroth, B., Abramova, K., Bornemann, N., Chetverova, A., Fedorova, I., et al. (2013). Baseline characteristics of climate, permafrost and land cover from a new permafrost observatory in the Lena River Delta, Siberia (1998–2011). *Biogeosciences* 10, 2105–2128. doi:10.5194/bg-10-2105-2013.

Box, J. E., Colgan, W. T., Christensen, T. R., Schmidt, N. M., Lund, M., Parmentier, F.-J. W., et al. (2019). Key indicators of Arctic climate change: 1971–2017. *Environ. Res. Lett.* 14, 045010. doi:10.1088/1748-9326/aafc1b.

Bronk Ramsey, C. (2008). Radiocarbon Dating: Revolutions in Understanding*. *Archaeometry* 50, 249–275. doi:10.1111/j.1475-4754.2008.00394.x.

Brown, J., Sidlauskas, F. J., and Delinski, G. (1997). Circum-Arctic map of permafrost and ground ice conditions.

Chapin, F. S. (2005). Role of Land-Surface Changes in Arctic Summer Warming. *Science* 310, 657–660. doi:10.1126/science.1117368.

Coplen, T. B., Brand, W. A., Gehre, M., Gröning, M., Meijer, H. A. J., Toman, B., et al. (2006). New Guidelines for δ^{13} C Measurements. *Anal. Chem.* 78, 2439–2441. doi:10.1021/ac052027c.

Czimczik, C. I., and Welker, J. M. (2010). Radiocarbon Content of CO_2 Respired from High Arctic Tundra in Northwest Greenland. *Arct. Antarct. Alp. Res.* 42, 342–350. doi:10.1657/1938-4246-42.3.342.

Czudek, T., and Demek, J. (1970). Thermokarst in Siberia and Its Influence on the Development of Lowland Relief. *Quat. Res.* 1, 103–120. doi:10.1016/0033-5894(70)90013-X.

Davidson, E. A., and Janssens, I. A. (2006). Temperature sensitivity of soil carbon decomposition and feedbacks to climate change. *Nature* 440, 165–173. doi:10.1038/nature04514.

De Vries, H. (1958). Atomic Bomb Effect: Variation of Radiocarbon in Plants, Shells, and Snails in the Past 4 Years. *Science* 128, 250–251. doi:10.1126/science.128.3318.250.

Dewald, A., Heinze, S., Jolie, J., Zilges, A., Dunai, T., Rethemeyer, J., et al. (2013). CologneAMS, a dedicated center for accelerator mass spectrometry in Germany. *Nucl. Instrum. Methods Phys. Res. Sect. B Beam Interact. Mater. At.* 294, 18–23. doi:10.1016/j.nimb.2012.04.030.

Dorsett, A., Cherrier, J., Martin, J. B., and Cable, J. E. (2011). Assessing hydrologic and biogeochemical controls on pore-water dissolved inorganic carbon cycling in a subterranean estuary: A 14C and 13C mass balance approach. *Mar. Chem.* 127, 76–89. doi:10.1016/j.marchem.2011.07.007.

Dutta, K., Schuur, E. A. G., Neff, J. C., and Zimov, S. A. (2006). Potential carbon release from permafrost soils of Northeastern Siberia: CARBON RELEASE FROM SIBERIAN PERMAFROST SOILS. *Glob. Change Biol.* 12, 2336–2351. doi:10.1111/j.1365-2486.2006.01259.x.

Estop-Aragonés, C., Cooper, M. D. A., Fisher, J. P., Thierry, A., Garnett, M. H., Charman, D. J., et al. (2018). Limited release of previously-frozen C and increased new peat formation after thaw in permafrost peatlands. *Soil Biol. Biochem.* 118, 115–129. doi:10.1016/j.soilbio.2017.12.010.

Fahrni, S. M., Wacker, L., Synal, H.-A., and Szidat, S. (2013). Improving a gas ion source for 14C AMS. *Nucl. Instrum. Methods Phys. Res. Sect. B Beam Interact. Mater. At.* 294, 320–327. doi:10.1016/j.nimb.2012.03.037.

Farquharson, L. M., Romanovsky, V. E., Cable, W. L., Walker, D. A., Kokelj, S. V., and Nicolsky, D. (2019). Climate Change Drives Widespread and Rapid Thermokarst Development in Very Cold Permafrost in the Canadian High Arctic. *Geophys. Res. Lett.* 46, 6681–6689. doi:10.1029/2019GL082187.

Faucherre, S., Jørgensen, C. J., Blok, D., Weiss, N., Siewert, M. B., Bang-Andreasen, T., et al. (2018). Short and Long-Term Controls on Active Layer and Permafrost Carbon Turnover Across the Arctic. *J. Geophys. Res. Biogeosciences* 123, 372–390. doi:10.1002/2017JG004069.

Fortier, D., Allard, M., and Shur, Y. (2007). Observation of rapid drainage system development by thermal erosion of ice wedges on Bylot Island, Canadian Arctic Archipelago. *Permafr. Periglac. Process.* 18, 229–243. doi:10.1002/ppp.595.

Garnett, M. H., and Murray, C. (2013). Processing of CO2 Samples Collected Using Zeolite Molecular Sieve for 14C Analysis at the NERC Radiocarbon Facility (East Kilbride, UK). *Radiocarbon* 55, 410–415. doi:10.1017/S0033822200057532.

Godwin, H. (1962). Half-life of Radiocarbon. *Nature* 195, 984–984. doi:10.1038/195984a0.

Gordeev, V. V., and Shevchenko, V. P. (1995). Chemical composition of suspended sediments in the Lena river and its mixing zone. *Berichte Zur Polar- Meeresforsch.* 176. Available at: https://elibrary.ru/item.asp?id=29052632 [Accessed September 30, 2021].

Griffith, D. R., McNichol, A. P., Xu, L., McLaughlin, F. A., Macdonald, R. W., Brown, K. A., et al. (2012). Carbon dynamics in the western Arctic Ocean: insights from full-depth carbon isotope profiles of DIC, DOC, and POC. *Biogeosciences* 9, 1217–1224. doi:10.5194/bg-9-1217-2012.

Grigoriev, M.N. (1993). Cryomorphogenesis of the Lena River mouth area. SB RAS, Yakutsk, 1-176. in Russian.

Grosse, G., Harden, J., Turetsky, M., McGuire, A. D., Camill, P., Tarnocai, C., et al. (2011). Vulnerability of high-latitude soil organic carbon in North America to disturbance. *J. Geophys. Res. Biogeosciences* 116. doi:10.1029/2010JG001507.

Grosse, G., Romanovsky, V., Walter, K., Morgenstern, A., Lantuit, H., and Zimov, S. (2008). Distribution of Thermokarst Lakes and Ponds at Three Yedoma Sites in Siberia. *Proceedings of the 9th International Conference on Permafrost, Fairbanks, Alaska, 29 June–3 July 2008*.

Guo, L., Ping, C.-L., and Macdonald, R. W. (2007). Mobilization pathways of organic carbon from permafrost to arctic rivers in a changing climate. *Geophys. Res. Lett.* 34. doi:10.1029/2007GL030689.

Gustafsson, Ö., van Dongen, B. E., Vonk, J. E., Dudarev, O. V., and Semiletov, I. P. (2011). Widespread release of old carbon across the Siberian Arctic echoed by its large rivers. *Biogeosciences* 8, 1737–1743. doi:10.5194/bg-8-1737-2011.

Harden, J. W., Mark, R. K., Sundquist, E. T., and Stallard, R. F. (1992). Dynamics of Soil Carbon During Deglaciation of the Laurentide Ice Sheet. *Science* 258, 1921–1924. doi:10.1126/science.258.5090.1921.

Hardie, S. M. L., Garnett, M. H., Fallick, A. E., Rowland, A. P., and Ostle, N. J. (2005). Carbon Dioxide Capture Using a Zeolite Molecular Sieve Sampling System for Isotopic Studies (13C and 14C) of Respiration. *Radiocarbon* 47, 441–451. doi:10.1017/S0033822200035220.

Hinzman, L. D., Kane, D. L., Gieck, R. E., and Everett, K. R. (1991). Hydrologic and thermal properties of the active layer in the Alaskan Arctic. *Cold Reg. Sci. Technol.* 19, 95–110. doi:10.1016/0165-232X(91)90001-W.

Hoefs, J. (2015). “Isotope Fractionation Processes of Selected Elements,” in *Stable Isotope Geochemistry*, ed. J. Hoefs (Cham: Springer International Publishing), 47–190. doi:10.1007/978-3-319-19716-6_2.

Houghton, R. A. (2007). Balancing the Global Carbon Budget. *Annu. Rev. Earth Planet. Sci.* 35, 313–347. doi:10.1146/annurev.earth.35.031306.140057.

Hugelius, G., Strauss, J., Zubrzycki, S., Harden, J. W., Schuur, E. A. G., Ping, C.-L., et al. (2014). Estimated stocks of circumpolar permafrost carbon with quantified uncertainty ranges and identified data gaps. *Biogeosciences* 11, 6573–6593. doi:10.5194/bg-11-6573-2014.

Hultén, E. (1937). Outline of the history of arctic and boreal biota during the Quaternary period.

Kane, D. L., Hinzman, L. D., and Zarling, J. P. (1991). Thermal response of the active layer to climatic warming in a permafrost environment. *Cold Reg. Sci. Technol.* 19, 111–122. doi:10.1016/0165-232X(91)90002-X.

Kanevskiy, M., Shur, Y., Fortier, D., Jorgenson, M. T., and Stephani, E. (2011). Cryostratigraphy of late Pleistocene syngenetic permafrost (yedoma) in northern Alaska, Itkillik River exposure. *Quat. Res.* 75, 584–596. doi:10.1016/j.yqres.2010.12.003.

Kittler, F., Heimann, M., Kolle, O., Zimov, N., Zimov, S., and Göckede, M. (2017). Long-Term Drainage Reduces CO2 Uptake and CH4 Emissions in a Siberian Permafrost Ecosystem. *Glob. Biogeochem. Cycles* 31, 1704–1717. doi:10.1002/2017GB005774.

Knoblauch, C., Beer, C., Sosnin, A., Wagner, D., and Pfeiffer, E.-M. (2013). Predicting long-term carbon mineralization and trace gas production from thawing permafrost of Northeast Siberia. *Glob. Change Biol.* 19, 1160–1172. doi:10.1111/gcb.12116.

Kokelj, S. V., Lacelle, D., Lantz, T. C., Tunnicliffe, J., Malone, L., Clark, I. D., et al. (2013). Thawing of massive ground ice in mega slumps drives increases in stream sediment and solute flux across a range of watershed scales. *J. Geophys. Res. Earth Surf.* 118, 681–692. doi:10.1002/jgrf.20063.

Koven, C. D., Schuur, E. A. G., Schädel, C., Bohn, T. J., Burke, E. J., Chen, G., et al. (2015). A simplified, data-constrained approach to estimate the permafrost carbon–climate feedback. *Philos. Trans. R. Soc. Math. Phys. Eng. Sci.* 373, 20140423. doi:10.1098/rsta.2014.0423.

Kuhry, P. (2008). Palsa and peat plateau development in the Hudson Bay Lowlands, Canada: timing, pathways and causes. *Boreas* 37, 316–327. doi:10.1111/j.1502-3885.2007.00022.x.

Kuhry, P., Bárta, J., Blok, D., Elberling, B., Faucherre, S., Hugelius, G., et al. (2020). Lability classification of soil organic matter in the northern permafrost region. *Biogeosciences* 17, 361–379. doi:10.5194/bg-17-361-2020.

Lee, H., Schuur, E. A. G., Inglett, K. S., Lavoie, M., and Chanton, J. P. (2012). The rate of permafrost carbon release under aerobic and anaerobic conditions and its potential effects on climate. *Glob. Change Biol.* 18, 515–527. doi:10.1111/j.1365-2486.2011.02519.x.

Lenton, T. M. (2012). Arctic Climate Tipping Points. *AMBIO* 41, 10–22. doi:10.1007/s13280-011-0221-x.

Lewkowicz, A. G. (2007). Dynamics of active-layer detachment failures, Fosheim Peninsula, Ellesmere Island, Nunavut, Canada. *Permafr. Periglac. Process.* 18, 89–103. doi:10.1002/ppp.578.

Lewkowicz, A. G., and Way, R. G. (2019). Extremes of summer climate trigger thousands of thermokarst landslides in a High Arctic environment. *Nat. Commun.* 10, 1329. doi:10.1038/s41467-019-09314-7.

Libby, W. F. (1946). Atmospheric Helium Three and Radiocarbon from Cosmic Radiation. *Phys. Rev.* 69, 671–672. doi:10.1103/PhysRev.69.671.2.

Lindgren, A., Hugelius, G., Kuhry, P., Christensen, T. R., and Vandenberghe, J. (2016). GIS-based Maps and Area Estimates of Northern Hemisphere Permafrost Extent during the Last Glacial Maximum. *Permafr. Periglac. Process.* 27, 6–16. doi:10.1002/ppp.1851.

Mauritz, M., Celis, G., Ebert, C., Hutchings, J., Ledman, J., Natali, S. M., et al. (2019). Using Stable Carbon Isotopes of Seasonal Ecosystem Respiration to Determine Permafrost Carbon Loss. *J. Geophys. Res. Biogeosciences* 124, 46–60. doi:10.1029/2018JG004619.

Mook, W. G., Bommerson, J. C., and Staverman, W. H. (1974). Carbon isotope fractionation between dissolved bicarbonate and gaseous carbon dioxide. *Earth Planet. Sci. Lett.* 22, 169–176. doi:10.1016/0012-821X(74)90078-8.

Morgenstern, A., Grosse, G., Günther, F., Fedorova, I., and Schirrmeister, L. (2011). Spatial analyses of thermokarst lakes and basins in Yedoma landscapes of the Lena Delta. *The Cryosphere* 5, 849–867. doi:10.5194/tc-5-849-2011.

Nitzbon, J., Westermann, S., Langer, M., Martin, L. C. P., Strauss, J., Laboor, S., et al. (2020). Fast response of cold ice-rich permafrost in northeast Siberia to a warming climate. *Nat. Commun.* 11, 1–11. doi:10.1038/s41467-020-15725-8.

Osterkamp, T. E., Jorgenson, M. T., Schuur, E. a. G., Shur, Y. L., Kanevskiy, M. Z., Vogel, J. G., et al. (2009). Physical and ecological changes associated with warming permafrost and thermokarst in Interior Alaska. *Permafr. Periglac. Process.* 20, 235–256. doi:10.1002/ppp.656.

Osterkamp, T. E., Viereck, L., Shur, Y., Jorgenson, M. T., Racine, C., Doyle, A., et al. (2000). Observations of Thermokarst and Its Impact on Boreal Forests in Alaska, U.S.A. *Arct. Antarct. Alp. Res.* 32, 303–315. doi:10.1080/15230430.2000.12003368.

Palonen, V., and Oinonen, M. (2013). Molecular Sieves in 14CO2 Sampling and Handling. *Radiocarbon* 55, 416–420. doi:10.1017/S0033822200057544.

Phillips, D. L., and Gregg, J. W. (2003). Source partitioning using stable isotopes: coping with too many sources. *Oecologia* 136, 261–269. doi:10.1007/s00442-003-1218-3.

Ping, C. L., Bockheim, J. G., Kimble, J. M., Michaelson, G. J., and Walker, D. A. (1998). Characteristics of cryogenic soils along a latitudinal transect in arctic Alaska. *J. Geophys. Res. Atmospheres* 103, 28917–28928. doi:10.1029/98JD02024.

Post, W. M., Emanuel, W. R., Zinke, P. J., and Stangenberger, A. G. (1982). Soil carbon pools and world life zones. *Nature* 298, 156–159. doi:10.1038/298156a0.

Pries, C. E. H., Schuur, E. A. G., Natali, S. M., and Crummer, K. G. (2016). Old soil carbon losses increase with ecosystem respiration in experimentally thawed tundra. *Nat. Clim. Change* 6, 214–218. doi:10.1038/nclimate2830.

Ramnarine, R., Wagner-Riddle, C., Dunfield, K. E., and Voroney, R. P. (2012). Contributions of carbonates to soil CO_2 emissions. *Can. J. Soil Sci.* 92, 599–607. doi:10.4141/cjss2011-025.

Reimer, P. J., Austin, W. E. N., Bard, E., Bayliss, A., Blackwell, P. G., Ramsey, C. B., et al. (2020). The IntCal20 Northern Hemisphere Radiocarbon Age Calibration Curve (0–55 cal kBP). *Radiocarbon* 62, 725–757. doi:10.1017/RDC.2020.41.

Rethemeyer, J., Fülöp, R.-H., Höfle, S., Wacker, L., Heinze, S., Hajdas, I., et al. (2013). Status report on sample preparation facilities for 14C analysis at the new CologneAMS center. *Nucl. Instrum. Methods Phys. Res. Sect. B Beam Interact. Mater. At.* 294, 168–172. doi:10.1016/j.nimb.2012.02.012.

Ruff, M., Wacker, L., Gäggeler, H. W., Suter, M., Synal, H.-A., and Szidat, S. (2007). A Gas Ion Source for Radiocarbon Measurements at 200 kV. *Radiocarbon* 49, 307–314. doi:10.1017/S0033822200042235.

Santos, G. M., Southon, J. R., Drenzek, N. J., Ziolkowski, L. A., Druffel, E., Xu, X., et al. (2010). Blank Assessment for Ultra-Small Radiocarbon Samples: Chemical Extraction and Separation Versus AMS. *Radiocarbon* 52, 1322–1335. doi:10.1017/S0033822200046415.

Santos, G. M., Southon, J. R., Griffin, S., Beaupre, S. R., and Druffel, E. R. M. (2007). Ultra small-mass AMS 14C sample preparation and analyses at KCCAMS/UCI Facility. *Nucl. Instrum. Methods Phys. Res. Sect. B Beam Interact. Mater. At.* 259, 293–302. doi:10.1016/j.nimb.2007.01.172.

Schädel, C., Schuur, E. A. G., Bracho, R., Elberling, B., Knoblauch, C., Lee, H., et al. (2014). Circumpolar assessment of permafrost C quality and its vulnerability over time using long-term incubation data. *Glob. Change Biol.* 20, 641–652. doi:10.1111/gcb.12417.

Schaefer, K., Lantuit, H., Romanovsky, V. E., Schuur, E. A. G., and Witt, R. (2014). The impact of the permafrost carbon feedback on global climate. *Environ. Res. Lett.* 9, 085003. doi:10.1088/1748-9326/9/8/085003.

Schirrmeister, L. (2011). Sedimentary characteristics and origin of the Late Pleistocene Ice Complex on north-east Siberian Arctic coastal lowlands and islands – A review. *Quat. Int.* 241, 3–25. doi:10.1016/j.quaint.2010.04.004.

Schirrmeister, L., Froese, D., Tumskoy, V., Grosse, G., and Wetterich, S. (2013). Yedoma: Late Pleistocene ice-rich syngenetic permafrost of Beringia. *Encycl. Quat. Sci. 2nd Ed.*, 542–552. Available at: http://www.sciencedirect.com/science/article/pii/B9780444536433001060 [Accessed September 30, 2021].

Schirrmeister, L., Grosse, G., Wetterich, S., Overduin, P. P., Strauss, J., Schuur, E. A. G., et al. (2011). Fossil organic matter characteristics in permafrost deposits of the northeast Siberian Arctic. *J. Geophys. Res. Biogeosciences* 116. doi:10.1029/2011JG001647.

Schneider von Deimling, T., Grosse, G., Strauss, J., Schirrmeister, L., Morgenstern, A., Schaphoff, S., et al. (2015). Observation-based modelling of permafrost carbon fluxes with accounting for deep carbon deposits and thermokarst activity. *Biogeosciences* 12, 3469–3488. doi:10.5194/bg-12-3469-2015.

Schuur, E. A. G., Bockheim, J., Canadell, J. G., Euskirchen, E., Field, C. B., Goryachkin, S. V., et al. (2008). Vulnerability of Permafrost Carbon to Climate Change: Implications for the Global Carbon Cycle. *BioScience* 58, 701–714. doi:10.1641/B580807.

Schuur, E. a. G., McGuire, A. D., Schädel, C., Grosse, G., Harden, J. W., Hayes, D. J., et al. (2015). Climate change and the permafrost carbon feedback. *Nature* 520, 171–179. doi:10.1038/nature14338.

Schuur, E. A. G., and Trumbore, S. E. (2006). Partitioning sources of soil respiration in boreal black spruce forest using radiocarbon. *Glob. Change Biol.* 12, 165–176. doi:10.1111/j.1365-2486.2005.01066.x.

Schuur, E. A. G., Trumbore, S. E., Druffel, E. R. M., Southon, J. R., Steinhof, A., Taylor, R. E., et al. (2016). “Radiocarbon and the Global Carbon Cycle,” in *Radiocarbon and Climate Change: Mechanisms, Applications and Laboratory Techniques*, eds. E. A. G. Schuur, E. Druffel, and S. E. Trumbore (Cham: Springer International Publishing), 1–19. doi:10.1007/978-3-319-25643-6_1.

Schwamborn, G., Rachold, V., Grigoriev, M. N., and Krbetschek, M. (2012). Sedimentation history in the Lena Delta, N-Siberia. in *EPIC3Russian-German cooperation in the scientific exploration of northern Eurasia and the adjacent Arctic ocean. Leopoldina Symposium in cooperation with St. Petersburg State University and the Russian Academy of Sciences, St. Petersburg, 2012-09-10-2012-09-12* (St. Petersburg). Available at: https://epic.awi.de/id/eprint/31152/ [Accessed September 30, 2021].

Stapel, J. G., Schirrmeister, L., Overduin, P. P., Wetterich, S., Strauss, J., Horsfield, B., et al. (2016). Microbial lipid signatures and substrate potential of organic matter in permafrost deposits: Implications for future greenhouse gas production. *J. Geophys. Res. Biogeosciences* 121, 2652–2666. doi:10.1002/2016JG003483.

Stettner, S., Beamish, A. L., Bartsch, A., Heim, B., Grosse, G., Roth, A., et al. (2018). Monitoring Inter- and Intra-Seasonal Dynamics of Rapidly Degrading Ice-Rich Permafrost Riverbanks in the Lena Delta with TerraSAR-X Time Series. *Remote Sens.* 10, 51. doi:10.3390/rs10010051.

Stolz, A., Dewald, A., Altenkirch, R., Herb, S., Heinze, S., Schiffer, M., et al. (2017). Radiocarbon measurements of small gaseous samples at CologneAMS. *Nucl. Instrum. Methods Phys. Res. Sect. B Beam Interact. Mater. At.* 406, 283–286. doi:10.1016/j.nimb.2017.03.031.

Stolz, A., Dewald, A., Heinze, S., Altenkirch, R., Hackenberg, G., Herb, S., et al. (2019). Improvements in the measurement of small 14CO2 samples at CologneAMS. *Nucl. Instrum. Methods Phys. Res. Sect. B Beam Interact. Mater. At.* 439, 70–75. doi:10.1016/j.nimb.2018.12.008.

Strauss, J., Schirrmeister, L., Grosse, G., Fortier, D., Hugelius, G., Knoblauch, C., et al. (2017). Deep Yedoma permafrost: A synthesis of depositional characteristics and carbon vulnerability. *Earth-Sci. Rev.* 172, 75–86. doi:10.1016/j.earscirev.2017.07.007.

Strauss, J., Schirrmeister, L., Mangelsdorf, K., Eichhorn, L., Wetterich, S., and Herzschuh, U. (2015). Organic-matter quality of deep permafrost carbon – a study from Arctic Siberia. *Biogeosciences* 12, 2227–2245. doi:10.5194/bg-12-2227-2015.

Stuiver, M., and Polach, H. A. (1977). Discussion Reporting of 14C Data. *Radiocarbon* 19, 355–363. doi:10.1017/S0033822200003672.

Tamir, G., Shenker, M., Heller, H., Bloom, P. R., Fine, P., and Bar-Tal, A. (2011). Can Soil Carbonate Dissolution Lead to Overestimation of Soil Respiration? *Soil Sci. Soc. Am. J.* 75, 1414–1422. doi:10.2136/sssaj2010.0396.

Tarnocai, C., Kimble, J., and Broll, G. (2003). Determining carbon stocks in Cryosols using the Northern and Mid Latitudes Soil Database. *Permafrost, vol. 2*, 1129– 1134.

Tarnocai, C., Canadell, J. G., Schuur, E. a. G., Kuhry, P., Mazhitova, G., and Zimov, S. (2009). Soil organic carbon pools in the northern circumpolar permafrost region. *Glob. Biogeochem. Cycles* 23. doi:10.1029/2008GB003327.

Tomirdiaro, S. V. (1996). Palaeogeography of Beringgia and Arctida. *Am. Begin.*, 58–69.

Turetsky, M. R., Abbott, B. W., Jones, M. C., Anthony, K. W., Olefeldt, D., Schuur, E. A. G., et al. (2020). Carbon release through abrupt permafrost thaw. *Nat. Geosci.* 13, 138–143. doi:10.1038/s41561-019-0526-0.

Urey, H. C., Lowenstam, H. A., Epstein, S., and McKinney, C. R. (1951). Measurement of Paleotemperatures and Temperatures of the Upper Cretaceous of England, Denmark, and the Southeastern United States. *GSA Bull.* 62, 399–416. doi:10.1130/0016-7606(1951)62[399:MOPATO]2.0.CO;2

Vasil'chuk, Yu. K., Budantseva, N. A., and Vasil'chuk, A. C. (2019). High-Resolution Oxygen Isotope Diagram of Late Pleistocene Ice Wedges of Seyakha Yedoma, Eastern Yamal Peninsula. *Dokl. Earth Sci.* 487, 823–826. doi:10.1134/S1028334X19070195.

Vas'kovsky, A. P. (1963). Stratigraphic outline of Quaternary deposits in northeastern Asia. *Geol. Koryaksky Mt.*, 24–53.

Wacker, L., Němec, M., and Bourquin, J. (2010). A revolutionary graphitisation system: Fully automated, compact and simple. *Nucl. Instrum. Methods Phys. Res. Sect. B Beam Interact. Mater. At.* 268, 931–934. doi:10.1016/j.nimb.2009.10.067.

Walker, H. J. (1998). Arctic Deltas. *J. Coast. Res.* 14, 719–738.

Walz, J., Knoblauch, C., Tigges, R., Opel, T., Schirrmeister, L., and Pfeiffer, E.-M. (2018). Greenhouse gas production in degrading ice-rich permafrost deposits in northeastern Siberia. *Biogeosciences* 15, 5423–5436. doi:10.5194/bg-15-5423-2018.

Weiss, N., Blok, D., Elberling, B., Hugelius, G., Jørgensen, C. J., Siewert, M. B., et al. (2016). Thermokarst dynamics and soil organic matter characteristics controlling initial carbon release from permafrost soils in the Siberian Yedoma region. *Sediment. Geol.* 340, 38–48. doi:10.1016/j.sedgeo.2015.12.004.

Welte, C., Hendriks, L., Wacker, L., Haghipour, N., Eglinton, T. I., Günther, D., et al. (2018). Towards the limits: Analysis of microscale 14C samples using EA-AMS. *Nucl. Instrum. Methods Phys. Res. Sect. B Beam Interact. Mater. At.* 437, 66–74. doi:10.1016/j.nimb.2018.09.046.

Wotte, A., Wischhöfer, P., Wacker, L., and Rethemeyer, J. (2017a). 14CO2 analysis of soil gas: Evaluation of sample size limits and sampling devices. *Nucl. Instrum. Methods Phys. Res. Sect. B Beam Interact. Mater. At.* 413, 51–56. doi:10.1016/j.nimb.2017.10.009.

Wotte, A., Wordell-Dietrich, P., Wacker, L., Don, A., and Rethemeyer, J. (2017b). 14CO2 processing using an improved and robust molecular sieve cartridge. *Nucl. Instrum. Methods Phys. Res. Sect. B Beam Interact. Mater. At.* 400, 65–73. doi:10.1016/j.nimb.2017.04.019.

Wu, H., Zhang, R., Wang, Y., Hong, M., Yan, H., and Zhu, J. (2021). Analyzing the effects of sea ice melting and atmospheric heat transport on the warming around arctic based on comparable analysis and coupling modes. *Atmospheric Res.* 258, 105630. doi:10.1016/j.atmosres.2021.105630.

Zhang, T., Barry, R. G., Knowles, K., Heginbottom, J. A., and Brown, J. (1999). Statistics and characteristics of permafrost and ground-ice distribution in the Northern Hemisphere [1]. *Polar Geogr.* 23, 132–154. doi:10.1080/10889379909377670.

Zimov, S. A., Davydov, S. P., Zimova, G. M., Davydova, A. I., Schuur, E. A. G., Dutta, K., et al. (2006). Permafrost carbon: Stock and decomposability of a globally significant carbon pool. Geophys. Res. Lett. 33, L20502. doi:10.1029/2006GL027484.

Manuscript I: Exploring sample size limits of AMS gas ion source ^{14}C analysis at CologneAMS

by

Jan Olaf Melchert[1], Alexander Stolz[2], Alfred Dewald[2], Merle Gierga[1], Philipp Wischhöfer[1], Janet Rethemeyer[1]

[1]Institute of Geology and Mineralogy, University of Cologne, Zuelpicher Str. 49b, 50674 Cologne, Germany
[2]Institute of Nuclear Physics, University of Cologne, Zuelpicher Str. 77, 50937 Cologne, Germany

published in

Radiocarbon 2018 Conference Proceedings Trondheim, Norway, June 17–22, 2018 Part 2 of 2

Volume 61 - Issue 6 - December 2019

Information regarding the acquisition of primary data:

The primary data relevant for this manuscript are stored and accessible on the server of the Institute of Geology and Mineralogy at the University of Cologne. Raw data needed to reproduce the presented calculations are included as supplementary material to this manuscript.

Jan Olaf Melchert[1], Alexander Stolz[2], Alfred Dewald[2], Merle Gierga[1], Philipp Wischhöfer[1], Janet Rethemeyer[1]

[1]Institute of Geology and Mineralogy, University of Cologne, Zuelpicher Str. 49b, 50674 Cologne, Germany
[2]Institute of Nuclear Physics, University of Cologne, Zuelpicher Str. 77, 50937 Cologne, Germany

Corresponding author Email: janet.rethemeyer@uni-koeln.de

Abstract

Increasing demands for small-scale ^{14}C analyses required the installation of a “SO-110 B” type ion source (HVE Europa B.V.) at our 6 MV Tandetron AMS (HVE) dedicated for the direct injection of CO_2 using either the gas injection system (GIS) from Ionplus AG or a EuroVector EA 3000 elemental analyzer (EA). We tested both systems with multiple series of ^{14}C-free and modern standards (2.5 – 50 µg C) combusted in quartz ampoules or EA containers and were able to quantify exogenous C introduced. In EA-GIS-AMS analysis exogenous C is mainly derived from the EA sample containers. Blank values for 50 µg C combusted in solvent-cleaned Sn vessels were 0.0127 ± 0.0012 $F^{14}C$ (boats) and 0.0090 ± 0.0010 $F^{14}C$ (capsules), while they were much higher for thermally-cleaned Ag capsules. The processing of gas samples for GIS-AMS yields similar blank values corresponding to 0.30 ± 0.08 µg exogenous C with 0.93 ± 0.23 $F^{14}C$ consisting of 0.28 µg C modern and 0.02 µg C fossil C. The combustion of larger amounts of blank material (1 mg C) in a single quartz tube split into aliquots, gives lower blanks (0.0064 ± 0.0008 $F^{14}C$; 50 µg C). Thus, ^{14}C analysis of small, gaseous samples is now possible at CologneAMS.

Introduction

The Centre of Accelerator Mass Spectrometry at the University of Cologne (CologneAMS) recently installed a second ion source (SO-110 B; Stolz et al., 2017) from High Voltage Engineering Europa B.V. (HVE, The Netherlands) at the HVE 6 MV Tandetron accelerator, which is used for ^{14}C analysis of CO_2 gas. Until now, all samples were converted to elemental carbon using the automated graphitization equipment AGE-2 (Ionplus AG, Switzerland). Samples smaller than 200 µg C, and older than about 25,000 yr BP were not measured so far, because we were not able to produce reliable results (Rethemeyer et al. 2013). Increasing demands for small-scale ^{14}C analysis of samples such as tiny macrofossils, organic molecules isolated with chromatographic methods, and CO_2 samples required the establishment of AMS gas ion source ^{14}C analysis at CologneAMS allowing the analysis of samples as small as 2.5 µg C.

The SO-110 B type ion source was first coupled with the gas injection system (GIS) from Ionplus AG, which introduces CO_2 provided in glass ampoules (GIS-AMS). Tests of this system

with ^{14}C-free CO_2 from gas bottles yielded a constant contamination of about 0.002 µg C. Blank values for samples >20 µg C correspond to 0.002 F^{14}C (Stolz et al. 2019). Secondly, an EA3000 elemental analyzer (EA; EuroVector, Italy) was coupled to the GIS (EA-GIS-AMS), in order to reduce pre-treatment steps and the time-consuming gas purification required for producing CO_2 samples in glass ampoules for GIS-AMS and to make small-scale ^{14}C analysis more efficient. Hence, samples only need to be packed into EA combustion vessels and are consequently combusted into CO_2. As soon as the system detects the CO_2 peak, the gas is streamed into a zeolite trap with helium. After that, the trap is heated and the released CO_2 is directly injected into the AMS using the GIS (Stolz et al. 2019). First tests of this coupled EA-GIS-AMS setup offered very promising results using IAEA reference standards (Stolz et al. 2019).

In this study, we conducted extensive tests to gain detailed information about the contamination introduced during the analysis of CO_2 samples using a) the GIS-AMS and b) the EA-GIS-AMS system. The relative importance of exogenous C contribution and its variability are increasing with decreasing sample size (e.g. Rethemeyer et al. 2013; Ruff et al. 2010b). Therefore, we determined the lower sample size and age limits of GIS-AMS by measuring multiple series of standards ranging from 2.5 – 50 µg C. For EA-GIS-AMS analysis, we additionally compared the contamination introduced during sample combustion using different types of vessels made of tin and silver.

Methods

Pre-treatment methods for GIS-AMS analysis

For the evaluation of lower size limits and blank values of the GIS-AMS system, different size series of a ^{14}C-free (Pocahontas, POC #3, Argonne Premium Coal) and of a modern standard (Ox-II; NIST SRM 4990C; nominal value 1.3407 F^{14}C) were prepared using sealed tube combustion. Outmost care was taken not to introduce any contamination during the preparation of the standards: The quartz glass ampoules (9 mm OD) for sample combustion and borosilicate glass tubes (4 mm OD), in which purified CO_2 samples are collected, were first visually checked for damages and then washed three times with Milli-Q water (Millipore, USA) and three times with acetone (PESTINORM® SUPRA TRACE, grade ≥99.9%, VWR® chemicals, Germany) to remove organic contaminants. The quartz ampoules, cupric oxide (CuO rods, 0.65 x 3 mm, p.a., MERCK KGaA, Germany), and silver wires (MERCK KGaA, Germany) were pre-combusted at 900°C for 4 h, while the borosilicate glass tubes were combusted at 450°C for 4 h. Then the sample was filled into the cleaned quartz tubes using tin boats for weighing and transferring together with the CuO (CuO:C ratio of about 60:1) and 5 mg silver wires (Santos and Xu 2017). Then, the ampoules were evacuated ($P < 10^{-4}$ mbar),

flame sealed, and heated in a muffle furnace to combust the standard material to CO_2 (900°C, 4 h). The gas was purification on a vacuum rig using a water trap (ethanol dry-ice slurry) and the CO_2 was finally trapped in a borosilicate glass ampoule (4 mm OD) placed in liquid nitrogen and was finally flame sealed (Wotte et al. 2017).

Pre-treatment methods for EA-GIS-AMS analysis

In order to determine blank values of different EA containers, we measured ^{14}C-free standards (POC #3) in a size range of 3.5 – 50 µg C. We tested Sn boats (4 x 4 x 11 mm), Sn capsules (3.5 x 9 mm) as well as Ag capsules (5 x 9 mm), all manufactured by Elementar (Germany). Prior to sample combustion, the containers were washed three times with dichloromethane (DCM; SupraSolv®, MERCK KGaA, Germany). The silver capsules were combusted at 450°C (4 h) in addition to DCM washing. We omit cleaning in an ultrasonic bath using organic solvents as handling experience showed that vessels become brittle.

System overview

To enable ^{14}C analysis of CO_2 at the HVE AMS system at CologneAMS, operation parameters of the SO-110 B type ion source were first optimized with the objective to maximize a stable C^- current output (maximum 12 ± 1 µA, 6 ± 2% C^- yield) (Stolz et al. 2017). In addition, a new gas-injection-control-software (GICS) controlling data acquisition and hardware was developed that substitutes the software from Ionplus AG (Stolz et al. 2019). The GIS sample magazine was also modified to be able to process 16 instead of previously 8 ampoules in one batch, which allows the extension of fully autonomous measurement periods.

Before starting an AMS measurement, all capillaries are flushed several times with He and a new target is loaded prior to sample CO_2 transfer (Stolz et al. 2019). Using EA-GIS, the CO_2 is transferred from the EA via a 13X zeolite trap into a syringe where it is mixed with He (mixing ratio CO_2:He 5%, Stolz et al. 2017). For GIS-AMS, CO_2 samples in glass ampoules are cracked in the ampoule cracker of the GIS, mixed with He, and injected into the ion source via syringe (flow rate 1.4 µg C min^{-1}, Stolz et al. 2017).

Quantification of contamination

The amount of exogenous C introduced during sample preparation and analysis can be quantified using the model of constant contamination as given by Hanke et al. (2017). It is based on the assumption that the total measured $F^{14}C$ (F_M) and its mass (m_M) are composed of the values of the standard itself (F_{Std}, m_{Std}) and of contributions from a constant exogenous contamination (F_C, m_C). As m_C cannot be determined directly, it is commonly assumed that the contamination is composed of two end-members, namely a ^{14}C-free ($F^{14}C = 0$) and a modern ($F^{14}C = 1$) proportion (e.g. Santos et al. 2007, Lang et al. 2013, Gierga et al. 2014). The

resulting $F^{14}C_c$ is therefore, depending on the contribution of each endmember between 0 and 1. In order to determine the respective proportions, size series of ^{14}C-free (POC #3) and modern (Ox-II) standards were prepared and measured. We only apply this model to POC#3 and Ox-II series analyzed with the GIS-AMS, but not to EA-GIS-AMS data consisting of only ^{14}C-free standard material. The amount of exogenous C (m_C) was determined by fitting the two independent parameters (F_M and m_M) using the Matlab script published by Haghipour et al. (2019).

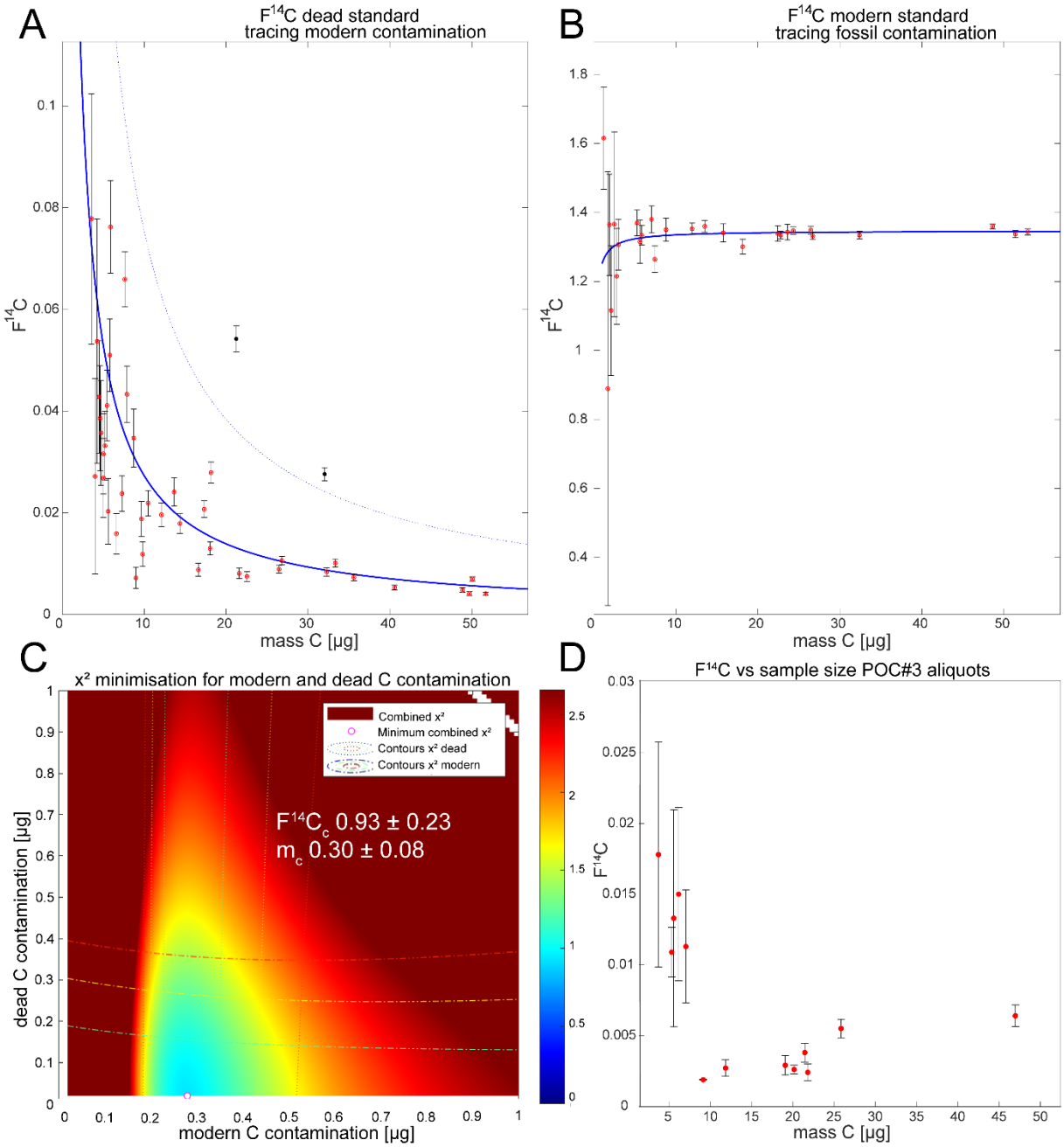

Figure 1: $F^{14}C$ vs mass C [µg] measured by GIS-AMS: A) for ^{14}C-free (POC#3) and B) modern (Ox-II) standard material (red circles). Fitting results are displayed as blue lines with 1-σ uncertainty (dashed blue lines). The fit assumes an error margin of 25%, outliers are displayed in black. C) shows the modelled solution space of χ^2 (indicated by colours) that depends on both contamination pools. The small circle indicates one possible solution

for the fitting procedure as displayed by $F^{14}C_c$ and m_c. D) displays the series of aliquot produced from one large sample, which has not been assessed using the χ^2 procedure, because only ^{14}C-free standards have been prepared as aliquots.

Results and Discussion

GIS-AMS measurements

In order to identify and quantify contamination introduced during sample preparation for CO_2 analysis with GIS-AMS, we prepared and measured four size series of ^{14}C-free (POC #3, Fig. 1A, D) and two series of modern standard material (Ox-II, Fig. 1B). Three of these size series of POC #3 (total n = 44) and two of the Ox-II series (total n = 27) were prepared by weighing defined amounts of standard material into individual quartz ampoules (Fig. 1A and B). For the fourth ^{14}C-free series (n = 14), standard material equivalent to ~1 mg C was combusted in one tube and split into aliquots (Fig. 1D) with sizes between 50 µg C and 2.5 µg C.

The ^{14}C results of the modern standard (Ox-II) do not show a distinct size dependency but rather scatter within 1-σ uncertainty around the consensus value (Fig. 1B). Contamination assessment using the Matlab script from Haghipour et al. (2019) for the Ox-II standards revealed a best fit when assuming minuscule amounts (0.02 µg C) of fossil exogenous C. Based on the used mixing model, we assume that mostly modern contamination is introduced during sample preparation (Fig. 1C).

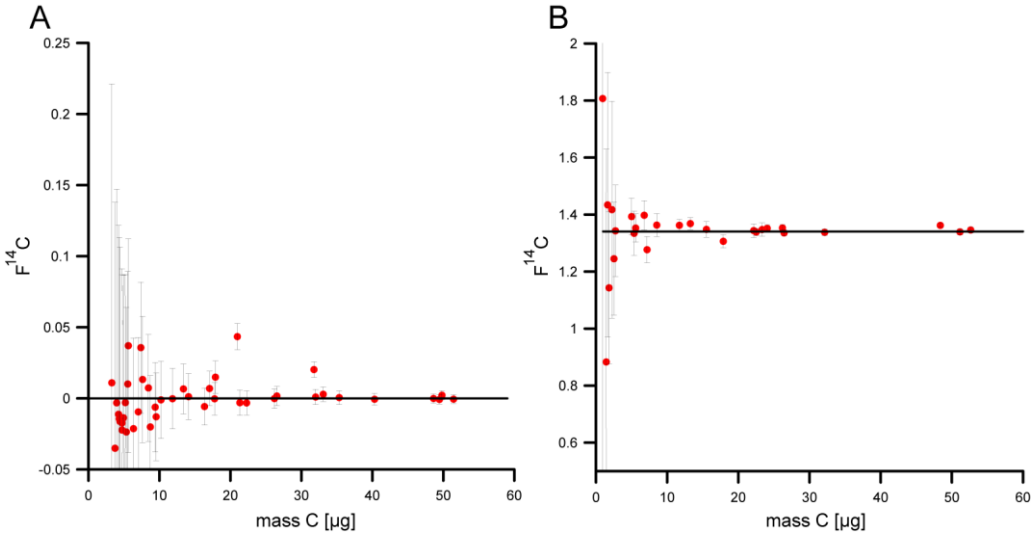

Figure 2: Combined data set of A) ^{14}C-free (POC#3) and B) modern (Ox-II) standard size series prepared in quartz ampoules for GIS-AMS analysis. Both sets have been corrected by the calculated contamination given in Fig.1C and scatter around consensus values (solid black lines).

The ^{14}C results of the three blank series weighed directly into quartz ampoules are in a similar range with an average of 0.0050 ± 0.0004 $F^{14}C$ (n = 4) for 50 µg C and increase in ^{14}C concentration at 20 µg C (0.0163 ± 0.0015 $F^{14}C$, n = 3, Fig. 1a), as smaller samples are increasingly affected by the constant contamination than larger ones. In contrast, the series of

aliquots prepared from one large sample gives much better blank values for smaller sample sizes of 2.5 - 20 µg C between 0.0029 ± 0.0007 $F^{14}C$ (20 µg C) and 0.0178 ± 0.0079 $F^{14}C$ (3.5 µg C; Fig. 1D), which indicates, that the contamination is mainly introduced during the pre-treatment including the weighing and transfer of samples/standards into the quartz ampoules and the subsequent combustion as also observed by Santos et al. (2010) and Santos and Xu (2017). The constant contamination for the total data set (n = 44 POC #3 and n = 27 Ox-II standards) consists of 0.30 ± 0.08 µg C (Fig. 1C). Based on our model, the corresponding isotopic ratio is $F^{14}C_c$ = 0.93 ± 0.23 of which 0.28 µg C is modern and 0.02 µg C fossil contamination.

Figure 2 shows the result of the total GIS-AMS data set (A: POC#3 blanks, n = 44; B: Ox-II, n = 27) that was corrected for the calculated contamination given in Fig. 1C. The data scatter close to the respective consensus values after application of the correction for contamination.

The constant contamination derived from the GIS system only, which was determined by directly injecting CO_2 from gas bottles into the AMS ion source, is 0.012 µg modern C (1 – 23 µg C, Stolz et al. 2019). Thus, sample preparation and combustion introduces most, about 0.30 ± 0.08 µg C, exogenous C.

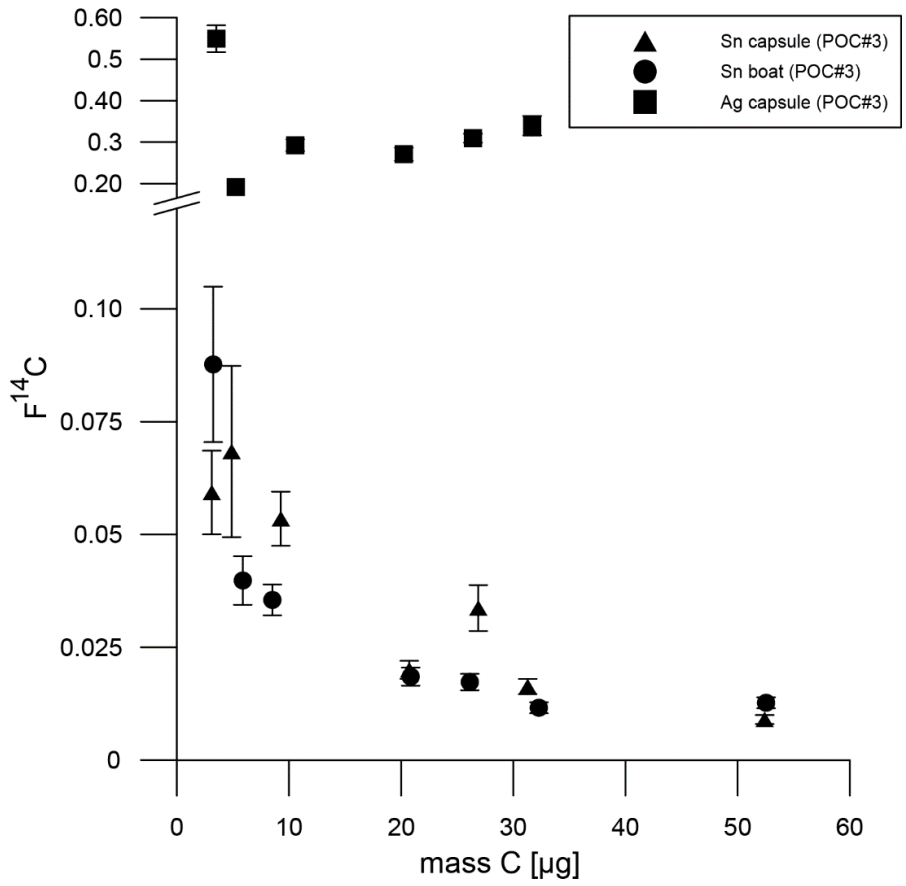

Figure 3: Overview of EA-GIS-AMS results for size series of blank material (POC#3) combusted in Sn boats (circle), Sn capsules (triangle), and in Ag capsules (square).

EA-GIS-AMS measurements

For ^{14}C analysis using EA-GIS-AMS, samples were weighed into containers for combustion in the EA. We investigated the contamination derived from different EA containers in three series using ^{14}C-free material (POC #3) combusted in Sn boats (n = 7), Sn capsules (n = 7), and Ag capsules (n = 6) (Fig. 3).

So far, only ^{14}C-free standards have been tested using the EA-GIS-AMS method due to a pending replacement of the EA and new installation of an isotope ratio mass spectrometer (IRMS). In order to quantify the amount of exogenous C using the contamination mixing model for this approach, we use a similar $F^{14}C_c$ of 0.93 like for GIS-AMS. This assumption is made to make results qualitatively comparable to other EA-GIS-AMS studies. We use this as a conservative estimation, because GIS-AMS sample handling involves more handling steps compared to EA-GIS-AMS, including the weighing of samples in Sn boats, the transfer of sample material from Sn boat into quartz ampoules as well as the handling and re-sealing on the vacuum line into a glass ampoule. More detailed investigations are planned once the new systems are operating.

In addition, we tested different EA sample containers including Sn boats and capsules cleaned with DCM, which removes contamination more efficient than Acetone or MQ-water (Welte et al. 2018, Ruff et al. 2010a), and Ag capsules cleaned by heating at 450°C. To directly compare the results for the Sn boats and Sn capsules, we calculated the amount of exogenous C for each series using the parameters obtained from the combined ampoule data set ($F^{14}C_c$ = 0.93 ± 0.23) (Tab.1). Blank values for Sn boats are 0.0127 ± 0.0012 $F^{14}C$ for 50 µg C and up to 0.0877 ± 0.0172 $F^{14}C$ for 3.5 µg C (m_c = 0.36 ± 0.09 µg C). Sn capsules have slightly better blank values of 0.0090 ± 0.0010 $F^{14}C$ (50 µg C) and 0.0593 ± 0.0093 $F^{14}C$ (3.5 µg C; m_c = 0.37 ± 0.09 µg C). Sn boats and capsules thus introduce similar amounts of contaminations. Our results determined with blank material combusted in Sn containers are in a similar range to results of other studies, which, however combusted empty Sn containers including Welte et al. (2018; m_c = 0.58 ± 0.04 µg C for DCM-washed Sn boats and m_c = 0.30 ± 0.03 µg C for DCM-washed Sn capsules) and Haghipour et al. (2019; m_c = 0.28 ± 0.08 µg C, $F^{14}C$ 0.6 ± 0.2).

We have so far not tested heat treatment (550°C) of DCM-washed Sn vessels, which can further reduce contamination levels (Welte et al. 2018). The size series combusted in Ag capsules gave ^{14}C concentrations, which are about one order of magnitude higher, between 0.1921 ± 0.0293 – 0.5492 ± 0.0322 $F^{14}C$, than for the Sn containers and the data show no size dependency but scatter strongly (Fig. 3). This result indicates a much higher and more variable contamination originating from the Ag capsules, which was likely introduced to the activated

surface of the capsule after heating, as suggested by Welte et al. (2018) and Haghipour et al. (2019).

Based on the results of our tests, we now chose for our laboratory routine Sn boats cleaned three-times with DCM. However, we plan to perform further tests with Ag capsules combusted at higher temperatures (800°C) as suggested by Fewlass et al. (2018) and Al containers that can be combusted at temperatures of up to 550°C, which may be an alternative to the usage of solvent-cleaned Sn suggested also by Welte et al. (2018).

Table 1: Summary of blank assessment for 50 µg and 3.5 µg C large samples measured with GIS-AMS and EA-GIS-AMS analysis. The quantification is based on ^{14}C-free standard material (POC#3) combusted in quartz ampoules (GIS) or in EA Sn containers using the Matlab script by Haghipour et al. (2019). We assume a similar F^{14}C for GIS-AMS as determined for EA-GIS-AMS.

	GIS-AMS		**EA-GIS-AMS**	
	Combined Series	**Aliquots**	**Sn boats**	**Sn capsules**
F^{14}C (50 µg C)	0.0050 ± 0.0004*[1]	0.0064 ± 0.0008	0.0127 ± 0.0012	0.0090 ± 0.0010
F^{14}C (3.5 µg C)	0.0163 ± 0.0015*[2]	0.0178 ± 0.0079	0.0877 ± 0.0172	0.0593 ± 0.0093
m_c [µg] + (F$^{14}C_c$)	0.30 ± 0.08 (0.93 ± 0.23)		0.36 ± 0.09 (0.93 ± 0.23)*[3]	0.37 ± 0.09 (0.93 ± 0.23)*[3]

*[1](n = 4); *[2](n = 3), *[3]based on GIS-AMS data evaluation

Conclusion

In this study, we investigated the contamination introduced during sample preparation for gas ion source ^{14}C analysis using our HVE 6 MV Tandetron accelerator coupled with the Ionplus AG GIS and an EuroVector EA3000. We prepared various size series of standards ranging from 2.5 – 50 µg C in glass ampoules for ^{14}C analysis using GIS-AMS and in different EA combustion containers for EA-GIS-AMS in order to quantify exogenous C contributions introduced applying the model of constant contamination. The constant contamination introduced during sample preparation for GIS-AMS analysis is 0.30 ± 0.08 µg C (F$^{14}C_c$ = 0.93 ± 0.23; 0.28 µg modern C, 0.02 µg fossil C). Blank values increase from 0.0050 ± 0.0004 F^{14}C for 50 µg C to 0.0163 ± 0.0015 F^{14}C for 20 µg C.

For EA-GIS-AMS analysis, the samples need to be weighed into EA combustion vessels, which introduce different amounts of contamination depending on the material and type of the vessel

itself and on the cleaning procedure. Lower blank values were obtained for ^{14}C-free material combusted in DCM-cleaned Sn boats (0.0127 ± 0.0012 $F^{14}C$ for 50 µg C and up to 0.0877 ± 0.0172 $F^{14}C$ for 3.5 µg C; m_c = 0.36 ± 0.09 µg C) compared to DCM-cleaned Sn capsules (0.0090 ± 0.0010 $F^{14}C$ for 50 µg C and 0.0593 ± 0.0093 $F^{14}C$ for 3.5 µg C; m_c = 0.37 ± 0.09 µg C). DCM-cleaned and heated Ag capsules produced the highest blank values indicating that either combustion at 450°C is not removing contamination sufficiently or that the containers surface is activated by heating and adsorbs contamination. $F^{14}C$ results of EA-GIS-AMS data are in similar ranges compared to our GIS-AMS results, except for the Ag capsule series, which have a higher and variable ^{14}C content (0.1921 ± 0.0293 – 0.5492 ± 0.0322 $F^{14}C$).

With our study we demonstrate, that small-scale ^{14}C analysis of gaseous samples using the HVE SO-110 B ion source and a modified GIS from Ionplus AG is now operational at CologneAMS. The amounts of exogenous C introduced during sample processing can be accounted for using adequate correction methods. As the sample preparation for EA-GIS-AMS is more time efficient and less expensive, we are planning further tests with a new set-up including an IRMS system. However, GIS-AMS analysis still remains the technique of choice for the ^{14}C analysis of small gas samples, e.g. from incubation studies.

Acknowledgements

This work was financially supported by German Science Foundation (DFG) within SFB 806 and FOR 1806 as well as by funds from the German Ministry of Science and Education (BMBF) within the project ‘KoPf’. We would like to thank Ulrike Patt for guidance and troubleshooting during sample pre-treatment as well as our student assistants (Thorsten Domann, Reaz Hossain, Elisabeth Krewer, and Vera Schmitt) that helped during sample processing.

References

Fewlass H, Talamo S, Tuna T, Fagault Y, Kromer B, Hoffmann H, Pangrazzi C, Hublin J-J, Bard E. 2018. Size Matters: Radiocarbon Dates of <200 µg Ancient Collagen Samples with AixMICADAS and Its Gas Ion Source. *Radiocarbon* 60: 425–439.

Gierga M, Schneider MPW, Wiedemeier DB, Lang SQ, Smittenberg RH, Hajdas I, Bernasconi SM, Schmidt MWI. 2014. Purification of fire derived markers for µg scale isotope analysis ($\delta^{13}C$, $\Delta^{14}C$) using high performance liquid chromatography (HPLC). *Org Geochem.* 70: 1–9.

Haghipour N, Ausin B, Usman MO, Ishikawa N, Wacker L, Welte C, Ueda K, Eglinton TI. 2019. Compound-Specific Radiocarbon Analysis by Elemental Analyzer-Accelerator Mass Spectrometry: Precision and Limitations*. Anal. Chem.* 91: 2042-2049.

Hanke UM, Wacker L, Haghipour N, Schmidt MWI, Eglinton TI, McIntyre CP. 2017. Comprehensive Radiocarbon Analysis of Benzene Polycarboxylic Acids (BPCAs) Derived From Pyrogenic Carbon in Environmental Samples. *Radiocarbon* 59: 1103-1116.

Lang SQ, Früh-Green GL, Bernasconi SM, Wacker L. 2013. Isotopic ($\delta^{13}C$, $\Delta^{14}C$) analysis of organic acids in marine samples using wet chemical oxidation. *Limnol Oceanogr Methods.* 11: 161–175.

Rethemeyer J, Fülöp R-H, Höfle S, Wacker L, Heinze S, Hajdas I, Patt U, König S, Stapper B, Dewald A. 2013. Status report on sample preparation facilities for ^{14}C analysis at the new CologneAMS center. *Nucl. Instrum. Methods Phys. Res. Sect. B Beam Interact. Mater. At.* 294: 168–172.

Ruff M, Fahrni S, Gäggeler HW, Hajdas I, Suter M, Synal H-A, Szidat S, Wacker L. 2010a. On-line Radiocarbon Measurements of Small Samples Using Elemental Analyzer and MICADAS Gas Ion Source. *Radiocarbon* 52: 1645–1656.

Ruff M, Szidat S, Gäggeler HW, Suter M, Synal H-A, Wacker L. 2010b. Gaseous radiocarbon measurements of small samples. *Nucl. Instrum. Methods Phys. Res. Sect. B Beam Interact. Mater. At.* 268: 790–794.

Santos GM, Southon JR, Griffin S, Beaupre SR, Druffel ERM. 2007. Ultra small-mass AMS ^{14}C sample preparation and analyses at KCCAMS/UCI Facility*. Nucl Instruments Methods Phys. Res. Sect. B Beam Interact. Mater. At.* 259(1): 293–302.

Santos GM, Southon JR, Drenzek NJ, Ziolkowski LA, Druffel E, Xu X, Zhang D, Trumbore S, Eglinton TI, Hughen KA. 2010. Blank Assessment for Ultra-Small Radiocarbon Samples: Chemical Extraction and Separation Versus AMS. *Radiocarbon* 52: 1322–1335.

Santos GM, Xu X. 2017. Bag of tricks: A set of techniques and other resources to help ^{14}C laboratory setup, sample processing, and beyond. *Radiocarbon* 59: 785–801.

Stolz A, Dewald A, Altenkirch R, Herb S, Heinze S, Schiffer M, Feuerstein C, Müller-Gatermann C, Wotte A, Rethemeyer J, Dunai T. 2017. Radiocarbon measurements of small gaseous samples at CologneAMS. *Nucl. Instrum. Methods Phys. Res. Sect. B Beam Interact. Mater. At.* 406: 283–286.

Stolz A, Dewald A, Heinze S, Altenkirch R, Hackenberg G, Herb S, Müller-Gatermann C, Schiffer M, Zitzer G, Wotte A, Rethemeyer J, Dunai T. 2019. Improvements in the measurement of small $^{14}CO_2$ samples at CologneAMS. *Nucl. Instrum. Methods Phys. Res. Sect. B Beam Interact. Mater. At*.

Welte C, Hendriks L, Wacker L, Haghipour N, Eglinton TI, Günther D, Synal H-A. 2018. Towards the limits: Analysis of microscale ^{14}C samples using EA-AMS. *Nucl. Instrum. Methods Phys. Res. Sect. B Beam Interact. Mater. At*. 437: 66-74.

Wotte A, Wordell-Dietrich P, Wacker L, Don A, Rethemeyer J. 2017. $^{14}CO_2$ processing using an improved and robust molecular sieve cartridge. *Nucl. Instrum. Methods Phys. Res. Sect. B Beam Interact. Mater.* 400: 65-73.

Supplementary Table S2: AMS results of all presented samples with their respective errors and masses.

GIS-AMS size series

POC#3	AMS ID	Standard type	$F^{14}C_m$	±	m_m [µg C]
	COL1000.0.0.31	POC#3	0.0196	0.0023	12.10
	COL1000.0.0.33	POC#3	0.0073	0.0006	35.59
	COL1000.0.0.36	POC#3	0.0778	0.0246	3.55
	COL1000.0.0.37	POC#3	0.0053	0.0005	40.57
	COL1000.0.0.38	POC#3	0.0075	0.0010	22.54
	COL1000.0.0.39	POC#3	0.0510	0.0071	5.80
	COL1000.0.0.40	POC#3	0.0188	0.0034	9.66
	COL1000.0.0.41	POC#3	0.0179	0.0020	14.36
	COL1000.0.0.44	POC#3	0.0207	0.0016	17.32
	COL1000.0.0.45	POC#3	0.0070	0.0004	50.07
	COL1000.0.0.46	POC#3	0.0219	0.0025	10.48
	COL1000.0.0.48	POC#3	0.0659	0.0054	7.64
	COL1000.0.0.49	POC#3	0.0101	0.0008	33.34
	COL1000.0.0.51	POC#3	0.0241	0.0027	13.64
	COL1000.0.0.52	POC#3	0.0433	0.0055	7.89
	COL1000.0.0.53	POC#3	0.0048	0.0004	48.88
	COL1000.0.0.56	POC#3	0.0411	0.0070	5.46
	COL1000.0.0.57	POC#3	0.0762	0.0091	5.88
	COL1000.0.0.58	POC#3	0.0081	0.0010	21.59
	COL1000.0.0.59	POC#3	0.0084	0.0008	32.27
	COL1000.0.0.60	POC#3	0.0041	0.0004	49.71
	COL1000.0.0.61	POC#3	0.0238	0.0035	7.28
	COL1000.0.0.64	POC#3	0.0542	0.0026	21.24
	COL1000.0.0.65	POC#3	0.0072	0.0021	8.98
	COL1000.0.0.67	POC#3	0.0279	0.0021	18.15
	COL1000.0.0.70	POC#3	0.0106	0.0009	26.81
	COL1000.0.0.71	POC#3	0.0088	0.0013	16.61
	COL1000.0.0.72	POC#3	0.0130	0.0013	18.03
	COL1000.0.0.73	POC#3	0.0332	0.0068	5.20
	COL1000.0.0.74	POC#3	0.0537	0.0240	4.24
	COL1000.0.0.75	POC#3	0.0347	0.0057	8.71
	COL1000.0.0.76	POC#3	0.0276	0.0013	32.03
	COL1000.0.0.77	POC#3	0.0089	0.0008	26.46
	COL 1000.0.0.99	POC#3	0.0119	0.0024	9.80
	COL 1000.0.0.100	POC#3	0.0269	0.0078	5.00
	COL 1000.0.0.101	POC#3	0.0428	0.0111	4.50
	COL 1000.0.0.102	POC#3	0.0316	0.0079	5.00
	COL 1000.0.0.103	POC#3	0.0159	0.0040	6.60
	COL 1000.0.0.104	POC#3	0.0357	0.0103	4.70
	COL 1000.0.0.105	POC#3	0.0272	0.0192	4.00
	COL 1000.0.0.106	POC#3	0.0386	0.0103	4.60
	COL 1000.0.0.107	POC#3	0.0203	0.0064	5.60
	COL 1000.0.0.108	POC#3	0.0041	0.0003	51.70

Ox-II	AMS ID	Standard type	$F^{14}C_m$	±	m_m [µg C]
	COL1002.0.0.19	Ox-II	1.3008	0.0216	18.15
	COL1002.0.0.20	Ox-II	1.3389	0.0228	22.42
	COL1002.0.0.21	Ox-II	1.3799	0.0396	7.04
	COL1002.0.0.22	Ox-II	1.2149	0.1386	2.79
	COL1002.0.0.23	Ox-II	1.2643	0.0383	7.44
	COL1002.0.0.24	Ox-II	1.3428	0.0226	23.61
	COL1002.0.0.25	Ox-II	1.3152	0.0627	5.62
	COL1002.0.0.26	Ox-II	1.3409	0.0260	15.78
	COL1002.0.0.27	Ox-II	1.3500	0.0336	8.80
	COL1002.0.0.31	Ox-II	1.3596	0.0068	48.64
	COL1002.0.0.34	Ox-II	1.3697	0.0370	5.27
	COL1002.0.0.35	Ox-II	1.3341	0.0113	22.78
	COL1002.0.0.36	Ox-II	1.3597	0.0174	13.52
	COL1002.0.0.37	Ox-II	1.3317	0.0092	26.69
	COL1002.0.0.38	Ox-II	1.3472	0.0108	24.32
	COL1002.0.0.39	Ox-II	1.3526	0.0166	11.98
	COL1002.0.0.40	Ox-II	1.3344	0.0105	32.39
	COL1002.0.0.41	Ox-II	1.3487	0.0112	26.46
	COL1002.0.0.43	Ox-II	1.3337	0.0287	5.84
	COL1002.0.0.44	Ox-II	1.3437	0.0094	52.91
	COL 1002.0.0.60	Ox-II	1.3065	0.0735	3.00
	COL 1002.0.0.61	Ox-II	1.3640	0.1465	1.90
	COL 1002.0.0.63	Ox-II	1.1158	0.1887	2.10
	COL 1002.0.0.64	Ox-II	1.6154	0.1478	1.20
	COL 1002.0.0.66	Ox-II	0.8890	0.6287	1.70
	COL 1002.0.0.67	Ox-II	1.3659	0.2680	2.50

Aliquots from 1 mg

POC#3	AMS ID	Standard type	$F^{14}C_m$	±	m_m [µg C]
	COL1000.0.0.79a	POC#3	0.0055	0.0006	25.86
	COL1000.0.0.79b	POC#3	0.0038	0.0007	21.47
	COL1000.0.0.79c	POC#3	0.0029	0.0007	19.10
	COL1000.0.0.79d	POC#3	0.0113	0.0040	7.06
	COL1000.0.0.79e	POC#3	0.0019	0.0000	9.16
	COL1000.0.0.79f	POC#3	0.0150	0.0061	6.18
	COL1000.0.0.79g	POC#3	0.0133	0.0077	5.59
	COL1000.0.0.78a	POC#3	0.0064	0.0008	46.98
	COL1000.0.0.78b	POC#3	0.0026	0.0003	20.17
	COL1000.0.0.78c	POC#3	0.0024	0.0006	21.83
	COL1000.0.0.78d	POC#3	0.0027	0.0006	11.86
	COL1000.0.0.78e	POC#3	0.0109	0.0018	5.34
	COL1000.0.0.78f	POC#3	0.0178	0.0079	3.74
	COL1000.0.0.78g	POC#3	0.0855	0.0349	2.82

EA-GIS-AMS

Sn boats (POC#3)	AMS ID	Standard type	$F^{14}C_m$	±	m_m [µg C]
	COL1000.0.0.0.1	POC#3	0.0877	0.0172	3.52
	COL1000.0.0.0.2	POC#3	0.0398	0.0054	6.16
	COL1000.0.0.0.3	POC#3	0.0355	0.0034	8.80
	COL1000.0.0.0.4	POC#3	0.0153	0.0020	21.12
	COL1000.0.0.0.5	POC#3	0.0173	0.0018	26.40
	COL1000.0.0.0.6	POC#3	0.0116	0.0012	32.56
	COL1000.0.0.0.7	POC#3	0.0127	0.0012	52.80

Sn capsules (POC#3)	AMS ID	Standard type	$F^{14}C_m$	±	m_m [µg C]
	COL1000.0.0.0.8	POC#3	0.0593	0.0093	3.52
	COL1000.0.0.0.9	POC#3	0.0684	0.0190	5.28
	COL1000.0.0.0.10	POC#3	0.0535	0.0060	9.68
	COL1000.0.0.0.11	POC#3	0.0200	0.0020	21.12
	COL1000.0.0.0.12	POC#3	0.0337	0.0051	27.28
	COL1000.0.0.0.13	POC#3	0.0163	0.0017	31.68
	COL1000.0.0.0.14	POC#3	0.0090	0.0010	52.80

Ag capsules (POC#3)	AMS ID	Standard type	$F^{14}C_m$	±	m_m [µg C]
	COL1000.0.0.0.15	POC#3	0.5492	0.0322	3.52
	COL1000.0.0.0.16	POC#3	0.1921	0.0293	5.28
	COL1000.0.0.0.17	POC#3	0.2924	0.0142	10.56
	COL1000.0.0.0.18	POC#3	0.2707	0.0156	20.24
	COL1000.0.0.0.19	POC#3	0.3093	0.0107	26.40
	COL1000.0.0.0.20	POC#3	0.3394	0.0234	31.68

Manuscript II: Sources of CO_2 produced in freshly thawed Pleistocene-age Yedoma permafrost

by

Jan Olaf Melchert[1], Philipp Wischhöfer[1], Christian Knoblauch[2,3], Tim Eckhardt[2,3], Susanne Liebner[4,5], Janet Rethemeyer[1]*

[1]Institute for Geology and Mineralogy, University of Cologne, Cologne, Germany

[2]Institute for Soil Science, University of Hamburg, Hamburg, Germany

[3]Center for Earth System Research and Sustainability, University of Hamburg, Hamburg, Germany

[4]German Research Centre for Geosciences (GFZ), Helmholtz Centre Potsdam, Potsdam, Germany

[5]Institute of Biochemistry and Biology, University of Potsdam, Potsdam, Germany

published in

Frontiers in Earth Science

January 2022

Information regarding the acquisition of primary data:

The primary data relevant for this manuscript are stored and accessible on the server of the Institute of Geology and Mineralogy at the University of Cologne. Raw data needed to reproduce the presented calculations are partially included as supplementary material to this manuscript and are available in the Zenodo online repository (https://doi.org/10.5281/zenodo.5644763)

Sample material that was used for the analyses presented in this manuscript is stored at the Institute of Geology and Mineralogy at the University of Cologne.

Jan Olaf Melchert[1], Philipp Wischhöfer[1], Christian Knoblauch[2,3], Tim Eckhardt[2,3], Susanne Liebner[4,5], Janet Rethemeyer[1]*

[1]Institute for Geology and Mineralogy, University of Cologne, Cologne, Germany

[2]Institute for Soil Science, University of Hamburg, Hamburg, Germany

[3]Center for Earth System Research and Sustainability, University of Hamburg, Hamburg, Germany

[4]German Research Centre for Geosciences (GFZ), Helmholtz Centre Potsdam, Potsdam, Germany

[5]Institute of Biochemistry and Biology, University of Potsdam, Potsdam, Germany

* Correspondence:
Corresponding Author
janet.rethemeyer@uni-koeln.de

Keywords: yedoma ice complex[1], permafrost[2], carbon cycle[3], climate change[4], thermokarst[5], radiocarbon[6], greenhouse gas[7]

Abstract

The release of greenhouse gases from the large organic carbon stock in permafrost deposits in the circumarctic regions may accelerate global warming upon thaw. The extent of this positive climate feedback is thought to be largely controlled by the microbial degradability of the organic matter preserved in these sediments. In addition, weathering and oxidation processes may release inorganic carbon preserved in permafrost sediments as CO_2, which is generally not accounted for. We used ^{13}C and ^{14}C analysis and isotopic mass balances to differentiate and quantify organic and inorganic carbon released as CO_2 in the field from an active retrogressive thaw slump of Pleistocene-age Yedoma and during a 1.5-year incubation experiment. The results reveal that the dominant source of the CO_2 released from freshly thawed Yedoma exposed as thaw mound is Pleistocene-age organic matter (48 - 80%) and to a lesser extent modern organic substrate (3 - 34%). A significant portion of the CO_2 originated from inorganic carbon in the Yedoma (17 - 26%). The mixing of young, active layer material with Yedoma at a site on the slump floor led to the preferential mineralization of this young organic carbon source. Admixtures of younger organic substrates in the Yedoma thaw mound were small and thus rapidly consumed as shown by lower contributions to the CO_2 produced during few weeks of aerobic incubation at 4°C corresponding to approximately one thaw season. Future CO_2 fluxes from the freshly thawed Yedoma will contain higher proportions of ancient inorganic (22%) and organic carbon (61 - 78%) as suggested by the results at the end, after 1.5 years of incubation. The increasing contribution of inorganic carbon during the incubation is favored by the accumulation of organic acids from microbial organic matter

degradation resulting in lower pH values and, in consequence, in inorganic carbon dissolution. Because part of the inorganic carbon pool is assumed to be of pedogenic origin, these emissions would ultimately not alter carbon budgets. The results of this study highlight the preferential degradation of younger organic substrates in freshly thawed Yedoma, if available, and a substantial release of CO_2 from inorganic sources.

Introduction

Permafrost deposits in the northern circumpolar regions contain about 1,300 to 1,600 Gt of organic carbon (OC) that accumulated over thousands of years and was stored at sub-zero temperatures (Schuur et al., 2015). More than one quarter, about 327 to 466 Gt OC, is stored in the loess-like Yedoma sediments that were deposited during the late Pleistocene and early Holocene in unglaciated areas of the Arctic region (Schirrmeister, 2011; Strauss et al., 2017). These up to 50 m thick sediments include massive syngenetic ice wedges (Schirrmeister, 2011) resulting in very high ground ice contents of up to 80 vol.% (Strauss et al., 2017), thus making Yedoma deposits especially vulnerable to rapid thaw in a warming world. The melting of the ground ice due to rising ground temperatures (Biskaborn et al., 2019) causes surface subsidence and thereby may expose the sedimentary OC abruptly to microbial degradation (Czudek and Demek, 1970; Grosse et al., 2011; Strauss et al., 2017; Nitzbon et al., 2020; Turetsky et al., 2020). In consequence, the previously freeze-locked organic matter (OM) is decomposed and released to the atmosphere as carbon dioxide (CO_2), methane (CH_4), and other greenhouse gasses (GHGs) causing a positive climate feedback (Schuur et al., 2015).

The extent of the permafrost-carbon feedback is still under debate because it not only depends on OC quantity but also on OM quality, i.e., microbial degradability, which is still uncertain due to the limited analytical data. Most studies assessing OM quality and degradability, respectively rely on incubation experiments at different temperatures (Schädel et al., 2014, 2016). The results of these laboratory studies may not necessarily apply to natural, more complex conditions. Additionally, chemical characterizations of the OM have been used to differentiate potentially labile and more recalcitrant OC pools based on OC/N ratios (e.g., Schädel et al., 2014; Kuhry et al., 2020) and characteristic organic compounds used as indicators for OM bioavailability and stage of degradation, respectively (e.g., Routh et al., 2014; Strauss et al., 2015; Stapel et al., 2016; Tanski et al., 2017; Jongejans et al., 2021).

Yedoma deposits were assumed to contain OM that accumulated and was freeze-locked quickly and thus has not undergone intense decomposition processes. Less transformed OM is supposed to be more reactive and thus more easily degradable upon thaw, which was reflected by high CO_2 fluxes measured in some incubation studies (Dutta et al., 2006; Zimov et al., 2006; Knoblauch et al., 2013) and the presence of easily biodegradable substrates

(Stapel et al., 2016; Jongejans et al., 2018). In contrast, other studies measured a higher degree of OM decomposition (Kuhry et al., 2020), which, however, did not result in lower respiration rates during some incubation studies (Weiss et al., 2016). The contrasting results may be attributed to the large spatial and temporal variability of OC contents and OM composition in Yedoma deposited under different environmental and climatic conditions (Strauss et al., 2015; Weiss et al., 2016; Stapel et al., 2018; Walz et al., 2018; Windirsch et al., 2020). In addition, thermokarst may alter the degradability of the ancient Yedoma OM by introducing younger material from overlying sediments and changing thermal and hydrological conditions (Grosse et al., 2011; Strauss et al., 2015; Wild et al., 2016). The mixing of sediments is particularly pronounced on retrogressive thaw slumps, a dynamic form of thermokarst in ice-rich areas, expanding inland by melting of the ground ice in the headwall (Lantuit and Pollard, 2008; Costard et al., 2021).

The release of GHGs deriving from the mineralization of modern and ancient OM can be differentiated by ^{14}C analyses, which has been applied in several field and incubation studies in high latitude regions (e.g., Schuur and Trumbore, 2006; Czimczik and Welker, 2010; Estop-Aragonés et al., 2018). In addition, organic and inorganic carbon sources can be identified and quantified by their $\delta^{13}C$ signature and by applying a dual isotopic mass balance calculation (Dorsett et al., 2011; Griffith et al., 2012; Pries et al., 2016). The contribution of inorganic carbon (IC) to CO_2 fluxes that may be released by abiotic processes (e.g., Biasi et al., 2008; Tamir et al., 2011; Ramnarine et al., 2012) has been neglected in most previous studies, which may thus have overestimated GHG fluxes from the mineralization of OC. Yedoma deposits contain substantial amounts of carbonates of about 0.2 to 18% in the north-east Siberian coastal lowlands (Schirrmeister, 2011) that may be released by dissolution processes (Zolkos et al., 2018, 2020).

The aim of this study is to quantify and differentiate between ancient and modern OC as well as IC contributions to the CO_2 emissions released from a retrogressive thaw slump in a Yedoma deposit in north-east Siberia by using a dual carbon isotopic approach. We selected two study sites on the thaw slump where freshly thawed Yedoma is a) exposed as thaw mounds and b) mixed with substrates from the overlaying Holocene terrace. To differentiate between Pleistocene and Holocene substrates, a third site on the Holocene terrace was sampled additionally. Beside field measurements, we incubated the sediments for 1.5 years and analyzed the isotopic compositions of the CO_2 after a few weeks and at the end of the long-term incubation. In addition, we analyzed the composition of the OM in the thaw layer at all sites to elucidate their potential effects on CO_2 production rates.

Study Site

The retrogressive thaw slump is located on the island of Kurungnakh, which lies beside the Olenyeksky Channel, in the southern part of the Lena River Delta in north-eastern Siberia (Tab. 1). Kurungnakh Island is mainly composed of late Quaternary sediments, so-called Yedoma or Ice Complex (Schirrmeister, 2011), which are up to 40 m thick and contain large ice wedges resulting in ground-ice contents of up to 80 vol.% (Wetterich et al., 2008a; Schirrmeister, 2011). The Pleistocene-age Yedoma deposit is overlain by Holocene polygonal tundra (Grigoriev, 1993; Schwamborn et al., 2002). The surface layer of the Yedoma deposits thaws for about four months per year during summer (Boike et al., 2008) and may reach a depth of about 80 cm (Tab. 1). Recorded data for the years 1998 - 2011 document an annual mean air temperature of -12.5°C (measured on the nearby Samoylov Island), with maximum mean air temperatures of 10.1°C in July and 8.5°C in August (Boike et al., 2013). The mean annual precipitation (rainfall and snow water equivalent) is about 190 mm (Boike et al., 2013).

For this study, three different sites were selected on the retrogressive thaw slump about 15 - 35 m above river level including the overlying Holocene terrace (HT1), an intact thaw mound of Pleistocene Yedoma (TM2), and a site on the slump floor (SF3) where both types of sediments were mixed during erosion (Fig.1)

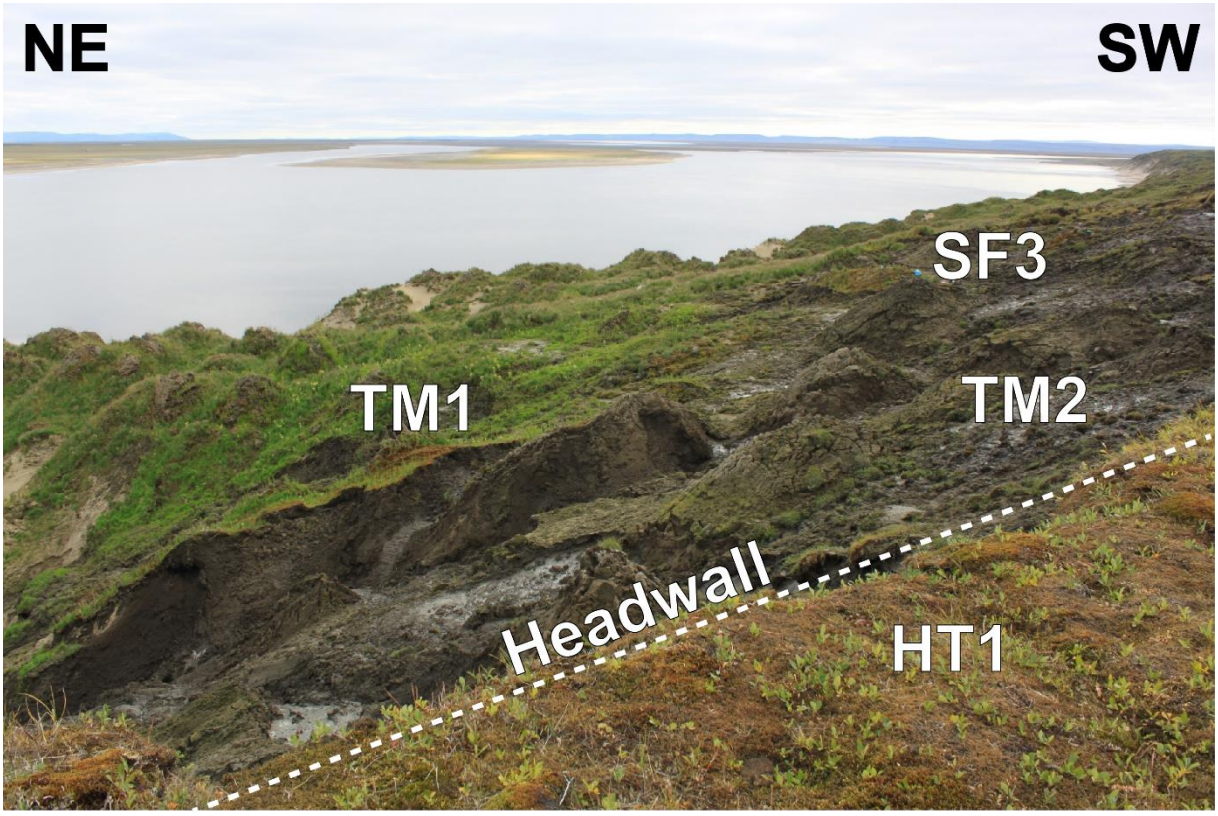

Figure 1: Study sites on the retrogressive thaw slump on Kurungnakh Island including two thaw mounds (TM) in Pleistocene Yedoma, a site on the slump floor (SF) where sediments were mixed, and the Holocene terrace (HT).

Table 3: Sampling locations on Kurugnakh Island and thaw depth (measured in August 2017).

Site		North [°dec]	East [°dec]	Thaw depth [cm]
SF3	**Thaw slump floor**	72.33900	126.29207	78
TM2	**Thaw mound**	72.33920	126.29199	70
HT1	**Holocene terrace**	72.33914	126.28945	21

Methods

Sediment sampling

Samples were collected from the active layer of the soil in the Holocene terrace and the Yedoma sediment in August 2017. At each site, one soil pit of about 1 x 1 m was dug down to the to the frozen ground and four replicates were sampled from the pit wall using a hand shovel. Samples were collected in 10 cm intervals for bulk elemental analysis. The incubation experiment was conducted with replicates of up to four depth intervals per site. Therefore, some of the sampled depth intervals were combined and homogenized. All samples were stored in sealed plastic bags and kept frozen at -20°C until analysis.

Gas sampling

Carbon dioxide was collected from three location in about 0.5 - 1 m distance at each study site according to Wotte et al. (2017) using PVC collars that were placed on the sediment. At SF3 and TM2, sprouts were carefully removed from the mostly barren soil surface to prevent the contribution of autotrophic (plant) respiration. At HT1, aboveground vegetation was clipped with a knife and the uppermost 8 cm of the sediment were carefully removed from the ground to minimize contributions from autotrophic respiration.

The plastic collars (polyvinylchloride, 25 cm OD, 25 cm height) were placed 10 cm in the ground and left for 12 hours prior to measurement. On the day of the measurement, an opaque chamber was placed on top of the collars and connected to an infrared gas analyzer (LI-840A, LI-COR Biosciences, Lincoln, USA). After closure of the chamber, the air was pumped in a closed loop for 5 min for CO_2 flux measurement. Moisture was removed using two traps filled with phosphorous pentoxide (Sicapent®, MERCK, Germany). Afterwards, atmospheric CO_2 was removed by pumping three chamber volumes through a soda lime trap (MERCK, Germany). Then, CO_2 emitted from the ground was trapped on a molecular sieve cartridge (MSC) filled with zeolite type 13X. The sampling time was about 30 minutes per site depending on CO_2 fluxes and volume of the emission chamber aiming to collect 2 mg of CO_2 on each MSC.

CO_2 fluxes were calculated from the recorded increase in CO_2 concentration inside the chamber during the first five minutes after closure. The first 30 seconds were discarded due to possible disturbances by closing the chamber. From the remaining data, the two-minute interval with the highest Pearson correlation coefficient (>0.9) was chosen for flux calculation.

Incubations

An aerobic long-term incubation experiment was conducted over a course of 1.5 years according to Knoblauch et al. (2013). Briefly, splits of the frozen sediment samples were thawed at 2°C and kept at 4°C for the duration of the incubation. The water content of each sample was determined prior to the start of the incubation. About 20 g of homogenized sediment was placed in 120 ml glass bottles, which were sealed by rubber stoppers and kept closed during the experiment to maintain constant moisture. The headspace of the bottles was flushed repeatedly with synthetic air prior to the start of the experiment to remove ambient CO_2 from each bottle. The CO_2 concentrations were recorded every week for the first 200 days and about every other month thereafter. If CO_2 concentrations exceeded 3%, the headspace was flushed repeatedly with synthetic air (20% O_2, 80% N_2). CO_2 samples were taken for isotope analysis at two times during the incubation: first, between 41 and 189 days after the samples had been flushed and again reached concentrations of about 3% CO_2. The second gas sampling was performed at the end of the experiment on day 537, regardless of the CO_2 concentration inside the bottles.

Sediment analysis

Bulk sediment analysis was performed on freeze-dried samples that were ground and thereby homogenized using a porcelain mortar. Total carbon (C), total OC and total nitrogen (N) contents were quantified using an elemental analyzer (vario MICRO, Elementar, Germany). For OC analysis, aliquots of the sediment were decalcified by treatment with 40 ml of 1% hydrochloric acid (HCl) for 1 hour at 60°C following 12 hours at room temperature as described in Rethemeyer et al. (2019). After the acid treatment, the samples were washed to neutral pH by adding Mili-Q water and dried at 60°C. pH values were measured after DIN ISO 10390:2005-12 in a suspension of 5 g dry mineral soil and 25 ml Milli-Q water after shaking (1 hour) and settling (1 hour) using a pH meter (FE20, Mettler-Toledo, Ohio, USA).

Radiocarbon analysis

^{14}C analysis of the bulk OC was performed by combustion and graphitization of the CO_2 as described in Rethemeyer et al. (2019). In short, an aliquot of the decalcified sediment was weighed into solvent-cleaned tin boats (4 x 4 x 11 mm, Elementar, Germany) for subsequent combustion in an elemental analyzer (VarioMicroCube, Elementar, Germany). The CO_2 produced was converted to elemental carbon ('graphite') in an automated graphitization

system (AGE; Wacker et al., 2010) using hydrogen and iron powder as catalyst. The ^{14}C content of the IC was measured by hydrolyzing the sediment, with phosphoric acid (99%) for 6 hours at 75°C. This was done without prior removal of OC from the sediment. Although experiences with this method were positive, we cannot exclude that small amounts of OC were dissolved along the IC and contributed to the ^{14}C analysis. The CO_2 evolved was then transferred into the AGE system with He and converted to graphite. The graphite was pressed into AMS target holders, which were analyzed with the 6 MV accelerator mass spectrometer (AMS) at CologneAMS (Dewald et al., 2013).

The CO_2 trapped on the MSCs was processed on a vacuum rig as described in Wotte et al. (2017). The MSC was heated to 500°C to release the CO_2 from the zeolite and flushed with He (grade 4.6) via a water trap immersed in dry ice-ethanol mixture (-80°C) to a CO_2 trap placed in liquid nitrogen. The amount of CO_2 was quantified in a calibrated volume with a pressure sensor and the glass tube containing the CO_2 was flame sealed.

The CO_2 from the aerobic incubation experiment was recovered from the glass bottles using sterile hypodermic needles. Similar to the MSC desorption procedure, the incubation-derived CO_2 was purified, quantified and flame sealed on the vacuum rig. ^{14}C analysis of the CO_2 was performed using the gas ion source of the AMS at the University of Cologne and the gas injection system described in (Stolz et al., 2017). ^{14}C results are reported in $F^{14}C$ (Reimer et al., 2013) and as uncalibrated years before present (BP; Stuiver and Polach, 1977).

Stable carbon isotope analysis

Stable carbon isotopes of OC were measured in sediment samples, which were decalcified with phosphoric acid, using an elemental analyzer (Flash 2000, Thermo Scientific, Germany) coupled to a Delta V (Thermo Scientific, Germany) isotope ratio mass spectrometer (IRMS) (Knoblauch et al., 2013). For $\delta^{13}C$ analysis of IC, ground sediment aliquots were weighed into 50 ml glass bottles and closed with a rubber stopper. Ambient air was removed from the bottles using He and phosphoric acid (5%) was added to convert the IC into CO_2. Carbon dioxide stable isotope analyses from IC, the incubation experiments and field samples were conducted by injecting gas samples into a Trace GC 1310 gas chromatograph connected to a DeltaVPlus IRMS (Thermo Scientific, Germany) (two replicates per sample). The range of replicate measurements was equal to or less than ± 0.3‰. The results of the stable carbon isotope measurements were calibrated with external standards and are reported in permille relative to the Vienna Pee Dee Belemnite (‰ VPDB).

Statistics and calculations

CO_2 production rates were compared with the elemental and isotopic compositions and the pH of the sediments using the ANOVA add-in from Microsoft Excel. For better comparison, the CO_2 production rate after 175 days of the incubation and at the end of the experiment, after 537 days, were used. Additionally, the CO_2 production rates were normalized for the amount of C available in the sample to eliminate bias by different C quantities. Furthermore, Pearson correlation coefficients were calculated to evaluate possible correlations between the data sets. Variances of data were compared using a F-test. Mean values of data sets were then compared using a t-test assuming either same or different variances, based on the F-test run previously.

The CO_2 samples taken from respiration chambers might contain contributions from atmospheric CO_2 leaking into the system through small cracks in the soil next to the chamber. To account for this effect, ^{14}C ($F^{14}C_s$) and ^{13}C ($\delta^{13}C_s$) contents of the CO_2 samples were corrected for the fraction of atmospheric CO_2 (f_{atm}) contributing to the total CO_2 and reported as $F^{14}C_c$. The $\delta^{13}C$ value of the CO_2 released in the incubation experiment ($\delta^{13}C_{inc}$) is free of atmospheric contamination that may be introduced in the field. It thus was used to correct the $\delta^{13}C$values of the CO_2 sampled in the field ($\delta^{13}C_c$). In addition, the ^{14}C ($F^{14}C_{atm}$) and ^{13}C contents ($\delta^{13}C_{atm}$) of an atmospheric air sample taken from HT1 were used to calculate the fraction of atmospheric CO_2 (f_{atm}) in the CO_2 samples and correct their ^{14}C content ($F^{14}C_c$) according to equations (1) and (2).

$$F^{14}C_c = \frac{(F^{14}C_s - f_{atm} * F^{14}C_{atm})}{(1 - f_{atm})} \quad (1)$$

$$\text{with } f_{atm} = \frac{(\delta^{13}C_s - \delta^{13}C_{inc})}{(\delta^{13}C_{atm} - \delta^{13}C_{inc})} \quad (2)$$

A mass balance approach was used to determine fractions of ancient (fOCa), and young organic carbon (fOCy) as well as of inorganic carbon (fIC) in the CO_2 flux using the $F^{14}C$ and $\delta^{13}C$ values of the potential sources (Tab. 2) and of the CO_2 released in the field and during the incubation experiment (Tab. S2, Fig. 5) according to equation 3 and 4:

$$\delta^{13}C_{CO2} = f_{IC} * \delta^{13}C_{IC} + f_{OCa} * \delta^{13}C_{OCa} + f_{OCy} * \delta^{13}C_{OCy} \quad (3)$$

and

$$F^{14}C_{CO2} = f_{IC} * F^{14}C_{IC} + f_{OCa} * F^{14}C_{OCa} + f_{OCy} * F^{14}C_{OCy} \quad (4)$$

$\delta^{13}C_{CO2}$ and $F^{14}C_{CO2}$ are the mean isotopic ratios of the CO_2 released from the thaw layer at each site. In the incubations, the mean isotopic values were weighted by the CO_2 production of each depth intervals per site.

Average isotopic values of IC and OC in the whole thaw layer ($F^{14}C_{IC/OC}$, $\delta^{13}C_{IC/OC}$), were calculated by weighing the respective values from the different depth intervals with their IC or OC content (IC_i/OC_i), respectively, and considering the bulk density (ρ_i) and thickness of the depth interval (h_i) according to equation 5 and 6.

$$\overline{F^{14}C_{IC/OC}} = \sum_{i=1}^{n} F^{14}C_i \times \left(\frac{\frac{IC/OC_i}{100} \times \rho_i \times h_i}{\sum_{i=1}^{n} \frac{IC/OC_i}{100} \times \rho_i \times h_i} \right) \quad (5)$$

$$\overline{\delta^{13}C_{IC/OC}} = \sum_{i=1}^{n} \delta^{13}C_i \times \left(\frac{\frac{IC/OC_i}{100} \times \rho_i \times h_i}{\sum_{i=1}^{n} \frac{IC/OC_i}{100} \times \rho_i \times h_i} \right) \quad (6)$$

For each site, different endmembers were used for defining young ($\delta^{13}C_{OCy}$ and $F^{14}C_{OCy}$) and ancient OC ($\delta^{13}C_{OCa}$ and $F^{14}C_{OCa}$) in the mass balance approach because the sediments are composed of different materials and the sites are situated at different heights above mean river level (a.m.r.l.) on the thaw slump (Tab. 2, S1). The thaw mound (TM2) in the Pleistocene Yedoma is located at 30 m a.m.r.l., which is 8 m below the Holocene terrace (HT1). We defined the ancient OC and IC endmembers of TM2 as the average $\delta^{13}C$ and $F^{14}C$ content of the thaw layer weighted by its OC or IC content and bulk density. Contributions of young OC were assumed to derive mainly from the thaw layer at HT1, which had a close to modern ^{14}C content (0.984 $F^{14}C$). At the slump floor (SF3), different sediments have been mixed due to erosional processes. As for TM2, we assumed that young OC was delivered mainly from the eroded thaw layer at HT1. SF3 is located at 29 m a.m.r.l., which is lower than TM2. Thus, we chose a nearby thaw mound (TM1) that is on the same height as SF3 as ancient endmember and calculated the average $\delta^{13}C$ and $F^{14}C$ for the thaw layer as for TM2. Because the IC content of the TM1 sediment was very low, only two depth intervals could be analyzed for ^{14}C in IC and results were averaged. At HT1, IC was below the detection limit. We therefore used a two-pool mixing model considering only ancient and young OC sources contributing to respired CO_2. The $F^{14}C$ and $\delta^{13}C$ values of atmospheric CO_2 measured at this site (Tab. S2) were used as young OC endmembers assuming that fresh plant OM contains the same isotopic ratios. The ancient OC endmember was defined by the lowest depth interval in the thaw layer at HT1.

Because of the differences in sediment ages at the three sites, the term 'ancient' refers to OC and IC older than 4,000 years BP at SF3 and HT1 and Pleistocene-aged at TM1, respectively. The term 'young' denotes OC younger than 4,000 years BP at TM1 and SF3, while it is near modern atmospheric ^{14}C concentrations at HT1 (Tab. 2).

To find feasible solutions for fIC, fOCa and fOCy in equations (4) and (5), the mass balance was solved using IsoSource (Phillips and Gregg, 2003). IsoSource iterates possible combinations of each source's contribution in pre-defined increments (1%) and within a defined tolerance (0.1‰). This underdetermined system (two equations with three variables) has no unique solution. Hence, a distribution of possible solutions is determined based on the isotopic ratios of three potential C sources (Tab. 2) that may contribute to the CO_2 emissions. By simplifying our model for HT1, fIC in equations (5) and (6) equals 0 and makes the equation system uniquely solvable.

Table 4: $\delta^{13}C$ and $F^{14}C$ values of the sedimentary C sources used in the mass balance calculation.

Site	$\delta^{13}C$			$F^{14}C$		
	IC	OCa	OCy	IC	OCa	OCy
HT1	-	-29.4	-27.3	-	0.597	1.021
TM2	-5.26	-26.8	-27.8	0.044	0.042	0.984
SF3	-7.46	-25.6	-27.8	0.047	0.038	0.984

The upper (maximum) and lower (minimum) limit of the calculated distributions of C sources were furthermore used to calculate the absolute amount of C released as CO_2 from the different C source at SF3 and TM2 after 175 and 537 days of the incubation experiment.

Results

Bulk sediment analysis

The undisturbed Yedoma exposed as thaw mound (TM2) had the lowest ^{14}C contents in the range of 0.023 to 0.109 $F^{14}C_{OC}$ in the thaw layer (0 - 70 cm depth) corresponding to conventional ^{14}C ages of 17,830 to 29,790 years BP (Tab. S1). The uppermost 10 cm had a higher ^{14}C content (0.109 $F^{14}C_{OC}$) than the underlying sediment at 10 to 70 cm depth (0.023 - 0.029 $F^{14}C_{OC}$). $F^{14}C_{OC}$ values in the thaw layer of the mixed sediment on the slump floor (SF3) ranged between 0.607 $F^{14}C_{OC}$ and 0.844 $F^{14}C_{OC}$ in 0 to 60 cm depth (1,370 – 4,010 years BP) and included two younger layers at 0 - 10 cm and 30 - 50 cm depth with 0.844 $F^{14}C_{OC}$ and 0.789 – 0.829 $F^{14}C_{OC}$ (1,370 and 1,500 – 1,900 yrs BP), respectively. The soil developed on the Holocene terrace (HT1) had the highest ^{14}C content between 0.597 and 0.946 $F^{14}C_{OC}$ in 0-17 cm depth. The organic layer on top of the mineral soil, which was removed prior to CO_2 analysis, had a ^{14}C content slightly above atmospheric levels (1.149 $F^{14}C$) indicating the contribution of OM produced during times of higher atmospheric ^{14}C levels due to above ground nuclear weapon testing.

The $\delta^{13}C_{OC}$ results ranged from -25.3 to -32.3‰ with no clear differences between sites and no relation to sediment depth or to other parameters (Tab. S1).

The OC and N contents did not change considerably with increasing sediment depth, except at HT1 (Tab. S1). Here, the highest OC content was measured in the uppermost layer (9.2 – 9.7%) and the lowest OC content in the bottom layer (3.0%). At the mixed site (SF3), OC contents ranged from 3.9 to 5.5%, while they were considerably lower in the intact thaw mound (TM2) with values of 1.0 to 2.0%. Here, higher values were measured in 0 – 10 cm than in 10 - 70 cm (Tab. S1). Similar to OC contents, the N content was highest in the uppermost layer at HT1 (0.70%) than in the lower layer (0.17%). Slightly lower N contents were determined SF3 (0.22 to 0.37%) and even lower values at TM2 (0.12 to 0.19%), which were higher in the upper 10 cm and lower below. The differences in OC and N content between the sites resulted in similar differences in OC/N ratios. HT1 had the highest values (14.0 - 37.6), SF3 slightly lower (13.9 – 17.4) and TM2 the lowest ratios (7.8 - 11.0).

No IC was measurable in the HT1 soil. At SF3, the IC content ranged from 1.1 – 2.8% in 0 – 50 cm, with considerably lower IC values of 0.2% and 0.7% in 20 – 30 cm and 50 – 60 cm depth, respectively. At TM2, IC contents were more consistent and ranged from 0.5 – 0.8%.

The ^{14}C and ^{13}C contents of the IC did not change with sediment depth. At SF3, $F^{14}C_{IC}$ values were in the range of 0.609 to 0.844 and thus were similar to the respective $F^{14}C_{OC,}$ while the $\delta^{13}C_{IC}$ values were much higher in the range of -9.1 to -12.8‰. At TM2, $F^{14}C_{IC}$ was between 0.019 and 0.056, which is higher than the respective $F^{14}C_{OC}$, except in the uppermost interval. Here, ^{14}C contents of the IC were lower compared to values of the OM. $\delta^{13}C_{IC}$ ranged from -4.5 to -7.0‰ in the thaw mound sediment.

The pH values at HT1 (4.3 - 5.8) and SF3 (4.9 - 6.1) were slightly acidic, while they were neutral to slightly alkaline (6.4 – 7.8) at TM2 (Tab. S1).

CO_2 fluxes and C isotopic signatures

The ^{14}C content of the CO_2 respired in the field differed distinctly between sites (Tab. S2). The CO_2 respired from TM2 had the lowest ^{14}C contents between 0.230 and 0.329 $F^{14}C$ (8.9 – 11.8 kyrs BP) compared to the two other sites on the thaw slump (Tab. S2). ^{14}C concentrations of the CO_2 released from SF3 ranged between 0.547 and 0.716 $F^{14}C$ (2.7 – 4.9 kyrs BP), while they were close to atmospheric contents (1.022 $F^{14}C$) at HT1 with 0.975 to 0.985 $F^{14}C$ matching values of bulk OC in the uppermost (0 – 11 cm) layer (0.946 $F^{14}C$) (Tab. S1).

The CO_2 fluxes measured prior to CO_2 sampling for isotopic analysis varied considerable between the different sites and between the three replicates taken at each site (Tab. S2). CO_2 fluxes were highest at TM2 (2.7 – 12.3 g CO_2 m^{-2} d^{-1}) and SF3 (6.1 – 11.6 g CO_2 m^{-2} d^{-1}) with

a considerable scatter, while they were much lower at HT1 (0.8 – 2.0 g CO_2 m^{-2} d^{-1}). However, the results were affected by weather conditions at the day of measurements and thus difficult to compare.

The stable carbon isotopic composition of CO_2 released in the incubation experiment differed between sites and duration of the incubation (Fig. 2, Tab. S3). At TM2, $\delta^{13}C$ values of the CO_2 released from the different depth intervals after the first incubation period ranged between -22.0 and -23.4‰ (Fig. 2 B), which is consistently heavier than values of OC from the corresponding bulk sediment (-25.3 to -30.8‰). Even higher values were determined for the CO_2 emitted from the mixed site, SF3, in the range of -19.5 to -24.6‰ (Fig. 2 C), while OC values of the corresponding bulk sediment ranged between -27.5 and -32.3‰. In contrast, CO_2 produced from the active layer of HT1 had the lowest isotopic ratios of -27.0 and -26.3‰ in 0 – 11 cm and 11 – 17 cm depth, respectively (Fig. 2 A). No depth trend of stable isotope signatures of the CO_2 produced in the incubations could be determined at all sites.

At TM2 and SF3 $\delta^{13}C$ values decreased at the end of the incubation by 0.9 to 2.0‰, except for the 20 – 40 cm interval and ranged between -21.1 and -22.9‰ at TM2 (Fig. 2 B) and -24.2 and -25.6‰ at SF3 (Fig. 2 C). The $\delta^{13}C$ of CO_2 released from HT1 remained close to values measured after the first incubation period at -27.3 to -28.5‰ with slightly lighter values for the 11 – 17 cm depth interval.

The overall lowest ^{14}C contents of the CO_2 released after the first incubation period were measured at TM2 and ranged from 0.147 – 0.188 $F^{14}C$ (Fig. 2 E; Tab. S3), which is higher than values of the bulk sediment (0.023 – 0.109 $F^{14}C$). At the mixed site, SF3, the released CO_2 had higher ^{14}C contents ranging from 0.585 to 0.718 $F^{14}C$ (Fig. 2 F) with higher values in the upper intervals 0 - 40 cm (0.702 – 0.718 $F^{14}C$) and lower values in 40 - 60 cm (0.585 $F^{14}C$), the latter being lower than the $F^{14}C$ of the bulk sediment. At HT1, CO_2 from the first incubation period had an overall higher ^{14}C content (Fig. 2 D) than the respective bulk sediment with 1.011 $F^{14}C$ in 0 - 11 cm, which is just below the atmospheric ^{14}C content measured at this site (1.021 $F^{14}C$; Tab. S2), while 0.859 $F^{14}C$ was measured for CO_2 of the incubations from 11 - 17 cm depth.

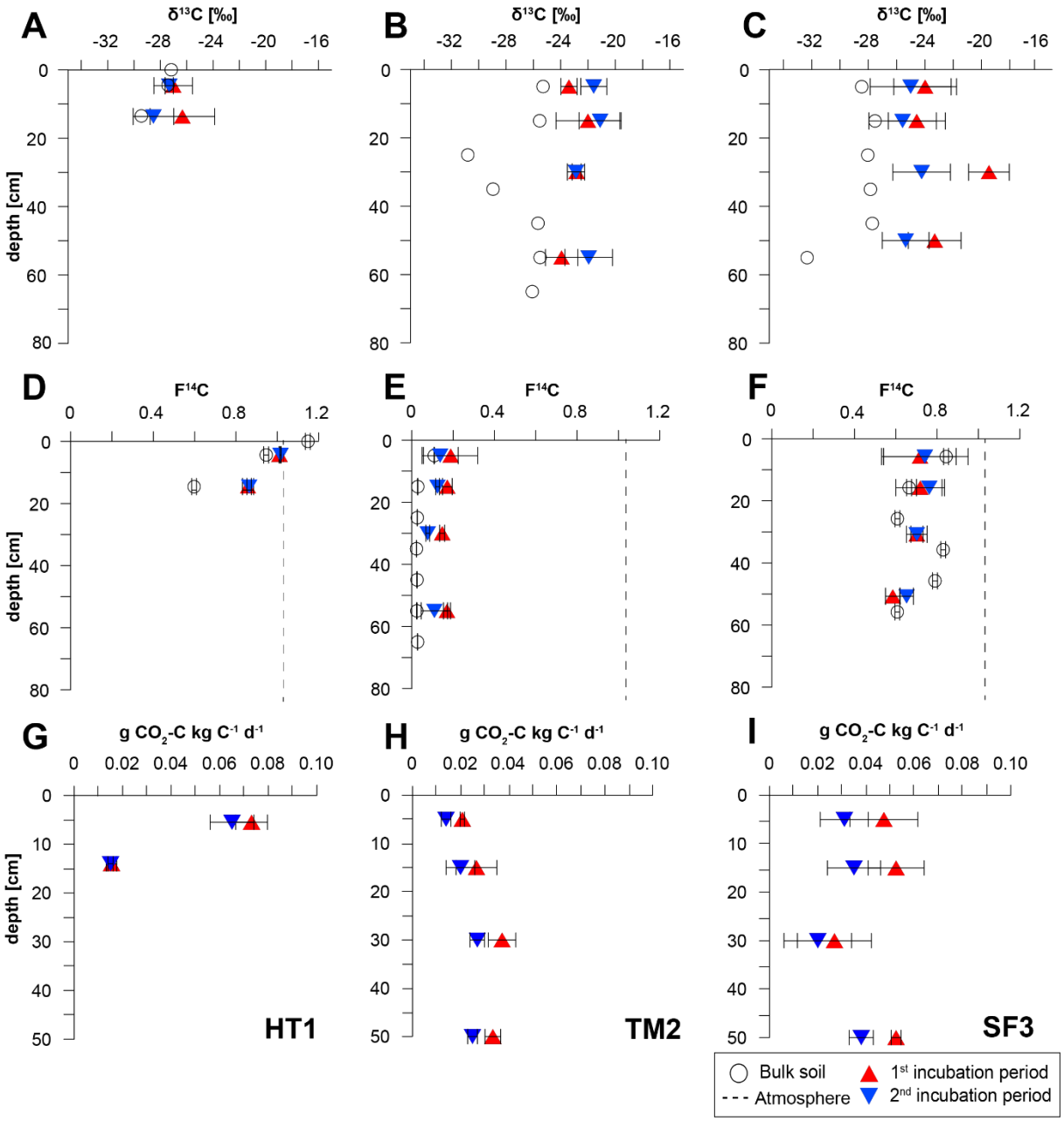

Figure 2: $\delta^{13}C$ (A, B, C) and ^{14}C contents (D, E, F) of bulk soil OC of the different sampling sites as well as CO_2 released from the incubation experiment (G, H, I) during the first (red triangles) and the second incubation period (blue triangles) normalized to the amount of soil carbon.

The ^{14}C contents of the CO_2 changed slightly at the end of the long-term incubation (Tab. S3). At TM2, consistently lower values were measured in all depth intervals (0.077 – 0.138 $F^{14}C$) after 1.5 years than after few weeks of incubation (Fig. 2 E). In contrast, ^{14}C contents increased during the incubation of SF3 sediment (0.652 – 0.762 $F^{14}C$), except for the CO_2 released from 20 – 40 cm (0.701 $F^{14}C$) (Fig. 2 F). The CO_2 produced from HT1 soil had similar values (0.864 – 1.016 $F^{14}C$) within the measurement uncertainty after few weeks and 1.5 years of incubation (Fig. 2 D).

The daily CO_2 production during the aerobic incubation differed considerably between sites and duration of the incubation (Tab. S3). The lowest cumulative CO_2 production was measured at TM2 in the range of 0.41 and 0.76 µg CO_2-C gdw^{-1} d^{-1} after 175 days. Higher CO_2 production rates were measured for the mixed sediments from SF3 of 1.18 to 2.85 µg CO_2-C gdw^{-1} d^{-1}. At HT1, most CO_2 was released from the uppermost depth interval after 175 days with 7.54 µg CO_2-C gdw^{-1} d^{-1}, while much less CO_2 was produced from 11 - 17 cm with 0.55 µg CO_2-C gdw^{-1} d^{-1}, which is comparable to the rates measured in TM2 sediment. When normalized to the amount of available thawed C, the daily release of C as CO_2 corresponds to 0.021 to 0.037 g CO_2-C kgC^{-1} d^{-1} at TM2 (Fig. 2 H), 0.027 to 0.052 g CO_2-C kgC^{-1} d^{-1} at SF3 (Fig. 2 I), and between 0.015 to 0.093 g CO_2-C kgC^{-1} d^{-1} at HT1 (Fig. 2 G, Tab. S3). The CO_2 production decreased towards the end of the incubation, after 1.5 years, by about 30% both, at TM2 (0.28 – 0.55 µg CO_2-C gdw^{-1} d^{-1}) and at SF3 (0.89 – 1.90 µg CO_2-C gdw^{-1} d^{-1}), and much less, by about 8%, at HT1 (0.51 – 6.68 µg CO_2-C gdw^{-1} d^{-1}). Accordingly, the normalized C release at the end of the incubation experiment decreased to 0.014 to 0.027 g CO_2-C kgC^{-1} d^{-1} at TM2, to 0.020 – 0.038 g CO_2-C kgC^{-1} d^{-1} at SF3, and to 0.015 to 0.065 g CO_2-C kgC^{-1} d^{-1} at HT1.

Contributions of organic and inorganic sources to CO_2 release

A three C pool, two isotope (^{13}C, ^{14}C) mass balance approach was used to calculate the contribution of different C sources to CO_2 emissions in the field and during the incubation experiment for sites TM2 and SF3 (Fig. 3). Since HT1 contained no IC, a two-pool model excluding IC was applied.

The range of possible contribution of the three different carbon sources to the CO_2 efflux is shown in Table 3 and the corresponding absolute amount of CO_2 released as C in Table S4. During the field measurements, most of the CO_2 (82%) released from the Yedoma thaw mound TM2 derived from OC sources including 15 to 34% of young OC and 48 to 67% of ancient OC. However, a significant amount of the CO_2 emissions of about 18% was of inorganic origin. At the mixed site SF3, a similar large amount of 74 - 76% of the CO_2 was released from organic sources. However, the majority of CO_2 at this site originated from young OC (51 - 72%) and less from ancient OC (2 - 25%). An even larger amount of 24 - 26% of the CO_2 derived from IC. At HT1, the two-pool model revealed that here mainly modern OM was mineralized and released as CO_2 (87 - 91%), while older substrates from greater depth made up only 9 to 13% of the CO_2 flux.

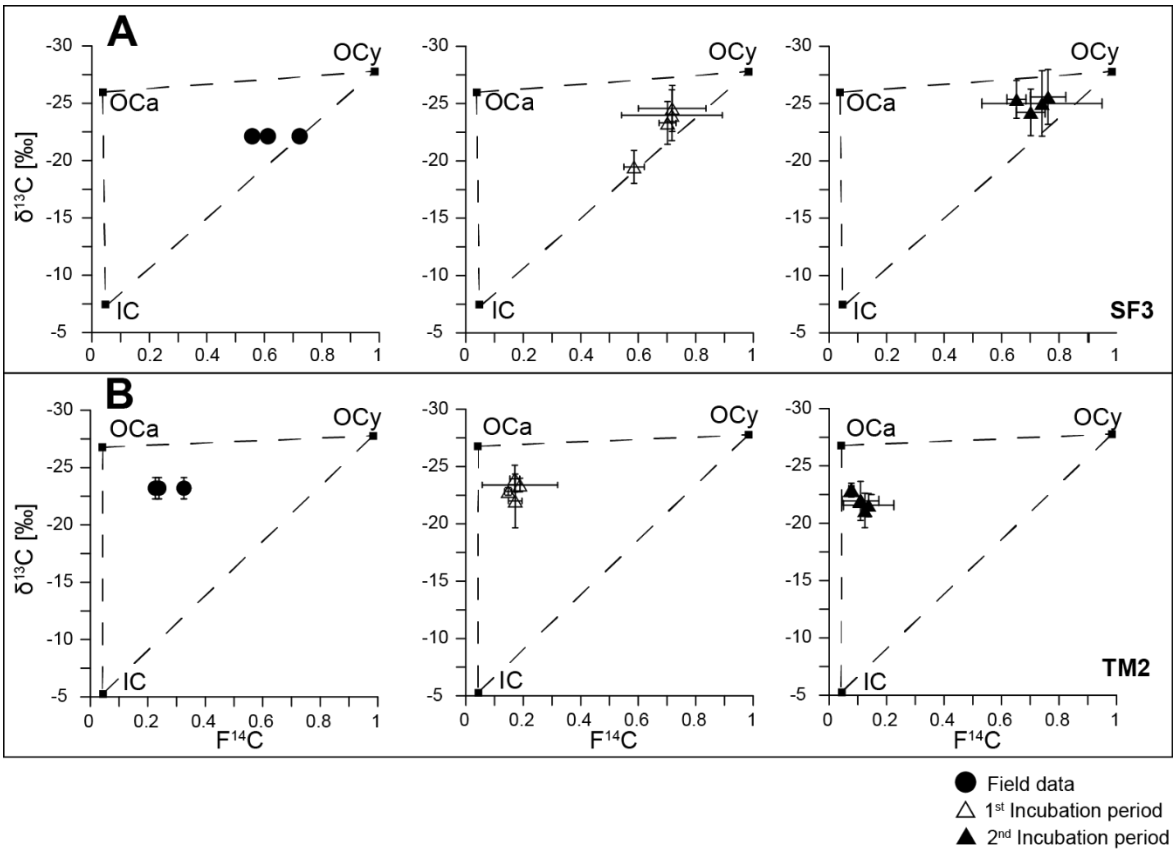

Figure 3: Carbon isotope biplots for (A) SF3 and (B) TM2 indicating endmembers (squares) on which the three-pool mass balance approach is based and including field and incubation data (mean values of depth intervals and standard deviation).

During the first 159 to 189 days of the aerobic incubation, until CO_2 was sampled, about 82% of the CO_2 produced from TM2 sediment was released from OC sources including 3 – 12% or 15 – 23% young (13 – 14% exceeds the 0.1‰ model tolerance) and 71 – 80% or 59 – 67% ancient OC. A significant amount of 17 to 18% of the CO_2 originated from IC. At SF3, slightly less CO_2 of about 74 – 76% was released from OC during the first 41 – 99 days until CO_2 sampling. Most of this CO_2, between 56 – 74%, was of young origin, while only 0 – 20% derived of ancient organic sources. The remaining 24 to 26% of the CO_2 originated from IC. At HT1, modern OC was the major CO_2 source (94 – 96%), while only 4 – 6% originated from older OM.

The largest change in C sources at the end of the incubation experiment (after 537 days) was measured at TM2. Here, the contribution of IC in the CO_2 produced increased to 22%, while the fraction of young OC decreased to 0 – 17% and the ancient OC contribution to 61 – 78%. At SF3, slightly more CO_2 was released from young (61 – 81%) and ancient OC (6 – 29%), respectively, while IC contributions decreased from 24 – 26% to 10 – 13%. No significant change in C sources during the incubation period was determined at HT1 (3 - 5% fOCa; 95 - 97% fOCy).

Table 5: Distributions of C pools contributing to the CO_2 released in the field and in the incubations.

Site	Minimum feasible fraction CO_2			Maximum feasible fraction CO_2		
	OCy	OCa	IC	OCy	OCa	IC
Field measurements						
TM2	0.15	0.48	0.18	0.34	0.67	0.18
SF3	0.51	0.02	0.24	0.72	0.25	0.26
HT1	0.87	0.09	-	0.91	0.13	-
1st incubation period						
TM2	0.03	0.59	0.17	0.23	0.80	0.18
SF3	0.56	0	0.24	0.74	0.20	0.26
HT1	0.94	0.04	-	0.96	0.06	-
2nd incubation period						
TM2	0	0.61	0.22	0.17	0.78	0.22
SF3	0.61	0.06	0.10	0.81	0.29	0.13
HT1	0.95	0.03	-	0.97	0.05	-

Discussion

Carbon sources of in situ CO_2 fluxes

The analyses of CO_2 collected in the field revealed that the largest proportion of the emissions (48 – 67%) released from freshly thawed Yedoma (TM2) derived from the degradation of ancient OM, while a much smaller amount is mineralized from young OM (15 – 34%). This result agrees well with high respiration rates of Pleistocene-age Yedoma measured in previous incubation experiments (Dutta et al., 2006; Zimov et al., 2006; Lee et al., 2012) that were related to higher amounts of labile OM than in Holocene deposits (Walz et al., 2018). The young OM at TM2 most likely was deposited on top of the thaw mound by melt water and erosion. The $\delta^{13}C$ signatures of the CO_2 released in the laboratory incubations indicate that about 18% of the CO_2 released at the field sites originated from IC sources. However, we cannot rule out that the CO_2 release from carbonates during the incubations was biased by the incubation conditions. Measurements of the stable C isotope signatures of CO_2 released from the thaw slump and flux measurements would be required to construct Keeling plots (Keeling, 1958; Köhler et al., 2006) giving direct evidence for IC dissolution under in situ conditions. Although the IC content of the sediment was relatively low (0.5 – 0.8%) and the pH neutral to slightly alkaline (7.3 - 7.8 in 0-60 cm and 6.4 in 60-70 cm) it is possible that in this pH range, the soil or sediment pH is buffered by carbonate dissolution to bicarbonate (HCO_3^-), which is dissolved in ground water (Guo et al., 2015; Raza et al., 2020). However, for net CO_2 emissions to be produced from IC, it has been speculated that the chemical equilibrium of chemical

weathering must have been shifted by organic acids towards carbonate dissolution (Zolkos et al., 2018). As suggested by Zolkos et al. (2018), thermokarst activity in retrogressive thaw slumps can increase HCO_3^- concentrations in the pore water of the sediments thus changing the chemical equilibrium to favor dissolution of carbonate and degassing of CO_2 (Fritz et al., 2015).

At the slump floor (SF3), where thermokarst processes caused the mixing of Pleistocene Yedoma with younger sediments eroded from the Holocene terrace, mostly young OM (51 – 72%) was released as CO_2 and much less derived from Pleistocene-age OM (2 – 25%). This indicates the preferential mineralization of the admixed Holocene-age OM. At SF3, thermokarst-related sediment mixing resulted in higher IC contents (0.2 - 2.8%) and lower pH values (4.9 – 6.1) promoting IC-derived CO_2 emissions. Here, the amount of IC in the CO_2 emissions (24 – 26%) was even larger than in the Yedoma thaw mound (TM2) supporting observations by (Zolkos et al., 2018, 2020) that thermokarst amplifies IC cycling. The lower pH of the mixed sediment may result from higher OC and N contents that possibly supported the formation of organic acids causing the dissolution of $CaCO_3$ (Ramnarine et al., 2012; Tamir et al., 2012; Zolkos et al., 2018).

The sedimentary IC most probably is not derived from lithogenic sources because it exhibited lower $\delta^{13}C$ values (Tab. S1) than average values for lithogenic IC in exchange with fresh water of about 2 – 4‰ PDB (Weber et al., 1965). Besides, the IC had similar ^{14}C concentrations like the sedimentary OC indicating coeval formation. Ca^{2+} may have been leached from silicate minerals to form pedogenic carbonate coatings on clay and silt-sized particles without lithogenic carbonates being present in the sediment (Schlesinger, 1985; Cailleau et al., 2005; Rovira and Vallejo, 2008; Ramnarine et al., 2012). Pedogenic carbonate may also have formed from HCO_3^- derived from CO_2 emitted by microbial degradation of the OM. The $\delta^{13}C$ of the pedogenic carbonate thus is lighter, in the range of -10 to 0‰ PDB, compared to lithogenic carbonate (Cerling, 1984). A further source of IC may be ostracods that lived in polygon centers during the Pleistocene and became part of the present Yedoma sediment. The $\delta^{13}C$ values of the sedimentary IC at SF3 (-9.1 to -12.8‰ PDB; Tab. S1) agree well with reported $\delta^{13}C$ values of subfossil ostracod valves found in thermokarst lakes at Kurungnakh Island (-6.9 to -7.1‰ PDB) and subfossil intrapolygonal ostracod valves (-10.8 to -11.1‰ PDB; Wetterich et al., 2008b). Thus, a fraction of the sedimentary IC may also have derived from dissolution of these fossil remains. Further investigations are needed to disentangle potential IC sources more precisely, because the dissolution of pedogenic carbonates would release CO_2 that originally formed from microbial degradation of OM and would therefore not alter the net CO_2 emissions of the sediment from where it is released (Zolkos et al., 2018).

The Holocene terrace (HT1) was investigated because it was used as modern endmember in the isotopic mass balance calculation. At HT1 mainly modern OM with atmospheric ^{14}C content was degraded and released as CO_2 (87 – 91%), while the remaining fraction of the CO_2 originated from the OM stored in the deeper mineral soil intervals, as indicated by the abrupt decrease in $F^{14}C$ of the bulk soil below 17 cm depth (Tab. S1). The soil did not contain any measurable IC. Although the vegetation was removed from HT1, small contributions of modern CO_2 derived from autotrophic respiration of roots cannot be fully excluded. However, these may be negligible, because the ^{14}C results of the CO_2, which were close to the atmospheric values, were corrected for atmospheric CO_2 contributions (Eq. 1 and 2). However, if any root remains released bomb-spiked enriched $^{14}CO_2$, it would have slightly skewed our results towards modern OM.

The CO_2 produced after few weeks of the aerobic incubation represent the emissions of approximately one thaw season, i.e., about 120 days (Boike et al., 2013). The results of the mass balance approach were similar to the field data at SF3 but slightly different at TM2 and HT1. No positive priming promoting the decomposition of the old OM as demonstrated in previous incubations (Wild et al., 2016; Walz et al., 2018; Pegoraro et al., 2019) took place at the slump floor SF3, where Holocene-age sediments were mixed with Pleistocene-age Yedoma (Tab. S4). Most CO_2 was released from young OM (2.6 – 6.8 g CO_2-C kgC^{-1}) and much less from ancient OM (0 – 1.8 g CO_2-C kgC^{-1}) indicating the preferential mineralization of young sources. In contrast to the field data, less CO_2 was produced from young OM (3 - 23%; 0.1 – 1.5 g CO_2-C kgC^{-1}) from the Yedoma thaw mound TM2 during the first few weeks of the incubation. This suggest that less young organic substrates were present and thus were rapidly consumed, i.e., within roughly one thawing season. This result agrees well with high CO_2 production rates measured in previous aerobic incubation studies of Yedoma that were attributed to the presence of labile OM, which can be readily mineralized after thawing (Dutta et al., 2006; Lee et al., 2012; Knoblauch et al., 2013; Walz et al., 2018). At SF3 and TM2, the contribution of IC to the total CO_2 flux was similar to the field data (17 – 18%). The CO_2 produced during 41 to 159 days of incubation of soil from the Holocene terrace (HT1) contained slightly, but statistically not significant higher amounts of young OC compared to the field data. This may be related to the CO_2 collection with respiration chambers giving a mixed signal that may also include CO_2 from deeper parts of the thawed layer (21 cm) containing older OC while the CO_2 in the incubation experiment was only released from the uppermost 17 cm.

The CO_2 production from the Yedoma thaw mound at TM2 during the first 175 days of (0.41 – 0.76 µg CO_2-C gdw^{-1} d^{-1}) was very low compared to previous results in which Pleistocene-age Yedoma from the Kolyma region was incubated for a shorter period (41 – 99 days) resulting in about five times larger CO_2 production rates compared to TM2 (Dutta et al., 2006), or, up to

one order of magnitude larger CO_2 production rates in an incubation at higher temperatures (15 °C, Lee et al., 2012). These differences may be related to different OM composition, stage of degradation and bioavailability, i.e., interaction with mineral particles in the heterogeneous Yedoma deposits and of cause to the different incubation temperatures.

The highest CO_2 production was measured in the uppermost, youngest layer at HT1 and much less in the lower depth interval (10 - 17 cm; 0.55 µg CO_2-C gdw^{-1} d^{-1}). This difference is related to the larger amounts of young (close to atmospheric ^{14}C levels), little degraded substrates in the surface layer having high OC content (9.7%) and OC/N ratio (14). Likewise, more than three times higher production rates were measured for the mixed sediment at the slump floor containing more OC compared to the Yedoma thaw mound (Tab. S1). These data underline the strong relation of CO_2 production to OC content ($R^2 = 0.9$; $p < 0.005$) persistent for all sites and both, field and incubation data, and, to a lesser extent, to OM quality represented by the OC/N ratio. The latter may have promoted the mineralization of OM, which has a lower stage of degradation at SF3 and HT1, suggested by higher OC/N ratios compared to TM2.

The CO_2 production rates normalized to the available C differed in a smaller range between the sites (Tab. S3). Most CO_2 was still produced from the carbon-rich surface soil at HT1, while about 40 – 70% less was generated from the mixed sediment SF3 (except from 20 – 40 cm depth) and about 25% less from the Yedoma thaw mound at SF3. The varying CO_2 production rates can be explained by the higher amount of younger OM that is preferentially degraded in HT1 soil and SF3 sediments. In addition, physical stabilization processes may reduce the bioavailability of the OM differently in the different sediments (Höfle et al., 2013; Gentsch et al., 2015).

The results measured after 1.5 years of incubations can give information on the future development of OM degradation and CO_2 production as shown in previous long-term incubation studies (Dutta et al., 2006; Knoblauch et al., 2013; Faucherre et al., 2018). The trend of young OM depletion in the thaw mound TM2, which was observed during the initial period of the incubation, continued resulting in a further decline of this OM pool by about 3 - 6% at the end of the incubation. Carbon dioxide emissions from ancient sources thus increased of which about 2% originate from the mineralization of Yedoma-derived OM and a larger proportion of 4 - 5% from the abiotic degradation of IC. Given the length of the long-term incubation, it is possible that the degradation of OM led to the oxidation of NH_4^+, which releases H^+ ions in aerated TM2 sediments during the incubation that decreased the pH and thus increased the dissolution of IC and consequently the contribution of IC to total CO_2 release (Tamir et al., 2012). The amino acids that are required for the microbial oxidation, if not present initially, may have been released into the sediment dissolved in water from melted ice wedges

(Drake et al., 2015), leading to acidification of the sediment, which was experimentally shown to occur rapidly within few weeks (Tamir et al., 2011, 2012).

At the mixed site SF3, slightly more CO_2 was released from both, young and old OM, while IC contribution declined at the end of the incubation. The lower contribution of IC may be caused by the overall decreasing heterotrophic respiration during the long-term incubation (Tab. S3). The 50% lower proportion of IC may be related to the reduction of microbial respiration and CO_2 production from OM. A decreased CO_2 concentration could slow down carbonate dissolution and reduce IC emissions. In contrast to TM2, the soil of SF3 had a lower pH that indicates a lower concentration of inorganic carbon. These could have dissolved the carbonates in the sediment, which may occur as rapidly as within one year (Biasi et al., 2008).

The CO_2 production from the thaw layer of the sediments at TM2 and SF3 decreased at the end of the incubation by about the same amount of approximately 24 to 34%, while it decreased much less, by 6 to 11%, at HT1. This decline in CO_2 production at all sites is smaller compared to previous long-term incubations, which attributed the reduction in production rates to a decline of labile OM (Dutta et al., 2006; Knoblauch et al., 2013; Walz et al., 2018). Thus, the lower decrease in CO_2 production in this study, may indicate that less labile OM was present here.

Overall, our source assessment indicates that relative proportions of CO_2 derived from young OM in Pleistocene-age Yedoma decline during the incubation (of TM2). However, when young OM is available in sufficient amounts, like in the mixed sediment SF3 and the soil in the Holocene terrace HT1, most of the CO_2 is produced from this young OM pool during the entire duration of the incubation. The reduction in CO_2 production thus may be related to other effects, e.g., changes in the microbial community as a result of the length of the experiment, the lack of nutrients that may have led to a decreased microbial diversity and favored conditions for slower metabolizing oligotrophic bacteria, which has been proposed but not yet experimentally verified (Schädel et al., 2020).

Conclusion

The dual carbon isotopic source assessment revealed that large proportions of up to 80% ancient organic and about 18% inorganic carbon, despite not being shown directly in the field, were likely released from freshly thawed, Pleistocene-age Yedoma exposed as thaw mound in a retrogressive thaw slump. A young OM pool, which derived from overlaying sediments or was transported by meltwater to the thaw mound, was preferentially respired. The contribution of ancient C sources, both organic and inorganic, to the CO_2 produced from thawed Yedoma may further increase (by about 6 - 7%) upon longer thaw as indicated at the end of the aerobic incubation at 4°C after 1.5 years. The mixing of Pleistocene-age Yedoma with Holocene

material at the slump floor by erosional processes did not cause a positive priming, i.e., increasing the release of ancient OC. Most of the CO_2 (51 - 72%) produced from the mixed sediments originated from young OM, which was available in sufficient quantities even at the end of the incubation. CO_2 production rates were positively correlated with sedimentary OC content and decreased over the course of the incubation. Considerable amounts of IC were abiotically released as CO_2 from the freshly thawed Yedoma and from the mixed sediments, which is supposed to be related to thermokarst activities and transport of HCO_3^- by meltwater from the ice wedges into the Yedoma causing dissolution of IC. Besides, pH values may be lower by the production of organic acids during microbial OM decomposition. The substantial IC contribution to CO_2 emissions from thawing Yedoma may overestimate CO_2 fluxes from organic sources. IC-related emissions may be even larger because significantly larger amounts of sedimentary IC were found in the circumarctic region compared to this study suggesting the possibility of a yet overseen source of CO_2 emissions. The dissolution of pedogenic carbonates that formed after Yedoma thaw, from bicarbonate of organic origin, would ultimately not alter the CO_2 budget, in contrast to lithogenic sources. However, the CO_2 budget might be altered if those pedogenic carbonates formed from OC over a longer time scale and were destabilized recently. Thus, further investigations are of interest and are required to determine precisely the potential sources of the sedimentary IC.

Data Availability Statement

The dataset of this study is available in the Zenodo online repository https://doi.org/10.5281/zenodo.5644763.

Conflict of Interest

The authors declare that the research was conducted in the absence of any commercial or financial relationships that could be construed as a potential conflict of interest.

Funding

This work was financially supported by the German Ministry of Science and Education (BMBF) within the project ‘KoPf’ (grant no. 03F0764A/E) and ‘KoPf’ Synthesis project (grant no. 03F0834A/D). C.K. received additional funds from the Clusters of Excellence CLICCS (EXC2037/1) at the Universität Hamburg funded by the German Research Foundation (DFG).

Acknowledgments

We are grateful for logistical support by AWI and station personnel during the Russian-German expedition Lena 2017. We thank Stefan Heinze, Svetlana John, Elisabeth Krewer, Ulrike Patt, Alexander Stolz and Anja Wotte (Cologne) for helping collecting and processing samples and

performing AMS ^{14}C analysis, Ralf Lendt (Hamburg) for stable carbon isotope analysis, and Jelena Gerloff (Hamburg) for helping with the incubation experiment.

References

Biasi, C., Lind, S. E., Pekkarinen, N. M., Huttunen, J. T., Shurpali, N. J., Hyvönen, N. P., et al. (2008). Direct experimental evidence for the contribution of lime to CO2 release from managed peat soil. *Soil Biol. Biochem.* 40, 2660–2669. doi:10.1016/j.soilbio.2008.07.011.

Biskaborn, B. K., Smith, S. L., Noetzli, J., Matthes, H., Vieira, G., Streletskiy, D. A., et al. (2019). Permafrost is warming at a global scale. *Nat. Commun.* 10, 1–11. doi:10.1038/s41467-018-08240-4.

Boike, J., Kattenstroth, B., Abramova, K., Bornemann, N., Chetverova, A., Fedorova, I., et al. (2013). Baseline characteristics of climate, permafrost and land cover from a new permafrost observatory in the Lena River Delta, Siberia (1998–2011). *Biogeosciences* 10, 2105–2128. doi:10.5194/bg-10-2105-2013.

Boike, J., Wille, C., and Abnizova, A. (2008). Climatology and summer energy and water balance of polygonal tundra in the Lena River Delta, Siberia. *J. Geophys. Res. Biogeosciences* 113. doi:10.1029/2007JG000540.

Cailleau, G., Braissant, O., Dupraz, C., Aragno, M., and Verrecchia, E. P. (2005). Biologically induced accumulations of $CaCO_3$ in orthox soils of Biga, Ivory Coast. *CATENA* 59, 1–17. doi:10.1016/j.catena.2004.06.002.

Cerling (1984). The stable isotopic composition of modern soil carbonate and its relationship to climate. *Earth Planet. Sci. Lett.* 71, 229–240. doi:10.1016/0012-821X(84)90089-X.

Costard, F., Dupeyrat, L., Séjourné, A., Bouchard, F., Fedorov, A., and Saint-Bézar, B. (2021). Retrogressive Thaw Slumps on Ice-Rich Permafrost Under Degradation: Results From a Large-Scale Laboratory Simulation. *Geophys. Res. Lett.* 48. doi:10.1029/2020GL091070.

Czimczik, C. I., and Welker, J. M. (2010). Radiocarbon Content of CO_2 Respired from High Arctic Tundra in Northwest Greenland. *Arct. Antarct. Alp. Res.* 42, 342–350. doi:10.1657/1938-4246-42.3.342.

Czudek, T., and Demek, J. (1970). Thermokarst in Siberia and Its Influence on the Development of Lowland Relief. *Quat. Res.* 1, 103–120. doi:10.1016/0033-5894(70)90013-X.

Dewald, A., Heinze, S., Jolie, J., Zilges, A., Dunai, T., Rethemeyer, J., et al. (2013). CologneAMS, a dedicated center for accelerator mass spectrometry in Germany. *Nucl. Instrum. Methods Phys. Res. Sect. B Beam Interact. Mater. At.* 294, 18–23. doi:10.1016/j.nimb.2012.04.030.

Dorsett, A., Cherrier, J., Martin, J. B., and Cable, J. E. (2011). Assessing hydrologic and biogeochemical controls on pore-water dissolved inorganic carbon cycling in a subterranean estuary: A ^{14}C and ^{13}C mass balance approach. *Mar. Chem.* 127, 76–89. doi:10.1016/j.marchem.2011.07.007.

Drake, T. W., Wickland, K. P., Spencer, R. G. M., McKnight, D. M., and Striegl, R. G. (2015). Ancient low–molecular-weight organic acids in permafrost fuel rapid carbon dioxide production upon thaw. *Proc. Natl. Acad. Sci.* 112, 13946–13951. doi:10.1073/pnas.1511705112.

Dutta, K., Schuur, E. A. G., Neff, J. C., and Zimov, S. A. (2006). Potential carbon release from permafrost soils of Northeastern Siberia: CARBON RELEASE FROM SIBERIAN

PERMAFROST SOILS. *Glob. Change Biol.* 12, 2336–2351. doi:10.1111/j.1365-2486.2006.01259.x.

Estop-Aragonés, C., Cooper, M. D. A., Fisher, J. P., Thierry, A., Garnett, M. H., Charman, D. J., et al. (2018). Limited release of previously-frozen C and increased new peat formation after thaw in permafrost peatlands. *Soil Biol. Biochem.* 118, 115–129. doi:10.1016/j.soilbio.2017.12.010.

Faucherre, S., Jørgensen, C. J., Blok, D., Weiss, N., Siewert, M. B., Bang-Andreasen, T., et al. (2018). Short and Long-Term Controls on Active Layer and Permafrost Carbon Turnover Across the Arctic. *J. Geophys. Res. Biogeosciences* 123, 372–390. doi:10.1002/2017JG004069.

Fritz, M., Opel, T., Tanski, G., Herzschuh, U., Meyer, H., Eulenburg, A., et al. (2015). Dissolved organic carbon (DOC) in Arctic ground ice. *The Cryosphere* 9, 737–752. doi:10.5194/tc-9-737-2015.

Gentsch, N., Mikutta, R., Shibistova, O., Wild, B., Schnecker, J., Richter, A., et al. (2015). Properties and bioavailability of particulate and mineral-associated organic matter in Arctic permafrost soils, Lower Kolyma Region, Russia: Organic matter stabilization in permafrost soils. *Eur. J. Soil Sci.* 66, 722–734. doi:10.1111/ejss.12269.

Griffith, D. R., McNichol, A. P., Xu, L., McLaughlin, F. A., Macdonald, R. W., Brown, K. A., et al. (2012). Carbon dynamics in the western Arctic Ocean: insights from full-depth carbon isotope profiles of DIC, DOC, and POC. *Biogeosciences* 9, 1217–1224. doi:10.5194/bg-9-1217-2012.

Grigoriev, M.N. (1993). Cryomorphogenesis of the Lena River mouth area. SB RAS, Yakutsk, 1-176. in Russian.

Grosse, G., Harden, J., Turetsky, M., McGuire, A. D., Camill, P., Tarnocai, C., et al. (2011). Vulnerability of high-latitude soil organic carbon in North America to disturbance. *J. Geophys. Res. Biogeosciences* 116. doi:10.1029/2010JG001507.

Guo, J., Wang, F., Vogt, R. D., Zhang, Y., and Liu, C.-Q. (2015). Anthropogenically enhanced chemical weathering and carbon evasion in the Yangtze Basin. *Sci. Rep.* 5, 1–8. doi:10.1038/srep11941.

Höfle, S., Rethemeyer, J., Mueller, C. W., and John, S. (2013). Organic matter composition and stabilization in a polygonal tundra soil of the Lena Delta. *Biogeosciences* 10, 3145–3158. doi:10.5194/bg-10-3145-2013.

Jongejans, L. L., Liebner, S., Knoblauch, C., Mangelsdorf, K., Ulrich, M., Grosse, G., et al. (2021). Greenhouse gas production and lipid biomarker distribution in Yedoma and Alas thermokarst lake sediments in Eastern Siberia. *Glob. Change Biol.* 27, 2822–2839. doi:10.1111/gcb.15566.

Jongejans, L. L., Strauss, J., Lenz, J., Peterse, F., Mangelsdorf, K., Fuchs, M., et al. (2018). Organic matter characteristics in yedoma and thermokarst deposits on Baldwin Peninsula, west Alaska. *Biogeosciences* 15, 6033–6048. doi:10.5194/bg-15-6033-2018.

Keeling, C. D. (1958). The concentration and isotopic abundances of atmospheric carbon dioxide in rural areas. Geochim. Cosmochim. Acta 13, 322–334. doi:10.1016/0016-7037(58)90033-4.

Knoblauch, C., Beer, C., Sosnin, A., Wagner, D., and Pfeiffer, E.-M. (2013). Predicting long-term carbon mineralization and trace gas production from thawing permafrost of Northeast Siberia. *Glob. Change Biol.* 19, 1160–1172. doi:10.1111/gcb.12116.

Kohler, P., Fischer, H., Schmitt, J., and Munhoven, G. (2006). On the application and interpretation of Keeling plots in paleo climate research – deciphering $\delta^{13}C$ of atmospheric CO_2 measured in ice cores. 18.

Kuhry, P., Bárta, J., Blok, D., Elberling, B., Faucherre, S., Hugelius, G., et al. (2020). Lability classification of soil organic matter in the northern permafrost region. *Biogeosciences* 17, 361–379. doi:10.5194/bg-17-361-2020.

Lantuit, H., and Pollard, W. H. (2008). Fifty years of coastal erosion and retrogressive thaw slump activity on Herschel Island, southern Beaufort Sea, Yukon Territory, Canada. *Geomorphology* 95, 84–102. doi:10.1016/j.geomorph.2006.07.040.

Lee, H., Schuur, E. A. G., Inglett, K. S., Lavoie, M., and Chanton, J. P. (2012). The rate of permafrost carbon release under aerobic and anaerobic conditions and its potential effects on climate. *Glob. Change Biol.* 18, 515–527. doi:10.1111/j.1365-2486.2011.02519.x.

Nitzbon, J., Westermann, S., Langer, M., Martin, L. C. P., Strauss, J., Laboor, S., et al. (2020). Fast response of cold ice-rich permafrost in northeast Siberia to a warming climate. *Nat. Commun.* 11, 1–11. doi:10.1038/s41467-020-15725-8.

Pegoraro, E., Mauritz, M., Bracho, R., Ebert, C., Dijkstra, P., Hungate, B. A., et al. (2019). Glucose addition increases the magnitude and decreases the age of soil respired carbon in a long-term permafrost incubation study. *Soil Biol. Biochem.* 129, 201–211. doi:10.1016/j.soilbio.2018.10.009.

Phillips, D. L., and Gregg, J. W. (2003). Source partitioning using stable isotopes: coping with too many sources. *Oecologia* 136, 261–269. doi:10.1007/s00442-003-1218-3.

Pries, C. E. H., Schuur, E. A. G., Natali, S. M., and Crummer, K. G. (2016). Old soil carbon losses increase with ecosystem respiration in experimentally thawed tundra. *Nat. Clim. Change* 6, 214–218. doi:10.1038/nclimate2830.

Ramnarine, R., Wagner-Riddle, C., Dunfield, K. E., and Voroney, R. P. (2012). Contributions of carbonates to soil CO_2 emissions. *Can. J. Soil Sci.* 92, 599–607. doi:10.4141/cjss2011-025.

Raza, S., Miao, N., Wang, P., Ju, X., Chen, Z., Zhou, J., et al. (2020). Dramatic loss of inorganic carbon by nitrogen-induced soil acidification in Chinese croplands. *Glob. Change Biol.* 26, 3738–3751. doi:10.1111/gcb.15101.

Reimer, P. J., Bard, E., Bayliss, A., Beck, J. W., Blackwell, P. G., Ramsey, C. B., et al. (2013). IntCal13 and Marine13 Radiocarbon Age Calibration Curves 0–50,000 Years cal BP. *Radiocarbon* 55, 1869–1887. doi:10.2458/azu_js_rc.55.16947.

Rethemeyer, J., Gierga, M., Heinze, S., Stolz, A., Wotte, A., Wischhöfer, P., et al. (2019). Current Sample Preparation and Analytical Capabilities of the Radiocarbon Laboratory at CologneAMS. *Radiocarbon* 61, 1449–1460. doi:10.1017/RDC.2019.16.

Routh, J., Hugelius, G., Kuhry, P., Filley, T., Tillman, P. K., Becher, M., et al. (2014). Multi-proxy study of soil organic matter dynamics in permafrost peat deposits reveal vulnerability to climate change in the European Russian Arctic. *Chem. Geol.* 368, 104–117. doi:10.1016/j.chemgeo.2013.12.022.

Rovira, P., and Vallejo, V. R. (2008). Changes in δ13C composition of soil carbonates driven by organic matter decomposition in a Mediterranean climate: A field incubation experiment. *Geoderma* 144, 517–534. doi:10.1016/j.geoderma.2008.01.006.

Schädel, C., Bader, M. K.-F., Schuur, E. A. G., Biasi, C., Bracho, R., Čapek, P., et al. (2016). Potential carbon emissions dominated by carbon dioxide from thawed permafrost soils. *Nat. Clim. Change* 6, 950–953. doi:10.1038/nclimate3054.

Schädel, C., Beem-Miller, J., Aziz Rad, M., Crow, S. E., Hicks Pries, C. E., Ernakovich, J., et al. (2020). Decomposability of soil organic matter over time: the Soil Incubation Database (SIDb, version 1.0) and guidance for incubation procedures. *Earth Syst. Sci. Data* 12, 1511–1524. doi:10.5194/essd-12-1511-2020.

Schädel, C., Schuur, E. A. G., Bracho, R., Elberling, B., Knoblauch, C., Lee, H., et al. (2014). Circumpolar assessment of permafrost C quality and its vulnerability over time using long-term incubation data. *Glob. Change Biol.* 20, 641–652. doi:10.1111/gcb.12417.

Schirrmeister, L. (2011). Sedimentary characteristics and origin of the Late Pleistocene Ice Complex on north-east Siberian Arctic coastal lowlands and islands – A review. *Quat. Int.* 241, 3–25. doi:10.1016/j.quaint.2010.04.004.

Schlesinger, W. H. (1985). The formation of caliche in soils of the Mojave Desert, California. *Geochim. Cosmochim. Acta* 49, 57–66. doi:10.1016/0016-7037(85)90191-7.

Schuur, E. a. G., McGuire, A. D., Schädel, C., Grosse, G., Harden, J. W., Hayes, D. J., et al. (2015). Climate change and the permafrost carbon feedback. *Nature* 520, 171–179. doi:10.1038/nature14338.

Schuur, E. A. G., and Trumbore, S. E. (2006). Partitioning sources of soil respiration in boreal black spruce forest using radiocarbon. *Glob. Change Biol.* 12, 165–176. doi:10.1111/j.1365-2486.2005.01066.x.

Schwamborn, G., Rachold, V., and Grigoriev, M. (2002). Late Quaternary sedimentation history of the Lena Delta. *Quat. Int.* 89, 119–134. doi:10.1016/S1040-6182(01)00084-2.

Stapel, J. G., Schirrmeister, L., Overduin, P. P., Wetterich, S., Strauss, J., Horsfield, B., et al. (2016). Microbial lipid signatures and substrate potential of organic matter in permafrost deposits: Implications for future greenhouse gas production. *J. Geophys. Res. Biogeosciences* 121, 2652–2666. doi:10.1002/2016JG003483.

Stapel, J. G., Schwamborn, G., Schirrmeister, L., Horsfield, B., and Mangelsdorf, K. (2018). Substrate potential of last interglacial to Holocene permafrost organic matter for future microbial greenhouse gas production. *Biogeosciences* 15, 1969–1985. doi:10.5194/bg-15-1969-2018.

Stolz, A., Dewald, A., Altenkirch, R., Herb, S., Heinze, S., Schiffer, M., et al. (2017). Radiocarbon measurements of small gaseous samples at CologneAMS. *Nucl. Instrum. Methods Phys. Res. Sect. B Beam Interact. Mater. At.* 406, 283–286. doi:10.1016/j.nimb.2017.03.031.

Strauss, J., Schirrmeister, L., Grosse, G., Fortier, D., Hugelius, G., Knoblauch, C., et al. (2017). Deep Yedoma permafrost: A synthesis of depositional characteristics and carbon vulnerability. *Earth-Sci. Rev.* 172, 75–86. doi:10.1016/j.earscirev.2017.07.007.

Strauss, J., Schirrmeister, L., Mangelsdorf, K., Eichhorn, L., Wetterich, S., and Herzschuh, U. (2015). Organic-matter quality of deep permafrost carbon – a study from Arctic Siberia. *Biogeosciences* 12, 2227–2245. doi:10.5194/bg-12-2227-2015.

Stuiver, M., and Polach, M. A. (1977). On the reporting of ^{14}C ages. *Radiocarbon 19*, 355-359.

Tamir, G., Shenker, M., Heller, H., Bloom, P. R., Fine, P., and Bar-Tal, A. (2011). Can Soil Carbonate Dissolution Lead to Overestimation of Soil Respiration? *Soil Sci. Soc. Am. J.* 75, 1414–1422. doi:10.2136/sssaj2010.0396.

Tamir, G., Shenker, M., Heller, H., Bloom, P. R., Fine, P., and Bar-Tal, A. (2012). Dissolution and Re-crystallization Processes of Active Calcium Carbonate in Soil Developed on Tufa. *Soil Sci. Soc. Am. J.* 76, 1606–1613. doi:10.2136/sssaj2012.0041.

Tanski, G., Lantuit, H., Ruttor, S., Knoblauch, C., Radosavljevic, B., Strauss, J., et al. (2017). Transformation of terrestrial organic matter along thermokarst-affected permafrost coasts in the Arctic. *Sci. Total Environ.* 581–582, 434–447. doi:10.1016/j.scitotenv.2016.12.152.

Turetsky, M. R., Abbott, B. W., Jones, M. C., Anthony, K. W., Olefeldt, D., Schuur, E. A. G., et al. (2020). Carbon release through abrupt permafrost thaw. *Nat. Geosci.* 13, 138–143. doi:10.1038/s41561-019-0526-0.

Wacker, L., Němec, M., and Bourquin, J. (2010). A revolutionary graphitisation system: Fully automated, compact and simple. *Nucl. Instrum. Methods Phys. Res. Sect. B Beam Interact. Mater. At.* 268, 931-934. doi: 10.1016/j.nimb.2009.10.067.

Walz, J., Knoblauch, C., Tigges, R., Opel, T., Schirrmeister, L., and Pfeiffer, E.-M. (2018). Greenhouse gas production in degrading ice-rich permafrost deposits in northeastern Siberia. *Biogeosciences* 15, 5423–5436. doi:10.5194/bg-15-5423-2018.

Weber, J.N., Bergenback, R.E., Williams, E.G. and Keith, M.L. (1965). Reconstruction of depositional environments in the Pennsylvanian Vanport basin by carbon isotope ratios. *Journal of Sedimentary Petrology* 35, 36-48. doi:10.1306/74D711EA-2B21-11D7-8648000102C1865D

Weiss, N., Blok, D., Elberling, B., Hugelius, G., Jørgensen, C. J., Siewert, M. B., et al. (2016). Thermokarst dynamics and soil organic matter characteristics controlling initial carbon release from permafrost soils in the Siberian Yedoma region. *Sediment. Geol.* 340, 38–48. doi:10.1016/j.sedgeo.2015.12.004.

Wetterich, S., Kuzmina, S., Andreev, A. A., Kienast, F., Meyer, H., Schirrmeister, L., et al. (2008a). Palaeoenvironmental dynamics inferred from late Quaternary permafrost deposits on Kurungnakh Island, Lena Delta, Northeast Siberia, Russia. *Quat. Sci. Rev.* 27, 1523–1540. doi:10.1016/j.quascirev.2008.04.007.

Wetterich, S., Schirrmeister, L., Meyer, H., Viehberg, F. A., and Mackensen, A. (2008b). Arctic freshwater ostracods from modern periglacial environments in the Lena River Delta (Siberian Arctic, Russia): geochemical applications for palaeoenvironmental reconstructions. *J. Paleolimnol.* 39, 427–449. doi:10.1007/s10933-007-9122-1.

Wild, B., Gentsch, N., Čapek, P., Diáková, K., Alves, R. J. E., Bárta, J., et al. (2016). Plant-derived compounds stimulate the decomposition of organic matter in arctic permafrost soils. *Sci. Rep.* 6, 25607. doi:10.1038/srep25607.

Windirsch, T., Grosse, G., Ulrich, M., Schirrmeister, L., Fedorov, A. N., Konstantinov, P. Y., et al. (2020). Organic carbon characteristics in ice-rich permafrost in alas and Yedoma deposits, central Yakutia, Siberia. *Biogeosciences* 17, 3797–3814. doi:10.5194/bg-17-3797-2020.

Wotte, A., Wischhöfer, P., Wacker, L., and Rethemeyer, J. (2017). 14CO2 analysis of soil gas: Evaluation of sample size limits and sampling devices. *Nucl. Instrum. Methods Phys. Res. Sect. B Beam Interact. Mater. At.* 413, 51–56. doi:10.1016/j.nimb.2017.10.009.

Zimov, S. A., Davydov, S. P., Zimova, G. M., Davydova, A. I., Schuur, E. A. G., Dutta, K., et al. (2006). Permafrost carbon: Stock and decomposability of a globally significant carbon pool. *Geophys. Res. Lett.* 33, L20502. doi:10.1029/2006GL027484.

Zolkos, S., Tank, S. E., and Kokelj, S. V. (2018). Mineral Weathering and the Permafrost Carbon-Climate Feedback. *Geophys. Res. Lett.* 45, 9623–9632. doi:10.1029/2018GL078748.

Zolkos, S., Tank, S. E., Striegl, R. G., Kokelj, S. V., Kokoszka, J., Estop-Aragonés, C., et al. (2020). Thermokarst amplifies fluvial inorganic carbon cycling and export across

watershed scales on the Peel Plateau, Canada. *Biogeosciences* 17, 5163–5182. doi:10.5194/bg-17-5163-2020.

Supplementary Table S1: Bulk sediment parameters in the thaw mounds (TM1, TM2), thaw slump floor (SF3) and Holocene terrace (HT1).

Site	Depth [cm]	Lab ID	$F^{14}C_{IC}$ ± 1σ	$\delta^{13}C_{IC}$ [‰]*1	$F^{14}C_{OC}$ ± 1σ	$\delta^{13}C_{OC}$ [‰]*1,2	pH	IC [wt.%]	OC [wt.%]	N [wt.%]	OC/N
TM1	0-10	COL5258	-	-4.9 ± 0.1	0.215 ± 0.002	-26.0 ± 0.1	7.9	0.2 ± 0.2	2.1 ± 0.2	0.16 ± 0.01	12.7 ± 1.4
	10-20	COL5259	0.050 ± 0.003	-6.0 ± 0.1	0.042 ± 0.001	-25.9 ± 0.2	8.2	0.4 ± 0.4	1.8 ± 0.1	0.19 ± 0.02	9.5 ± 1.2
	20-30	COL5260	-	-7.2 ± 0.2	0.026 ± 0.001	-26.1 ± 0.1	8.2	0.4 ± 0.2	1.9 ± 0.1	0.19 ± 0.02	10.0 ± 1.1
	30-40	COL5261	-	-5.3 ± 0.2	0.035 ± 0.001	-26.2 ± 0.2	8.1	0.2 ± 0.1	2.2 ± 0.1	0.20 ± 0.02	10.6 ± 1.2
	40-50	COL5262	0.043 ± 0.003	-6.9 ± 0.1	0.030 ± 0.001	-26.0 ± 0.1	7.9	0.3 ± 0.5	2.3 ± 0.2	0.22 ± 0.02	10.8 ± 1.6
	50-60	COL5263	-	-7.0 ± 0.1	0.023 ± 0.001	-26.0 ± 0.1	7.6	0.3 ± 0.3	2.6 ± 0.1	0.23 ± 0.01	11.4 ± 0.7
	60-70	COL5264	-	-11.6 ± 0.1	0.016 ± 0.001	-25.6 ± 0.3	7.9	0.2 ± 0.1	3.3 ± 0.1	0.31 ± 0.01	10.5 ± 0.2
	70-80	COL5265	-	-19.1 ± 0.1	0.007 ± 0.001	-26.1 ± 0.6	7.7	0.1 ± 0.1	3.3 ± 0.1	0.31 ± 0.01	10.7 ± 0.2
	80-90	COL5266	-	-19.6 ± 0.1	0.007 ± 0.001	-25.9 ± 0.2	6.8	0.0 ± 0.4	7.8 ± 0.4	0.58 ± 0.01	13.5 ± 0.7
TM2	0-10	COL5999	0.056 ± 0.001	-5.3 ± 0.1	0.109 ± 0.001	-25.3	7.6	0.7 ± 0.4	2.0 ± 0.1	0.19 ± 0.02	10.4 ± 1.1
	10-20	COL6000	0.055 ± 0.004	-4.5 ± 0.1	0.029 ± 0.001	-25.5	7.8	0.7 ± 0.3	1.5 ± 0.2	0.17 ± 0.02	8.9 ± 1.3
	20-30	COL6001	0.057 ± 0.004	-7.0 ± 0.1	0.027 ± 0.001	-30.8	7.3	0.5 ± 0.4	1.9 ± 0.1	0.18 ± 0.02	10.3 ± 1.3
	30-40	COL6002	0.044 ± 0.004	-5.4 ± 0.1	0.023 ± 0.001	-29.0	7.3	0.6 ± 0.2	1.0 ± 0.1	0.13 ± 0.00	7.8 ± 0.4
	40-50	COL6003	0.038 ± 0.004	-4.6 ± 0.1	0.025 ± 0.001	-25.7	7.3	0.8 ± 0.4	1.6 ± 0.3	0.17 ± 0.00	9.1 ± 1.5
	50-60	COL6004	0.019 ± 0.001	-5.2 ± 0.1	0.025 ± 0.001	-25.5	7.3	0.5 ± 0.2	1.4 ± 0.2	0.13 ± 0.00	11.0 ± 1.3
	60-70	COL6005	0.035 ± 0.004	-5.2 ± 0.1	0.028 ± 0.001	-26.1	6.4	0.8 ± 0.5	1.1 ± 0.0	0.12 ± 0.05	9.1 ± 1.5
SF3	0-10	COL6006	0.812 ± 0.009	-12.8 ± 0.1	0.844 ± 0.012	-28.5	5.8	1.9 ± 1.2	4.4 ± 0.6	0.31 ± 0.02	13.9 ± 2.1
	10-20	COL6007	0.668 ± 0.010	-10.8 ± 0.1	0.664 ± 0.012	-27.5	5.5	1.1 ± 0.8	4.2 ± 0.4	0.32 ± 0.03	12.9 ± 1.6
	20-30	COL6008	0.593 ± 0.008	-9.1 ± 0.1	0.608 ± 0.012	-28.0	5.1	0.2 ± 1.5	3.9 ± 1.3	0.22 ± 0.03	17.4 ± 6.2
	30-40	COL6009	0.179 ± 0.003	-11.8 ± 0.1	0.829 ± 0.012	-27.9	6.1	2.8 ± 0.5	5.5 ± 0.1	0.33 ± 0.03	16.6 ± 1.5
	40-50	COL6010	0.764 ± 0.010	-10.2 ± 0.1	0.789 ± 0.012	-27.7	5.5	2.2 ± 1.2	5.5 ± 0.1	0.37 ± 0.05	15.0 ± 2.1
	50-60	COL6011	0.609 ± 0.007	-9.6 ± 0.1	0.607 ± 0.012	-32.3	4.9	0.7 ± 0.4	4.3 ± 0.1	0.28 ± 0.02	15.4 ± 1.0
HT1	+8	COL6014	-	-	1.149 ± 0.012	-27.2	4.5	-	9.2 ± 6.0	0.44 ± 0.01	37.6 ± 0.4
	0-11	COL6012	-	-	0.946 ± 0.012	-27.4	5.8	-	9.7 ± 0.4	0.70 ± 0.00	14.0 ± 0.6
	11-17	COL6013	-	-	0.597 ± 0.012	-29.4	4.3	-	3.0 ± 0.1	0.17 ± 0.02	17.8 ± 2.1

***1 [‰ VPDB]; *2 n = 1 for TM2, SF3, HT1**

Supplementary Table S2: Measured (s) and contamination corrected (c) $\delta^{13}C$, $F^{14}C$ values and conventional ^{14}C ages of CO_2 emissions and and atmospheric sample (Atm) as well as surface CO_2 fluxes.

Site	Lab ID	$F^{14}C_s \pm 1\sigma$	$F^{14}C_c \pm 1\sigma$	Age (yrs BP)	$\delta^{13}C_s$ [‰ VPDB]	$\delta^{13}C_c$ [‰ VPDB] (n=1 per site)	Flux [g CO_2 m^{-2} d^{-1}]
TM2	COL5014	0.419 ± 0.004	0.242 ± 0.001	11400 ± 120	-19.8 ± 0.1		12.3
	COL5015	0.234 ± 0.003	0.230 ± 0.001	11800 ± 170	-23.1 ± 0.1	-23.1 ± 0.6	6.7
	COL5016	0.583 ± 0.005	0.329 ± 0.002	8940 ± 90	-17.7 ± 0.3		2.7
SF3	COL5011	0.829 ± 0.007	0.602 ± 0.004	4070 ± 40	-14.9 ± 0.3		7.4
	COL5012	0.689 ± 0.006	0.547 ± 0.002	4850 ± 50	-18.2 ± 0.1	-22.5 ± 0.9	6.1
	COL5013	0.771 ± 0.006	0.716 ± 0.001	2690 ± 30	-19.9 ± 0.3		11.6
HT1	COL5017	1.002 ± 0.007	0.985 ± 0.003	120 ± 5	-18.4 ± 0.2		2.0
	COL5018	1.004 ± 0.008	0.967 ± 0.005	270 ± 5	-14.2 ± 0.3	-27.0 ± 1.7	0.8
	COL5019	1.010 ± 0.008	0.975 ± 0.006	210 ± 5	-13.0 ± 0.1		0.9
Atm	COL5025	1.021 ± 0.008	-	present	-8.4 ± 0.3	-	-

Supplementary Table S3: ^{13}C and ^{14}C contents of CO_2 with daily and normalized CO_2 production during the incubation (means + std. dev).

		1st incubation period				2nd incubation period			
Site	**Depth [cm]**	**$\delta^{13}C \pm 1\sigma$ [‰ vs. VPDB]**	**$F^{14}C \pm 1\sigma$**	**µg CO_2-C g dw^{-1} d^{-1}**	**g CO_2-C kg C^{-1} d^{-1}**	**$\delta^{13}C \pm 1\sigma$ [‰ vs. VPDB]**	**$F^{14}C \pm 1\sigma$**	**µg CO_2-C g dw^{-1} d^{-1}**	**g CO_2-C kg C^{-1} d^{-1}**
TM2	0-10	-23.4 ± 0.6	0.188 ± 0.131	0.41 ± 0.09	0.021 ± 0.001	-21.6 ± 1.0	0.138 ± 0.088	0.28 ± 0.06	0.014 ± 0.002
	10-20	-22.0 ± 2.3	0.172 ± 0.023	0.48 ± 0.24	0.027 ± 0.009	-21.1 ± 1.5	0.124 ± 0.010	0.36 ± 0.11	0.020 ± 0.006
	20-40	-22.8 ± 0.3	0.147 ± 0.012	0.76 ± 0.15	0.037 ± 0.006	-22.9 ± 0.6	0.077 ± 0.009	0.55 ± 0.06	0.027 ± 0.003
	40-70	-23.9 ± 1.2	0.171 ± 0.017	0.51 ± 0.08	0.033 ± 0.003	-21.9 ± 1.7	0.110 ± 0.064	0.39 ± 0.04	0.025 ± 0.002
SF3	0-10	-24.0 ± 2.2	0.717 ± 0.175	2.31 ± 1.47	0.047 ± 0.014	-25.0 ± 2.9	0.741 ± 0.209	1.53 ± 0.70	0.031 ± 0.010
	10-20	-24.6 ± 2.0	0.718 ± 0.118	2.85 ± 1.09	0.052 ± 0.012	-25.6 ± 2.4	0.762 ± 0.061	1.90 ± 0.61	0.035 ± 0.011
	20-40	-19.5 ± 1.4	0.702 ± 0.029	1.18 ± 0.92	0.027 ± 0.015	-24.2 ± 2.0	0.701 ± 0.050	0.89 ± 0.55	0.020 ± 0.014
	40-60	-23.3 ± 1.9	0.585 ± 0.035	2.02 ± 0.10	0.052 ± 0.002	-25.4 ± 1.7	0.652 ± 0.033	1.48 ± 0.20	0.038 ± 0.005
HT1	0-11	-27.0 ± 1.5	1.011 ± 0.003	7.54 ± 1.70	0.093 ± 0.009	-27.3 ± 0.3	1.016 ± 0.003	6.68 ± 0.95	0.065 ± 0.009
	11-17	-26.3 ± 2.5	0.859 ± 0.027	0.55 ± 0.24	0.015 ± 0.002	-28.5 ± 1.5	0.864 ± 0.011	0.51 ± 0.06	0.015 ± 0.001

Supplementary Table S4: Absolute C released (means + std. dev.) calculated from min. and max. distributions of the mass balance approach.

Site	Depth [cm]	Minimum absolute produced CO_2			Maximum absolute produced CO_2		
		OCa	OCy	IC	OCa	OCy	IC
		175 days of incubation [g CO_2-C kgC^{-1}]					
TM2	0-10	2.14 ± 0.06	0.11 ± 0.01	0.87 ± 0.03	2.91 ± 0.09	0.84 ± 0.02	0.94 ± 0.03
	10-20	2.75 ± 0.72	0.14 ± 0.04	1.12 ± 0.29	3.73 ± 0.97	1.07 ± 0.28	1.21 ± 0.32
	20-40	3.85 ± 0.48	0.20 ± 0.02	1.57 ± 0.19	5.22 ± 0.65	1.50 ± 0.19	1.70 ± 0.21
	40-70	3.46 ± 0.28	0.18 ± 0.01	1.41 ± 0.11	4.68 ± 0.38	1.35 ± 0.11	1.52 ± 0.12
SF3	0-10	0	4.64 ± 1.12	1.99 ± 0.48	1.66 ± 0.40	6.14 ± 1.49	2.16 ± 0.52
	10-20	0	5.14 ± 0.93	2.20 ± 0.40	1.84 ± 0.33	6.79 ± 1.23	2.39 ± 0.43
	20-40	0	2.64 ± 1.23	1.13 ± 0.53	0.94 ± 0.44	3.49 ± 1.62	1.22 ± 0.57
	40-60	0	5.14 ± 0.16	2.20 ± 0.07	1.84 ± 0.06	6.79 ± 0.22	2.39 ± 0.08
		537 days of incubation [g CO_2-C kgC^{-1}]					
TM2	0-10	4.59 ± 0.40	0	1.66 ± 0.15	5.87 ± 0.51	1.28 ± 0.11	1.66 ± 0.15
	10-20	6.58 ± 1.57	0	2.37 ± 0.57	8.41 ± 2.01	1.83 ± 0.44	2.37 ± 0.57
	20-40	8.77 ± 0.89	0	3.16 ± 0.32	11.22 ± 1.13	2.45 ± 0.25	3.16 ± 0.32
	40-70	8.31 ± 0.64	0	3.00 ± 0.23	10.63 ± 0.82	2.32 ± 0.18	3.00 ± 0.23
SF3	0-10	1.00 ± 0.25	10.21 ± 2.59	1.67 ± 0.42	4.69 ± 1.19	13.56 ± 3.43	2.18 ± 0.55
	10-20	1.13 ± 0.28	11.45 ± 2.84	1.88 ± 0.47	5.26 ± 1.30	15.21 ± 3.77	2.44 ± 0.60
	20-40	0.66 ± 0.36	6.69 ± 3.63	1.10 ± 0.60	3.07 ± 1.67	8.88 ± 4.82	1.43 ± 0.77
	40-60	1.24 ± 0.13	12.59 ± 1.30	2.06 ± 0.21	5.78 ± 0.60	16.72 ± 1.72	2.68 ± 028

Manuscript III: A new setup for ^{14}C analysis of CH_4 at CologneAMS

by

Jan Olaf Melchert[1], Merle Gierga[1], Janet Rethemeyer[1]

[1]Institute for Geology and Mineralogy, University of Cologne, Cologne, Germany

Information regarding the acquisition of primary data:

The primary data relevant for this manuscript are stored and accessible on the server of the Institute of Geology and Mineralogy at the University of Cologne.

Jan Olaf Melchert[1], Merle Gierga[1], Janet Rethemeyer[1]

[1]Institute of Geology and Mineralogy, University of Cologne, Cologne, Germany.

Abstract

The radiocarbon analysis of CH_4 required the development of a new sample handling routine and the establishment of a new vacuum system that converts CH_4 to CO_2 for direct measurement with the gas injection system of the AMS at the CologneAMS facility. First tests with multiple series of ^{14}C-free and modern standards, as well with a biogas mixture with sample sizes ranging from 20 to 50 µg C resulted in a CH_4 to CO_2 conversion efficiency of 94 – 97%. Processed standards were further evaluated for contamination with extraneous carbon. With this new set up blank values achieved 0.006 ± 0.003 $F^{14}C$, which is comparable to blank values achieved with our routinely used CO_2 vacuum system. With the processed standard series, we were able to quantify a low contribution of 0.26 ± 0.13 µg modern and 0.33 ± 0.12 µg dead exogenous carbon, respectively, for the new system. Both sources of contamination resulted in 0.58 ± 0.18 µg of extraneous C, introduced during sample handling and pre-treatment, with a corresponding $F^{14}C$ of 0.447 ± 0.245. First tests with a near modern CH_4:CO_2 biogas mixture delivered reproducible results with a ^{14}C content of 0.978 – 1.010 $F^{14}C$, after applying the correction for extraneously introduced carbon.

Introduction

The global atmospheric methane (CH_4) concentration doubled since the 19th century and is increasing even more rapidly since 2007 (Kirschke et al., 2013; Turner et al., 2017). Besides carbon dioxide (CO_2), methane is considered to be the second most important greenhouse gas with a 20-fold warming potential (Milich, 1999). The atmosphere balances CH_4 emissions from other terrestrial or aquatic sources, thus acting as a CH_4 sink. In general, there are three main categories of CH_4 sources: Biogenic (methanogenic microbes), thermogenic (geological processes) and pyrogenic (incomplete combustion of biomass through wildfires and fuels) sources release CH_4 with characteristic ^{13}C and ^{14}C isotopic signatures. Methanogenic microorganisms, for example, produce CH_4 that is depleted in its ^{13}C content and likely enriched in its ^{14}C content, whereas thermogenic CH_4, produced over millions of years, would contain more ^{13}C compared to biogenic sources and no ^{14}C. While the sources of CH_4 contributing to the atmosphere are generally known, it is still uncertain to which extent individual carbon (C) sources are contributing to the CH_4 budget (Kirschke et al., 2013). Numerous studies have been conducted over the last years, analysing CH_4 emissions to distinguish between C sources based on ^{14}C content directly from the atmosphere (Graven et al., 2019), peatlands (Garnett et al., 2016; Cooper et al., 2017) or aquatic environments (Pohlman et al., 2009; Joung et al., 2019).

Gas samples taken from the environment or even from laboratory incubations contain other C carrying gases that need to be separated from CH_4, by utilizing carrier gases (noble gas or synthetic air, Pohlman et al., 2009) or pressure differences (Garnett et al., 2019) by which the sample is moved. The CH_4 separation during sample processing may be achieved through chemical adsorbents (Garnett et al., 2019), cryogenic traps (Petrenko et al., 2008; Pack et al., 2015), oxidation furnaces (Pack et al., 2015) or a combination of those (Garnett et al., 2019), in order to perform a meaningful C-isotope analysis. The approach presented in this study utilizes a combination of methods taken from recent studies. The sample is flushed through a set of cryogenic traps and an oxidation furnace, using a carrier gas at reduced pressure.

Environmental gas samples most prominently contain CO_2, and water (H_2O), but also carbon monoxide (CO) and other hydrocarbon gases in smaller quantities. As these gases are potentially emitted from different organic or inorganic sources and therefore feature different isotopic compositions, it is necessary to separate them (Petrenko et al., 2008). H_2O is removed by using dry ice slurries (DI) or adsorbents (Garnett et al., 2019) while CO_2 is fixated at low temperatures by utilizing liquid nitrogen (LN, Petrenko et al., 2008; Pack et al., 2015) or adsorbed through molecular sieves containing zeolite (Garnett et al., 2019). Ultimately, the purified CH_4 is oxidized in a furnace with an oxygen donor and converted to CO_2 and H_2O. The choice of the catalyst varies from laboratory to laboratory. Most prominently, cupric oxide (CuO) filled columns (Kessler and Reeburgh, 2005; Pack et al., 2015), platinized alumina beads contained in quartz glass tubes (Garnett et al., 2019) or platinized quartz wool are used as catalysts (Petrenko et al., 2008; Sparrow and Kessler, 2017). After the reaction, the CH_4 derived CO_2 can be quantified and prepared for ^{14}C analysis via gas injection (Stolz et al., 2017) or graphitization.

Here we present a new setup for the purification and conversion of CH_4 samples to CO_2 at the CologneAMS facility. Gas samples are flushed with synthetic air at reduced pressures through cryogenic traps, separating CH_4 from other gases and subsequently oxidized to CO_2 for ^{14}C analysis using a gas ion source. We performed tests with different standards including a modern CH_4:CO_2 biogas mixture, as well as ^{14}C-free CH_4 mixed with ^{14}C-enriched CO_2 to quantify the trapping efficiency and CH_4 to CO_2 conversion and recovery rates. With this setup sample injection, purification and oxidation, as well as sealing for AMS analysis, is possible in less than 1 h.

Methods

System overview

The new CH_4 oxidation system consists of three units (Fig. 1): (1) the mixing unit, where samples or standard gas mixtures are prepared and injected via the gas supplies. (2) The purification unit consists of furnaces and cryotraps to separate and trap gases in order to isolate CH_4. (3) The sealing unit consists of pressure transducers (PKR 361, Pfeiffer© Vacuum, Germany; Baratron® 628B, MKS Instruments Deutschland GmbH, Germany), a series of calibrated volumes, and ultra-torr fittings equipped with glass ampoules where the sample can be quantified and CO_2 aliquots corresponding to 20 - 50 µg C are sealed off for subsequent AMS measurement.

The mixing unit (Fig. 1) was built to handle gases from different containers (i.e., gas cylinders, serum bottles or vials). Each connection is individually maintainable by a respective valve allowing the injection and mixing of defined volumes of gas mixtures. CH_4 and CO_2 are supplied either in small pressurized 15 l bottles that are directly connected to the mixing unit with a pressure regulator and regular ferrule fittings (Swagelok®, USA) from a self-assembled stainless-steel cylinder (304L-HDF4-1GAL, Swagelok®, USA), that is equipped with a pressure gauge (-1 – 3 bar, PGI-63B-BC3-LAQX, Swagelok®, USA) and sept port (SS-4-TA-1-4STKZ, Swagelok®, USA), or the gases are taken from sealed serum bottles. Similar to the sample cylinder, a sept port (S, Fig.1) is used for syringe injection of gases at the mixing unit. Gases are injected with a 10 ml gas tight syringe (Gastight 1010 LTN, Hamilton®, USA). In order to mix bottled gas with gases from the syringe, a 2.5 ml stainless-steel vacuum syringe (S_V, Fig.1, KDScientific Inc., USA), featuring a screw thread for standard vacuum fittings was installed permanently next to the syringe port in order to quantify and temporarily hold injected volumes. The valves are permanently regulating the gas flow so that a gas stream of 60 ml min^{-1} cannot be exceeded. The flow is permanently monitored by a flow meter (F, Fig.1-, FMA-1606, Omega™ Engineering Inc., USA) that is installed prior to the purification unit of the oxidation rig.

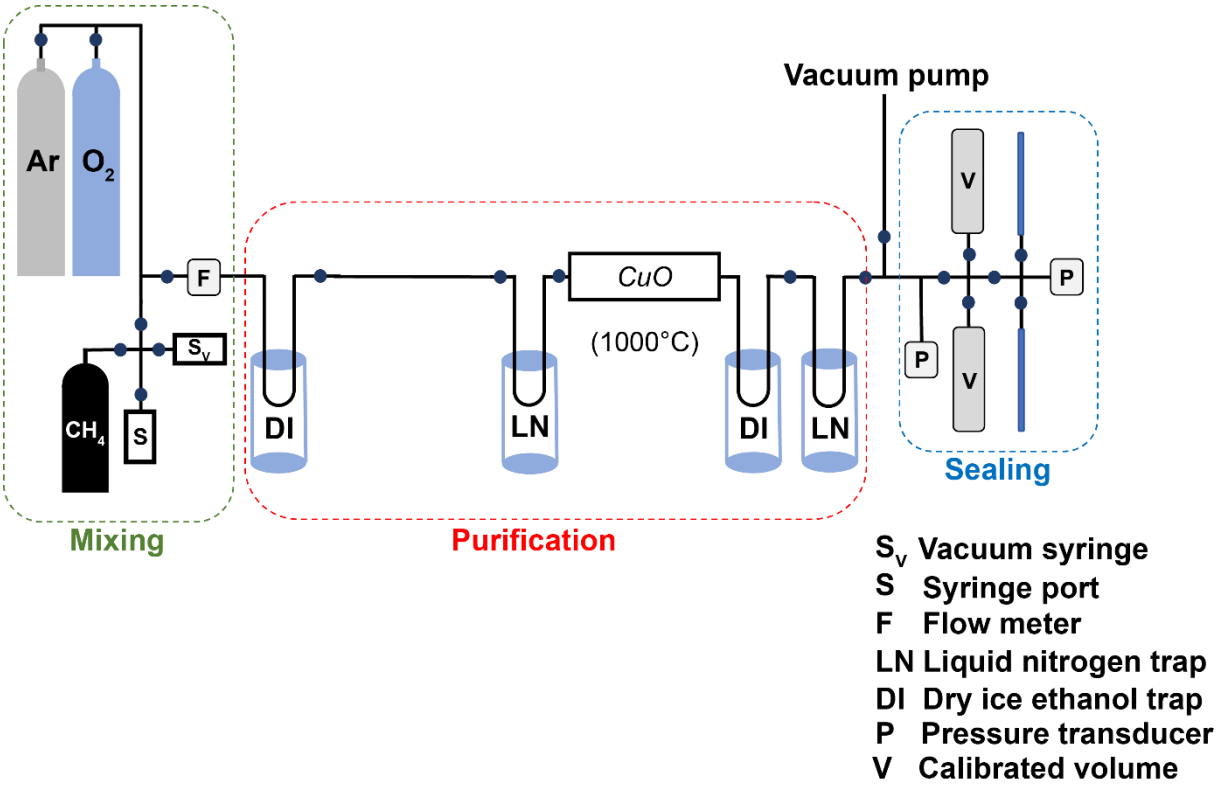

Figure 1: Schematic overview of the oxidation rig, consisting of the mixing (green), purification (red) and sealing (blue) units.

A tube furnace was installed in line with the cryogenic traps that oxidizes CH_4 to H_2O and CO_2 (red frame, Fig. 1). Gases are flushed from the mixing unit through two U-shaped tubes. The first U-tube is submerged in a Dewar flask filled with DI that immobilizes any excess moisture, while the second U-tube is submerged in a Dewar flask filled with LN to immobilize any CO_2 from the gas stream. Subsequently, the gas stream enters the furnace (Carbolite Gero GmbH & Co. KG) with a CuO filled quartz glass tube and is heated to 1000°C in order to oxidize CH_4 to CO_2. In a final set of cryogenic traps H_2O and CO_2 are collected within U-tubes submerged in DI and LN, respectively. Any non-reactive and non-condensable gases left in the gas stream are now evacuated through the vacuum pump and the isolated CO_2 is transferred to the sealing unit.

The sealing unit (blue frame, Fig. 1) is constructed like a standard vacuum rig with pressure transducers, calibrated volumes, and ultra-torr fittings equipped with glass ampoules (4 or 6 mm OD), that are used to seal CO_2 samples (Wotte et al., 2017). The sample CO_2 is trapped into one of the calibrated volumes by applying a LN filled Dewar flask. After transferring the CO_2 into the calibrated volume, valves are shut, and the LN is removed to mobilize the gas. The evolving gas builds up pressure that can be directly related to the amount of C. Defined amounts of CO_2 can be transferred to a second calibrated volume by applying LN. These aliquots can be further used for AMS analysis after transferring them to the glass ampoules.

While the CO_2 is still immobilized inside the glass ampoule submerged in LN, the valves to the vacuum pump are briefly opened and non-condensable gases are removed. After this evacuation, glass ampoules are sealed with a hand-torch.

Setup maintenance and preparation

Prior to sample processing, the tube furnace is heated up to 1000°C and maintained at this temperature for 30 minutes to ensure that the CuO filled quartz glass tubes are heated up, as well. The mixing and purification units of the system are flushed three times with 40 ml min^{-1} argon (Ar) gas for 10 min and evacuated afterwards below 10^{-3} mbar. This is done prior and in between samples to maintain a low line blank and prevent memory effects (Pack et al., 2015). After the third evacuation, synthetic air is set up to flow at a rate of 10 ml min^{-1} during the entire sample preparation procedure. This is monitored with the flow meter that is installed at the beginning of the purification unit. With the synthetic air being set up, a pressure of < 20 mbar is maintained throughout the sample processing. A pressure of <20 mbar still allows the fixation and removal of other hydrocarbon gases from the gas phase into the LN trap but more importantly prevents the condensation of oxygen, which might pose a safety hazard (Sparrow and Kessler, 2017). The rightmost part of the system, which is used for sample quantification and sealing is not flushed and kept at a constant vacuum below 10^{-7} mbar to maintain cleanliness.

Depending on the type of sample or standard that needs to be handled, different injection and mixing procedures are possible at the mixing unit of the oxidation rig that will be addressed individually in more detail in the following. All samples and standards were treated similarly after injection. Injected gas mixtures are transported with the synthetic air stream from the mixing unit through the furnaces and cryogenic traps installed at the purification unit into the calibrated volumes and glass ampoules at the sealing unit.

Preparation of standards

Different types of standards were prepared to test the overall cleanliness of the setup, as well as the trapping efficiency and the CH_4 to CO_2 conversion rate of the oxidation rig. In a first test run, the overall C-blank of the line was tested by preparing pure, C-free N_2 gas with the system. The N_2 (99.999% purity, Linde GmbH, Germany) was filled via a Teflon tube attached to sterile injection needles (Sterican® size 18, B.Braun SE, Germany) into 100 ml serum bottles, sealed with crimped butyl rubber stoppers. A second injection needle was inserted into the butyl stopper as an escape opening for the ambient air sealed into the bottle during crimping. The serum bottles were washed with Milli-Q water (MQ; Millipore, USA) water and subsequently combusted at 450°C for 3 hours in a muffle furnace prior to usage. The butyl stoppers were washed with MQ water. The bottles were flushed at ambient pressure with N_2 at ambient

pressure with at least three bottle volumes in order to ensure that no ambient air remained inside. A 10 ml gas tight syringe, that was pre-cleaned with dichloromethane (DCM; SupraSolv®, MERCK KGaA, Germany) to remove residual lubricants, was used to extract 10 ml N_2 from the sealed serum bottle in order to inject the N_2 gas into the oxidation rig via the sept port (S, Fig. 1).

^{14}C-enriched CO_2 standards (Ox-II; NIST SRM 4990C; nominal value 1.3407 $F^{14}C$) were prepared with sealed tube combustion of oxalic acid crystals according to the methods described in Melchert et al. (2019). In summary, oxalic acid powder equalling 3 mg of C was weighed into DCM-cleaned Sn boats (4 x 4 x 11 mm, Elementar, Germany) and transferred into quartz tubes (MQ-washed and pre-combusted at 900°C) along with CuO as a combustion catalyst. The filled quartz tubes were then evacuated at a vacuum rig below 10^{-3} mbar and sealed using a blow torch. Subsequently, the sealed quartz tubes were combusted at 900°C for 4 hours in the muffle furnace to oxidize the oxalic acid to CO_2. The quartz tubes with the Ox-II derived CO_2 were left to cool down after combustion, wiped with acetone (PESTINORM® SUPRA TRACE, grade ≥99.9%, VWR® chemicals, Germany) and put in a tube cracker at our vacuum rig, where they were cracked under a stream of He. The CO_2 was flushed with the He stream through a dry-ice ethanol slurry to remove any excess moisture and then through a LN-filled cryotrap to fixate the CO_2. Using calibrated volumes with pressure reading inside the vacuum rig, the amount of CO_2 was quantified and sealed off in a smaller glass ampoule. Afterwards, the glass ampoule containing the CO_2 standard was carefully inserted inside a 100 ml serum bottle, sealed with a butyl stopper and flushed with 40 ml min^{-1} of He for 10 min via injection needles at ambient pressure. After flushing, the needles were removed, and the serum bottle was thoroughly shaken to break the glass ampoule inside in order to release the CO_2. Lastly, a 10 ml aliquot of the CO_2:He mixture was extracted using the gas tight syringe and injected into the oxidation rig via the syringe port.

Bottled ^{14}C-free CH_4 (99.995% purity, Westfalen AG, Germany) was connected to the mixing unit of the oxidation rig and 2 ml were injected at ambient pressure as a radiocarbon free standard and, in a second series, mixed with ^{14}C-enriched CO_2 from oxalic acid. With this second series we tested the efficiency to trap CO_2 that does not originate from CH_4 and separate it from CH_4-derived CO_2. A ratio of 2 ml CH_4 to 10 ml of He:CO_2 gas mixture was injected to provide a sensitive measure for the separation of ^{14}C-free CO_2 derived from CH_4 and ^{14}C-enriched CO_2 originated from Ox-II. Therefore, the synthetic air stream was closed, and the mixing unit was evacuated until no mass flow was readable anymore on the flow meter. Then, the CH_4 bottle was opened and set up at 1 bar to fill the 2 ml vacuum syringe. The valve next to the vacuum syringe and the CH_4 supply were then closed, and the system left to evacuate. After no mass flow was readable anymore, the synthetic air stream was opened

again and set up at 10 ml min^{-1}. Up to this point, no cryogenic traps were yet attached and the residual CH_4 was pumped out of the system. 10 ml aliquots of the Ox-II derived CO_2:He mixture were extracted from the 100 ml serum bottles using the gas tight syringe and inserted into the sept port. Dry-ice ethanol slurry and LN were then filled into their respective traps and attached to the U-tubes. Consequently, the valves connecting the vacuum syringes as well as the sept port to the line were opened, and the gases expanded into the system and were flushed through the line with the stream of synthetic air. After the syringes were emptied completely, the valves to the sept port and vacuum syringe were closed and the system left for about 10 minutes with the synthetic air stream open to ensure that the gas mixture has moved completely through the whole setup.

Relatively ^{14}C enriched biogas was collected from a nearby biogas facility (Randkanal Nord; Dormagen, Germany) in a stainless-steel cylinder and used as a near-modern CH_4 laboratory standard. Prior to the gas collection, the cylinder was connected to our vacuum line and the ambient air in the tank was fully evacuated. At the biogas facility, the cylinder was directly connected to one of the maintenance gas outlets via a Teflon coated tube. The cylinder had opening valves on both sides allowing a proper flushing. The valves were opened after connecting the tube so that the gas was allowed to flush through the cylinder for about 5 minutes. The biogas mainly consists of CH_4 and CO_2 among other trace gases (56% CH_4, 44% CO_2, quantified on the oxidation rig). 10 ml aliquots were extracted from the cylinder at ambient pressure by connecting a second valve with sept port to the cylinder and using the gas tight syringe. The gas was then immediately injected into the prepared oxidation rig, similar to the procedure for the previously described Ox-II CO_2 standards.

Quantification of extraneous carbon contributions

Radiocarbon analysis of small samples is sensitive to the introduction of contamination (Santos et al., 2007). It is assumed that the apparent ^{14}C content and the mass of a sample ($F^{14}C_S$, m_S) consist of the real ^{14}C content of the sample and its mass ($F^{14}C_R$, m_R), as well as contribution from extraneously introduced carbon ($F^{14}C_{EXT}$, m_{EXT}):

$$F^{14}C_S * m_S = F^{14}C_R * m_R + F^{14}C_{EXT} * m_{EXT} \quad (1)$$

and $m_R = m_S - m_{EXT}$ (2)

The results of the ^{14}C analysis of different standards were used to calculate two principal contamination pools introduced during pre-treatment and sample injection into the system. A ^{14}C-free ($F^{14}C = 0$) or dead pool is estimated by evaluation of ^{14}C enriched standards and a modern ($F^{14}C = 1.01$) contamination pool by evaluation of ^{14}C-free standards:

$$m_{EXT} = \frac{F^{14}C_s * m_S - F^{14}C_R * m_R}{F^{14}C_{EXT} - F^{14}C_R} \quad (3)$$

Consequently, the two individually calculated pools are combined to a single extraneous carbon pool featuring a mean ^{14}C content of the individually calculated ^{14}C-free (dead) and modern contamination pools (Gierga et al., 2014):

$$F^{14}C_{EXT} = \frac{F^{14}C_{dead} * m_{dead} + F^{14}C_{modern} * m_{modern}}{m_{dead} + m_{modern}} \quad (4)$$

After quantifying m_{dead} and m_{modern} in addition to their respective $F^{14}C$ by evaluating different standards and solving equations (3) and (4), the ^{14}C data obtained from the biogas analysis were corrected for both, modern and dead contamination, by rearranging and solving equations (1) and (2). The associated errors were calculated using Gauss error propagation.

Results and Discussion

In order to test our oxidation system for recovery efficiency, as well as for contamination, a total of 33 aliquots from multiple 2 ml and 10 ml injections, divided into different series, containing between 20 and 50 µg C were processed for AMS analysis. The results of the different series are summarized in figure 2 and table 1.

Table 1: Comparison of different standard series handled on the CH_4 oxidation rig, expected and measured $F^{14}C$ (average value with standard deviation), as well as recovery efficiency.

Sample	***n***	***Expected $F^{14}C_R$***	***Measured $F^{14}C_S \pm 1\sigma$***	***Efficiency [%]***
CH_4:CO_2 (dead:Ox-II)	13	0	0.006 ± 0.006	94.4
CH_4:CO_2 (biogas)	9	~1	0.983 ± 0.016	97.3
CH_4 (dead)	5	0	0.006 ± 0.003	-
CO_2 (Ox-II)	4	1.341	1.331 ± 0.012	-
N_2 (C-free)	5	-	-	-

^{14}C analysis of standards

CO_2 produced from pure ^{14}C-free CH_4 had an average $F^{14}C$ of 0.006 ± 0.003 (n = 5). The same CH_4, that was mixed with Ox-II derived CO_2, resulted the same amount of ^{14}C (0.006 ± 0.006 $F^{14}C$; n = 13). An overview of blank values presented in other studies in comparison to our results is given in table 2. Although the data set is limited, due to the small number of total samples processed, the blank values obtained from these series are comparable to blank standards of a similar size, prepared on our CO_2 vacuum line used for compound specific radiocarbon analysis ($F^{14}C$ 0.005 ± 0.0004; n = 4; Melchert et al., 2019). Compared to other studies, the blank values shown here are higher, however, due to the difference in the measurement of CO_2 vs. graphite, graphite samples usually achieve lower blank values.

Further, our samples that are processed for the direct AMS measurement of CO_2, not graphite, are much smaller. Thus, the blank values are more sensitive to contamination in addition to the higher blank value limitation (Tab. 2). The ^{14}C content of pure CO_2 produced from Ox-II (n = 4) is close to that of the consensus value with a $F^{14}C$ of 1.331 ± 0.012, while the injection of carbon-free N_2 gas resulted no quantifiable amount of C via AMS analysis. This indicates that the system operates without quantifiable leakages. The results of the ^{14}C-enriched CO_2, ^{14}C-free CH_4 and the C-free N_2 injections further indicate that the sample handling, which includes the sealing of gas in serum bottles and transfer of aliquots via syringes, does not introduce severe amounts of contamination.

Estimating extraneous carbon

A first estimate of extraneous C, introduced during sample processing, calculated from the ^{14}C data of standard CH_4 and CO_2, resulted an average of 0.33 ± 0.12 µg C of ^{14}C-free contamination and of 0.26 ± 0.13 µg C of modern contamination. The amount of modern contamination presented here is similar to the modern contamination reported for the oxidation of ^{14}C-free CH_4 in Pack et al. (2015), as well as Sparrow and Kessler (2017). Combined to a single pool of extraneous carbon according to (4), we estimated that on average 0.58 ± 0.18 µg C with a $F^{14}C_{EXT}$ of 0.447 ± 0.245 were introduced during sample processing, which is about twice the amount of contamination assessed from the analysis of ^{14}C-free and modern material, for CH_4 oxidation setup presented by Petrenko et al. (2008). Compared to our CO_2 vacuum system, twice the amount of extraneous C is introduced with about half the ^{14}C content (m_{EXT} = 0.30 ± 0.08 µg C; $F^{14}C_{EXT}$ = 0.93 ± 0.23, Melchert et al., 2019). The pre-treatment for the preparation of Ox-II standards involved more steps compared to the preparation of ^{14}C-free standards and unexpectedly both methods introduced the same amount of contamination. This could either indicate, that during the extra steps of oxalic acid handling no more additional contaminate has been added or that the size of the standards (10 ml Ox-II:He mixture) is too large to be a sensitive indicator for additional contamination. In contrast to our CO_2 vacuum system study, we observed a fraction of ^{14}C-free contamination, which could have been introduced by the butyl stoppers used to seal the serum bottles. After long storage times, Pack et al. (2015) showed that the butyl stoppers introduce old CO_2 by outgassing, which was initially reported by Gao et al. (2014).

Table 2: Overview over blank values and quantified contamination of other studies compared to the data assessed in this study as well as measured (S) and contamination corrected (R) ^{14}C data from biogas analysis (own data are mean values with propagated errors).

Author	$F^{14}C_{dead}$ CH_4	m_{modern} [µg C]	$F^{14}C_{EXT}$	m_{EXT} [µg C]	m_S [µg C]
This study	0.006 ± 0.003	0.3 ± 0.1	0.447 ± 0.245	0.58 ± 0.18	20 - 50
Pack et al. (2015)	0.0016 ± 0.0003	0.4 ± 0.2	-	-	>500
Garnett et al. (2019)	0.0011 – 0.0016	1.9 – 3.8	-	-	>500
Palonen et al. (2017)	0.0006 ± 0.0007*[1]	-	-	-	1000
Petrenko et al. (2008)	0.0022 ± 0.0004	-	0.236 ± 0.162	0.23 ± 0.16	130 - 190
Sparrow & Kessler (2017)	0.0023 ± 0.0007	0.24	-	-	451 - 839
Biogas					
Author	$F^{14}C_S$		$F^{14}C_R$		m_S [µg C]
This study	0.967 – 1.001		0.978 – 1.010		20 - 50
Garnett et al. (2019)	-		0.978 – 0.987*[2]		>500
Palonen et al. (2017)	-		1.045 ± 0.005*[1]		1000

[1] background corrected for 0.004 ± 0.001 $F^{14}C$; *[2] background corrected for 0.0017 $F^{14}C$

However, the injection of pure N_2 gas from sealed serum bottles did not contain any C, which either indicates that the outgassing of butyl only happens after longer storage or is below detection limit of the pressure transducers at the oxidation system. Given that the presented data set is limited, and the uncertainty associated with the ^{14}C content of the contamination is large, the results are merely an estimate that nevertheless shows that the system is operating with a reasonable quality and that sources of contamination are identifiable.

^{14}C analysis of biogas

Near modern biogas was collected at a nearby biogas facility and used as a ^{14}C-enriched in-house CH_4 standard. Buyable CH_4 gas is mostly produced from natural gas and oil residues and is therefore ^{14}C-depleted. Alternatives, that are usable as a modern CH_4 standard are therefore difficult to obtain. The sample sizes ranged from 20 to 50 µg C (n = 9) and resulted a ^{14}C content in the range of 0.967 to 1.001 $F^{14}C$ (Tab. 1 and Tab. 2). The data demonstrate that the ^{14}C analysis of the biogas gives reliable and reproducible results. Further, we observed a small decrease in $F^{14}C$ with decreasing sample size. The estimation of extraneous carbon

from the ^{14}C data of processed standards allows for the correction of our biogas data. After correction the biogas ^{14}C content slightly increased, now ranging from 0.978 to 1.010 $F^{14}C$. Because the presented data are the first tests with this biogas and the ^{14}C content of the biogas changes, depending on the organic matter that was used for its production, we have no distinct reference values (Palonen et al., 2017; Garnett et al., 2019).

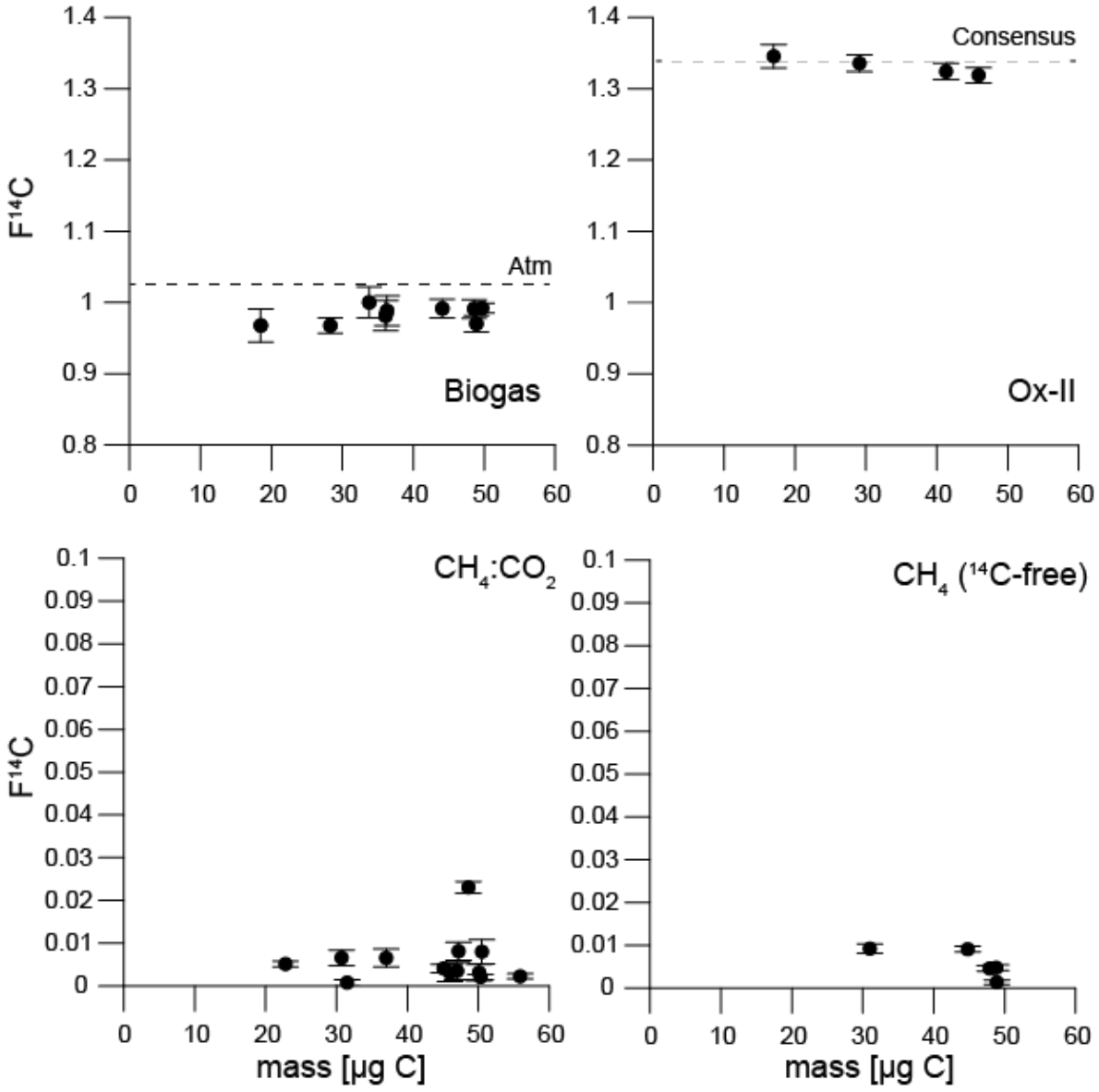

Figure 2: Results of ^{14}C AMS measurements for the biogas mixture, modern standard and ^{14}C-free standard as well as the CH_4:CO_2 gas mixture.

However, other studies present results for the ^{14}C analysis of biogas that yielded data with a comparable ^{14}C content (Tab. 2, Palonen et al., 2017; Garnett et al., 2019).

CH_4 oxidation efficiency and recovery

After the oxidation of pure ^{14}C-free CH_4, about 94.4% of the CH_4 was trapped as CO_2 in the LN trap. The low ^{14}C content of the CH_4:CO_2 gas mixture, which is in agreement with the ^{14}C

content of the pure CH_4 standards, suggests that the separation of CO_2 from CH_4 derived CO_2 is sufficient. The CH_4:CO_2 biogas mixture resulted an even higher recovery of 97.3% CH_4-derived CO_2 after the oxidation. A temporary installation of a second LN trap, as suggested by various authors, did not increase the recovery efficiency, from which we deduced that our traps work sufficiently (Petrenko et al., 2008; Pack et al., 2015; Sparrow and Kessler, 2017). There are small uncertainties associated with the quantification of the oxidation efficiency, because the sample extraction and subsequent injection with the syringe are performed manually, which possibly leads to small losses of sample material during transfer which would decrease the calculated recovery. Furthermore, differences in the oxidation efficiency, or recovery, are likely linked to the type of catalyst and to the packing and compaction of the catalyst inside the oxidation tube (Sparrow and Kessler, 2017). We decided to use CuO rods, because they are easy to handle and cost efficient, moreover, they are already routinely used in our laboratory. Pack et al. (2015) reported a very high oxidation efficiency of about 100% with CuO, while Sparrow and Kessler (2017) exchanged CuO for platinized quartz wool to achieve consistently high efficiencies. The quartz tube that we used to hold the CuO is rather loosely packed over almost the entire length of about 30 cm and fixated on each side with quartz wool, which should allow the gas to heat up properly and react with the catalyst without restricting gas flow.

The injection of pure CO_2 at different flow rates of synthetic air up to 80 ml min^{-1} gave no changes in the amount of CO_2 trapped with LN. The decreasing recovery and precision of samples with increasing flow rates has been assessed by Pack et al. (2015) and was improved by installing an additional CO_2 trap. Achieved flow rates and the pressure inside the system are highly dependent on the scale of the setup, i.e., length and diameter of the used capillaries and components, therefore advise given on optimal setup conditions are, unfortunately, not universally applicable. Decreasing recovery rates might occur at even higher flow rates in our system, which are, however, omitted at our setup to keep the overall pressure inside the system below 200 mbar as explained in the method section.

Conclusion

The first test series and estimations of contamination and error sources of a new CH_4 to CO_2 oxidation system was presented. ^{14}C-depleted CH_4, ^{14}C-enriched CO_2 as well as the mixture of both in addition to a near modern biogas CH_4:CO_2 mixture was processed for AMS analysis at CologneAMS. All samples were in the size range between 20 and 50 µg C. With the given results from the standards, we estimated a dead and modern contamination of about 0.33 ± 0.12 µg C and 0.26 ± 0.13 µg C, respectively. In total 0.58 ± 0.18 µg extraneous carbon with a $F^{14}C$ of 0.447 ± 0.245 are introduced during sample handling. While the large uncertainty associated with the extraneous carbon is most likely caused by the small data set, the results

show that the evaluated background is identifiable. Further tests are however required to quantify background values and contamination pools more thoroughly.

The collection and analysis of near modern biogas resulted precise and reproducible results (0.978 – 1.010 $F^{14}C$) that we were able to correct for the previously estimated extraneous carbon. The CH_4 to CO_2 conversion rate of about 94 – 97% calculated from the ^{14}C-free CH_4 standard and biogas are satisfying. Even higher conversion rates, presented in recent studies (99 – 100%), are likely linked to different types and packing of the oxidation catalyst inside the furnace. Improvements might be achieved in future test runs.

With this study we demonstrate, that the ^{14}C analysis of CH_4 derived CO_2 using the new oxidation vacuum system is operational at CologneAMS. The current pre-treatment methods and handling of a sample within 1h is time efficient, while the usage of CuO catalysts and cryogenic traps instead of chemicals is quite cost efficient. Further tests, as well as the processing of first field samples are planned in the near future.

References

Cooper, M. D. A., Estop-Aragonés, C., Fisher, J. P., Thierry, A., Garnett, M. H., Charman, D. J., et al. (2017). Limited contribution of permafrost carbon to methane release from thawing peatlands. *Nat. Clim. Change* 7, 507–511. doi:10.1038/nclimate3328.

Gao, P., Xu, X., Zhou, L., Pack, M. A., Griffin, S., Santos, G. M., et al. (2014). Rapid sample preparation of dissolved inorganic carbon in natural waters using a headspace-extraction approach for radiocarbon analysis by accelerator mass spectrometry. *Limnol. Oceanogr. Methods* 12, 174–190. doi:10.4319/lom.2014.12.174.

Garnett, M. H., Gulliver, P., and Billett, M. F. (2016). A rapid method to collect methane from peatland streams for radiocarbon analysis. *Ecohydrology* 9, 113–121. doi:10.1002/eco.1617.

Garnett, M. H., Murray, C., Gulliver, P., and Ascough, P. L. (2019). Radiocarbon Analysis of Methane at the NERC Radiocarbon Facility (East Kilbride). *Radiocarbon* 61, 1477–1487. doi:10.1017/RDC.2019.3.

Gierga, M., Schneider, M. P. W., Wiedemeier, D. B., Lang, S. Q., Smittenberg, R. H., Hajdas, I., et al. (2014). Purification of fire derived markers for µg scale isotope analysis (δ13C, Δ14C) using high performance liquid chromatography (HPLC). *Org. Geochem.* 70, 1–9. doi:10.1016/j.orggeochem.2014.02.008.

Graven, H., Hocking, T., and Zazzeri, G. (2019). Detection of Fossil and Biogenic Methane at Regional Scales Using Atmospheric Radiocarbon. *Earths Future* 7, 283–299. doi:10.1029/2018EF001064.

Joung, D., Leonte, M., and Kessler, J. D. (2019). Methane Sources in the Waters of Lake Michigan and Lake Superior as Revealed by Natural Radiocarbon Measurements. *Geophys. Res. Lett.* 46, 5436–5444. doi:10.1029/2019GL082531.

Kessler, J. D., and Reeburgh, W. S. (2005). Preparation of natural methane samples for stable isotope and radiocarbon analysis: Methane isotope analysis. *Limnol. Oceanogr. Methods* 3, 408–418. doi:10.4319/lom.2005.3.408.

Kirschke, S., Bousquet, P., Ciais, P., Saunois, M., Canadell, J. G., Dlugokencky, E. J., et al. (2013). Three decades of global methane sources and sinks. *Nat. Geosci.* 6, 813–823. doi:10.1038/ngeo1955.

Melchert, J. O., Stolz, A., Dewald, A., Gierga, M., Wischhöfer, P., and Rethemeyer, J. (2019). Exploring sample size limits of AMS gas Ion Source 14C analysis at Cologneams. *Radiocarbon* 61, 1785–1793. doi:10.1017/RDC.2019.143.

Milich, L. (1999). The role of methane in global warming: where might mitigation strategies be focused? *Glob. Environ. Change* 9, 179–201. doi:10.1016/S0959-3780(98)00037-5.

Pack, M. A., Xu, X., Lupascu, M., Kessler, J. D., and Czimczik, C. I. (2015). A rapid method for preparing low volume CH4 and CO2 gas samples for 14C AMS analysis. *Org. Geochem.* 78, 89–98. doi:10.1016/j.orggeochem.2014.10.010.

Palonen, V., Uusitalo, J., Seppälä, E., and Oinonen, M. (2017). A portable methane sampling system for radiocarbon-based bioportion measurements and environmental CH4 sourcing studies. *Rev. Sci. Instrum.* 88, 075102. doi:10.1063/1.4993920.

Petrenko, V. V., Smith, A. M., Brailsford, G., Riedel, K., Hua, Q., Lowe, D., et al. (2008). A New Method for Analyzing 14C of Methane in Ancient Air Extracted from Glacial Ice. *Radiocarbon* 50, 53–73. doi:10.1017/S0033822200043368.

Pohlman, J. W., Kaneko, M., Heuer, V. B., Coffin, R. B., and Whiticar, M. (2009). Methane sources and production in the northern Cascadia margin gas hydrate system. *Earth Planet. Sci. Lett.* 287, 504–512. doi:10.1016/j.epsl.2009.08.037.

Santos, G. M., Southon, J. R., Griffin, S., Beaupre, S. R., and Druffel, E. R. M. (2007). Ultra small-mass AMS 14C sample preparation and analyses at KCCAMS/UCI Facility. *Nucl. Instrum. Methods Phys. Res. Sect. B Beam Interact. Mater. At.* 259, 293–302. doi:10.1016/j.nimb.2007.01.172.

Sparrow, K. J., and Kessler, J. D. (2017). Efficient collection and preparation of methane from low concentration waters for natural abundance radiocarbon analysis. *Limnol. Oceanogr. Methods* 15, 601–617. doi:10.1002/lom3.10184.

Stolz, A., Dewald, A., Altenkirch, R., Herb, S., Heinze, S., Schiffer, M., et al. (2017). Radiocarbon measurements of small gaseous samples at CologneAMS. *Nucl. Instrum. Methods Phys. Res. Sect. B Beam Interact. Mater. At.* 406, 283–286. doi:10.1016/j.nimb.2017.03.031.

Turner, A. J., Frankenberg, C., Wennberg, P. O., and Jacob, D. J. (2017). Ambiguity in the causes for decadal trends in atmospheric methane and hydroxyl. *Proc. Natl. Acad. Sci.* 114, 5367–5372. doi:10.1073/pnas.1616020114.

Wotte, A., Wordell-Dietrich, P., Wacker, L., Don, A., and Rethemeyer, J. (2017). 14CO2 processing using an improved and robust molecular sieve cartridge. *Nucl. Instrum. Methods Phys. Res. Sect. B Beam Interact. Mater. At.* 400, 65–73. doi:10.1016/j.nimb.2017.04.019.

Synthesis and overall Discussion

Evaluation of sample size limits and exogenous carbon

This thesis provides new insights about the decomposability of recently thawed Yedoma deposits in the Lena River Delta. These results were only possible after a critical evaluation of the laboratory setup and a quantification of the sources of contamination. Very small samples (2.5 – 50 µg C) are especially sensitive to the introduction of exogenous C. Contamination can be added during sample handling, which includes the actual transfer and weighing of solid and liquid material that is converted to CO_2 during sealed tube combustion, as well as the processing of the CO_2 on a vacuum setup to prepare for AMS analysis. Therefore, utmost care must be taken to keep the contamination with exogenous C particularly low. There are several possibilities, by which contamination can be introduced, given by the different procedures to prepare C for ^{14}C and ^{13}C analysis (i.e., graphitization of bulk sediment, sampling and storage of in-situ respired CO_2, purification, and handling of CO_2 for GIS-AMS measurement). The following section provides a summary of the findings and limitations of the analytical method assessments and a summary of the results of the application of said methods.

The ^{14}C analysis of CO_2 directly via the GIS-AMS is a key method in the presented studies omitting the need for graphitization and allowing the analysis of very small samples down to 20 µg C. The evaluation of our pre-treatment procedures and the sample handling by running several series of different standards revealed small amounts of contamination, mostly modern exogenous carbon, that is likely introduced during weighing and sample transfer at the CO_2 vacuum system (manuscript I). Our study revealed that there is a constant contamination of about 0.30 ± 0.08 µg C (0.93 ± 0.23 $F^{14}C$) added to a sample. Therefore, we recommend not to analyze samples smaller than 20 µg C in order to obtain reliable results according to accuracy and reliability. If less sample material is available, ^{14}C analysis down to a size of 2.5 µg C can be performed but the associated uncertainty is large. We demonstrated that most exogenous C is introduced during the pre-treatment and preparation for sealed tube combustion of standard materials (Santos et al., 2010; Santos and Xu, 2017), which is especially relevant for the measurement of small samples that are not gaseous. Thus, for CO_2 samples the applied corrections based on standards produced by sealed tube combustion is considered as a conservative approach.

The usage of MSCs enabled the collection of sufficiently large samples of in-situ respired CO_2 for ^{14}C GIS-AMS analysis performed at CologneAMS as well as ^{13}C analysis at the University of Hamburg (manuscript II). A maximum amount of CO_2 corresponding to 2 mg C can be collected per MSC, from which 50 µg C aliquots were processed for ^{14}C analysis. Processing such a large amount of C further dilutes the small amount of contamination that is introduced

with the vacuum system and the usage of the MSC. However, this is only possible if the environmental conditions allow sampling of sufficient amounts of CO_2. Sampling time and CO_2 emissions are highly variable, depending on the sampling location and the overall temperature. Long sampling intervals via respiration chambers may disturb the natural CO_2 gradient below the surface (Conen and Smith, 2000) and there is a higher risk of intake of ambient air through small leakages at the sampling equipment's connections or through gaps and dry-cracks in the sediment, which might contaminate the sample. The contamination assessment for the in-situ collection of CO_2 performed by Wotte et al. (2017a) suggested that the majority of modern and ^{14}C-free contamination of 2.0 and 3.0 µg C, respectively, is introduced by the usage of MSCs. This demonstrates that most of the exogenous contamination is introduced by the MSC sampling container itself, however, assuming an MSC is filled up completely during sampling, the sum of the contamination makes up for only 0.25% of total C contained in one sample. Furthermore, results of the in-situ $^{14}CO_2$ analysis have been corrected for modern contamination from atmospheric air, most probably introduced during sampling, which should further diminish influence of exogenous C on $F^{14}C$ values (manuscript II). For the incubation experiments (manuscript II) CO_2 was sealed in serum bottles. This sample gas is flushed with He-gas via injection needles through the vacuum system. We found out that the main part of the contamination comes from the vacuum system itself in addition to ambient air that is probably introduced during handling of the injection needles. The risk for ambient air being introduced is, however, minimized by first inserting the injection needles in an empty serum bottle and flushing with He for 10 minutes through the system prior to handling of the sample.

There are first estimates for the contamination assessment for the new oxidation system that has been designed for the oxidation of CH_4 samples to CO_2. They are based on a small data set of different standards and showed a contamination of 0.58 µg C (manuscript III). This is roughly twice the contamination that is introduced with the CO_2 vacuum system (manuscript I). We determined the endmembers of contamination, namely the values for ^{14}C-free and modern (i.e., $F^{14}C$ close to atmospheric values), that were in the same range with about 0.3 ± 0.1 µg C, respectively. The preparation of modern standards through sealed tube combustion of oxalic acid requires more preparatory steps compared to the injection of ^{14}C-free gas directly into the system, but the quantified contamination for both types of standards is the same. This is indicating that either the amount of injected standard material was too large to be a sensitive enough indicator of contamination or that the additional handling of the solid oxalic acid did not introduce any significant additional amount of contamination. However, major sources of contamination are the handling of the material and the sealed tube combustion procedure to produce Ox-II-derived CO_2, as has been suggested by Santos et al. (2010) and Santos and Xu (2017). Compared to other studies that presented a setup for the conversion of CH_4 to CO_2

for ^{14}C analysis, the contamination reported in manuscript III tends to be larger, however, these other studies graphitized their samples and therefore rely on larger sample sizes. Although natural CH_4 concentrations can vary considerably (Palonen et al., 2017), the ability to directly inject the CH_4-derived CO_2 on micro-scale sample sizes into the AMS is a significant advantage and a requirement for the study of permafrost soils. Furthermore, the GIS-AMS analysis of CH_4-derived CO_2 gives the opportunity to handle anaerobic incubations of permafrost soils, that have been shown to very slowly generate CH_4 emissions (Knoblauch et al., 2013). If individual samples had to be graphitized first in order to analyze them, a major limiting factor will be the accumulation of enough CH_4 through the incubation experiment. It has been shown that the most significant changes in GHG production occur during the initial period (weeks to a few months), during which GIS-AMS analysis of micro-scale samples are in contrast to graphitization possible (Dutta et al., 2006; Knoblauch et al., 2013; Schädel et al., 2014).

The ^{14}C analysis of bulk OC and IC, that was required for the assessment of C sources contributing to CO_2 emission (manuscript II), was performed on graphitized sample material and therefore was not subject to the contamination evaluated for the vacuum system and the MSC. The recent evaluation of the graphitization procedure shows low blank values of 0.0025 ± 0.0007 $F^{14}C$ in the sample size range of 250 – 650 µg C (Rethemeyer et al., 2019). This corresponds to 0.92 µg C of modern contamination, introduced by the graphitization procedure, which is accounted for by correction through routine measurements of materials with known ^{14}C content and which additionally should not negatively influence ^{14}C results, given the large sample sizes compared to the amount of contamination.

Limitations and future improvements of the actual systems

The possibility to measure the ^{14}C content of very small amounts of CO_2 and CH_4 opens up the possibility for analyses that have not been previously possible due to the size limitations given by the graphitization. However, analyzing GHGs in the µg-range amplifies the influence of contamination, which is a limiting factor for reliable results. The improvement of pre-treatment methods and the handling of samples will most likely only lead to minor improvements on the CO_2 vacuum system and therefore, the focus for future improvements should be set on thorough quantification of the contamination that is introduced. This holds especially true for the CH_4 vacuum system, because the so far acquired data are limited and the determined contamination should rather be considered as a first estimate. Additionally, the workflow for the conversion of CH_4 to CO_2 can possible be improved (e.g., the conversion efficiency of the system, or testing of other catalysts). Other changes of the overall setup are already planned and include the addition of a second furnace and further cryotraps in order to remove carbon monoxide from the sample gas, which would otherwise be converted along with CH_4 to CO_2 and potentially mix carbon sources (Pack et al., 2015). These changes are

necessary for the analysis of CH_4 samples directly collected from soils. However, the existing system is designed to analyze CH_4 from incubation experiments where the sample gas is supplied in high concentrations in sealed serum bottles.

Furthermore, the contamination that is introduced via MSCs is small relative to the amount of C that can be potentially stored during sampling. This contamination is most likely introduced via the sampling setup itself including the respiration chamber and gas analyzer attached via several valves and tubes. Natural CH_4 emissions have been shown to be variable (Natali et al., 2015) and therefore the sampling time to collect sufficient amounts for ^{14}C analysis also varies, which also gives exogenous carbon more time to enter the equipment and contaminate the sample. Provided a method for CH_4 collection is developed similar to the CO_2 collection method, changes in either the setup or the whole sampling routine have to be made for the sampling of CH_4 from permafrost soils. This can be achieved by either reducing the number of connections that are potentially leaking or by including mobile traps that remove all unwanted gases and excess moisture as best as possible.

Degradability of Yedoma OM

The careful assessment of the limitations of ^{14}C analysis demonstrated that the results from 20 – 50 µg C sized CO_2 samples are reliably possible. With the confirmation that the analytical routine is functioning and that sources of errors are identifiable and thus being accounted for, the application to real field measurements was enabled as the next logical step. The vast permafrost areas of the northern hemisphere are able to potentially release large amounts of OC as GHGs into the atmosphere. The Yedoma deposits of Beringia, that extent deep below the active layer (Schaefer et al., 2014; Koven et al., 2015), are especially at risk for GHG release and are considered as one of the potential climate tipping elements (Lenton, 2012; Strauss et al., 2017). They are especially vulnerable to rapidly induced thaw by a warming climate due to their high ice-content. The study and identification of the degradability of these Yedoma deposits and the sources of released GHGs are essential for more concise climate models predicting the future development of global warming (Schneider von Deimling et al., 2015).

In the frame of this thesis an evaluation of sources contributing to overall CO_2 emissions was carried out by applying a combined mass-balance approach from ^{14}C and ^{13}C isotopic analysis of sediment and gas samples taken from an active retrogressive thaw slump on Kurungnakh Island in the Lena River Delta (manuscript II). Freshly thawed Pleistocene-aged Yedoma deposits have been exposed on the thaw slump through thermal erosion, overlain by intact Holocene polygonal tundra, which is eroded down onto the thaw slump and mixes with the Yedoma sediments. As a result, the thaw slump allowed the investigation of unique sites in

close proximity of each other: the freshly thawed Yedoma, which is exposed as thaw mounds (TM1, TM2), the intact Holocene polygonal tundra on top of the thaw slump (HT1), as well as the slump floor (SF3) at which the Holocene soils and recent plant-derived OM mixes with melt water and eroded Yedoma OM. It has been shown that, labile and young substrates are being degraded first, and mostly ancient OM from Pleistocene-aged Yedoma sediments is released as CO_2 upon thaw. More importantly, the data indicate that a significant amount of CO_2 released from the thaw slump is derived from inorganic carbon sources, likely favoured by low pH values and the presence of organic acids. These findings were substantially based on micro-scale isotopic analysis of CO_2 ($\delta^{13}C$ and ^{14}C). The application of ^{14}C and ^{13}C data in a dual isotope mass-balance approach has been done for over a decade now, however, the application in the context of assessing OM degradability from permafrost deposits is rather new (Dorsett et al., 2011; Griffith et al., 2012; Pries et al., 2016) and made possible through the development of methods to sample CO_2 from remote locations by using MSCs (Hardie et al., 2005; Garnett and Murray, 2013; Wotte et al., 2017b).

Furthermore, the analysis of bulk sediment parameters including TOC and TIC contents, OC/N ratios, as well as $\delta^{13}C$, and ^{14}C, was used to assess the state of Yedoma OM degradation. With continuous degradation of OM, TOC content, as well as OC/N ratios tend to decrease whereas the $\delta^{13}C$ values increase due to enrichment of ^{13}C through microbial discrimination (Schädel et al., 2014; Gentsch et al., 2015; Strauss et al., 2015). The bulk sediment data obtained from TM1 and TM2 delivered comparable results to previous studies of Yedoma deposits at Kurungnakh Island (Wetterich et al., 2008; Knoblauch et al., 2013). The analysis of the bulk sediment (Tab S2, manuscript II) shows that the thaw mounds TM1 and TM2 are similar in composition, highlighted by OC and IC content. Compared to the uppermost interval from the Holocene tundra, which mainly consists of plant material, OC/N ratios of TM1 and TM2 are low. However, the OC/N ratios of the Holocene mineral soil below are much lower compared to the recent organic cover on top and slightly higher compared to the thaw mounds, which possibly suggests that the Yedoma OM is preserved rather well (Dutta et al., 2006; Strauss et al., 2015) and comparable to the Holocene tundra regarding degradability. At the slump floor site (SF3) where Pleistocene and Holocene sediments are mixed, OC as well as IC contents are higher compared to the thaw mounds and the OC/N ratios are similar to those of the mineral soils sampled at the Holocene tundra (HT1), indicating incorporation of younger OM substrates into the sediment mixture.

The average radiocarbon content of the thaw mound sediments indicates that the outcropped sediments likely belong to the upper Yedoma unit IV (Wetterich et al., 2008). The radiocarbon content of the CO_2 released in-situ and during the laboratory incubation differ from the bulk sediments at both Yedoma sites. The CO_2 collected from the TM2 incubation resulted a lower

^{14}C content compared to the in-situ collected CO_2 (after correction for atmospheric contamination). The mass-balance approach (Tab. 3, manuscript II) showed that mostly ancient OM was released as CO_2 at TM2, whereas mostly young OM was released at the slump floor SF3.

It can be deduced from the discrepancy between the elevated ^{14}C content of the emission compared to the parent material that the most labile components of the OM are metabolized initially, which also includes young OM. This is supported by the decrease in CO_2 production rates over the course of the incubation experiment (Tab. S3, manuscript II), as it indicates ongoing depletion of labile, easily degradable OM (Knoblauch et al., 2013; Schädel et al., 2014). However, this decrease in CO_2 production is observed for all sampling sites, independent of the age of the parent material and therefore indicates that the ancient Yedoma OM likewise contains labile components.

Further, the results of the mass-balance calculation indicate that during the in-situ measurement, a larger fraction of CO_2 from young OM sources was collected with the MSCs compared to the incubation experiment. The ^{14}C content of the uppermost interval from the TM2 bulk sediment is significantly higher (Tab. S1, manuscript II) compared to the sediments below, which is either caused by an onset of vegetation or via erosion from the Holocene tundra above. The vegetation was removed prior to measurement, thus incorporation of young OM through erosion is more likely. This possibly explains the difference in the average radiocarbon age of the bulk sediment compared to the CO_2 collected during the field measurements.

Expectedly, the admixture of Holocene sediments with Yedoma at the slump floor resulted in higher radiocarbon contents of the bulk sediment, corresponding to an average age of 2,680 years BP. In contrast, the results of the field measurement at the slump floor indicate that CO_2 with a lower ^{14}C content compared to the incubation was released. The small offset between the data can also be explained with the results of the mass-balance approach. At SF3, slightly less young OM was degraded and released as CO_2 compared to the incubation experiment, possibly through heterogeneity of the sampled sediments, as the differences are not strongly pronounced. Due to the admixture of young OM with thawed Pleistocene-aged Yedoma OM positive priming was expected to occur. The degradation of young OM has been previously documented to stimulate the microbial degradation of ancient OM (Wild et al., 2016; Girkin et al., 2018; Walz et al., 2018; Pegoraro et al., 2019) the absolute amounts of CO_2 released during the incubation experiment could, however, not confirm priming to occur during the experiment (Tab. S4, manuscript II).

Limitations and future perspectives of the field study

The surveillance of the occurrence of positive priming during the field measurements is an interesting aspect for future research. This would require a larger data set of CO_2 flux data. With this additional data, the calculation of the absolute amounts of CO_2 released per quantified OM pools for both sites would be enabled, and the comparison of the amounts of released CO_2 during field measurements and incubation experiment would be possible.

The CO_2 fluxes in the field are measured with the same respiration chamber that is used to collect the CO_2. This method is very sensitive towards environmental conditions such as the air and soil temperature (Dutta et al., 2006; Treat et al., 2015) on the day of the measurement, as well as the wind strength and moisture of the sediment. Therefore, more measurements on consecutive days are necessary to compensate for changing weather and temperature conditions. Furthermore, a larger and more refined data set on in-situ CO_2 fluxes would allow for a better comparison towards CO_2 production during incubation experiments and allow for a proper upscaling. Improvements of the field equipment could include a more sophisticated respiration chamber with built in sensors for temperature and moisture enabling more stable and comparable data sets.

The potential annual release of C from deep permafrost could be estimated (Schuur et al., 2009; Biasi et al., 2014) and linked to the results of the mass-balance approach, which would give valuable information about the availability of freshly thawed Yedoma OM. However, generalizations about the overall degradability and vulnerability of Yedoma based on data generated from one locality are hardly possible (Walz et al., 2018). This is mainly due to variations of the regional climate and depositional conditions (anaerobic wet vs. aerobic dry) at the time of OM incorporation during the formation of the Yedoma deposits. Thus, data regarding the OM decomposability should be interpreted against the paleoenvironmental background of the study region (Walz et al., 2018). Recently, efforts have been undertaken to establish global databases in which incubation (Schädel et al., 2020) as well as soil respiration data sets (Bond-Lamberty et al., 2020) are collected. This possibly opens opportunities for future studies under similar experimental conditions and therefore making datasets accessible for comparison. With the data being easier accessible, interpretation of cross-regional Yedoma OM degradability might become possible.

The findings gained by applying a dual carbon isotope mass-balance approach are promising. It enables the identification of individual C sources and quantification of their respective contribution to GHG emissions, which, in turn, opens further possibilities for the development of better constrained climate models and improvement of the overall understanding of OM degradability. Modelling the contribution of C sources to soil respiration and GHG fluxes further

improves current C budgeting approaches, as indicated by the finding of an IC pool contributing to CO_2 release from Yedoma deposits (manuscript II).

In manuscript II, the analysis of ^{14}C and ^{13}C from inorganic carbon suggested that a fraction of that inorganic carbon is younger and isotopically lighter than expected. This inorganic carbon pool potentially formed pedogenically by using up CO_2 released from microbial degradation of Yedoma OM (Zolkos et al., 2018). As a result, a later release of CO_2 from said pedogenic carbonate would ultimately not alter a CO_2 budget. However, these estimates are strongly limited by the constraints made to the mass-balance approach and the quality of the data used to model. To prove the hypothesis of pedogenic carbonates contributing to CO_2 emissions, refined and additional data are required. Thus, the mass-balance approach could be improved by including a fourth carbon source to distinguish between lithogenic and pedogenic carbonates. This, in return, requires reliable information about the isotopic composition of lithogenic and pedogenic carbonates to properly constrain the calculation: The difference in $\delta^{13}C$ values between lithogenic and pedogenic carbonates should be distinct, enabled by the consumption of microbially respired, $\delta^{13}C$-light CO_2 to form pedogenic carbonate versus the $\delta^{13}C$-heavier lithogenic carbonate (see discussion, manuscript II). However, the set-up models from mass-balance approaches need to be critically evaluated and not taken at face value immediately. Comparisons of three-pool and four-pool approaches should indicate similar inorganic fractions between both models. The sum of lithogenic and pedogenic IC, calculated from the four-pool model should equal the IC pool, calculated from the three-pool model. If this was not the case, the chosen endmembers for each carbon source need to be reconsidered. Furthermore, information about the mineral composition (Schirrmeister et al., 2020) and fractions of sediment could improve knowledge about regional sedimentary mechanisms that led to Yedoma formation and enable more sophisticated estimates about an inorganic carbon stock. The analysis of DOC as well as DIC might answer from where organic acids possibly accumulated, favoring dissolution of carbonate minerals, as well as show if significant amounts of inorganic carbon were mobilized in watery solutions (Drake et al., 2015, 2018).

Conclusion

Following the discussion of main findings presented in the manuscripts included in this thesis, the following key findings can be summarized:

- The evaluation of pre-treatment methods for micro-scale AMS analysis showed that 0.30 ± 0.08 µg of exogenous C ($F^{14}C$ = 0.93 ± 0.23; 0.28 µg modern C, 0.02 µg fossil C) are introduced during sample treatment, enabling reliable measurements down to sample sizes of 20 µg C.

- Critically evaluating and refining sampling and analysis methods is crucial for a meaningful application to field studies.
- The GIS-AMS analysis of CO_2 collected from Yedoma sediments on an active retrogressive thaw slump demonstrated that ancient OC is the dominant source of CO_2 emission, while the admixture with younger organic substrates did not cause positive priming, it led to the preferential mineralization of young OC.
- A significant fraction of the released CO_2 originates from IC, that possibly formed pedogenically which would not necessarily alter C budgets.
- The results of AMS analysis of CO_2 collected from a 1.5-year aerobic incubation of Yedoma sediments suggests a rather rapid depletion of labile OM pools that lead to decreased CO_2 production rates after initial thaw. Future CO_2 emissions are estimated to contain more IC-derived CO_2.
- First tests of the new vacuum system for the GIS-AMS analysis of CH_4 showed that 0.58 ± 0.18 µg of extraneous C ($F^{14}C$ of 0.447 ± 0.245; 0.26 ± 0.13 µg modern, 0.33 ± 0.12 µg fossil C) are introduced during sample treatment.
- Blank values achieved with the new system of 0.006 ± 0.003 $F^{14}C$ are similar to blank values achieved with the CO_2 vacuum system.
- Multiple series of CH_4 standard and CH_4 biogas injections demonstrate a CH_4 to CO_2 conversion efficiency of 94 – 97%.
- The quantification of sources of exogenous C indicates that correction of CH_4 data is possible, more data for further investigations are, however, required.
- Provided additional data show similar or even better results, the new CH_4 vacuum system is ready for the analysis of first CH_4 samples collected from anaerobic incubation of Yedoma sediments.

References

Biasi, C., Jokinen, S., Marushchak, M. E., Hämäläinen, K., Trubnikova, T., Oinonen, M., et al. (2014). Microbial Respiration in Arctic Upland and Peat Soils as a Source of Atmospheric Carbon Dioxide. *Ecosystems* 17, 112–126. doi:10.1007/s10021-013-9710-z.

Bond-Lamberty, B., Christianson, D. S., Malhotra, A., Pennington, S. C., Sihi, D., AghaKouchak, A., et al. (2020). COSORE: A community database for continuous soil respiration and other soil-atmosphere greenhouse gas flux data. *Glob. Change Biol.* 26, 7268–7283. doi:10.1111/gcb.15353.

Conen, F., and Smith, K. A. (2000). An explanation of linear increases in gas concentration under closed chambers used to measure gas exchange between soil and the atmosphere. *Eur. J. Soil Sci.* 51, 111–117. doi:10.1046/j.1365-2389.2000.00292.x.

Dorsett, A., Cherrier, J., Martin, J. B., and Cable, J. E. (2011). Assessing hydrologic and biogeochemical controls on pore-water dissolved inorganic carbon cycling in a

subterranean estuary: A 14C and 13C mass balance approach. *Mar. Chem.* 127, 76–89. doi:10.1016/j.marchem.2011.07.007.

Drake, T. W., Guillemette, F., Hemingway, J. D., Chanton, J. P., Podgorski, D. C., Zimov, N. S., et al. (2018). The Ephemeral Signature of Permafrost Carbon in an Arctic Fluvial Network. *J. Geophys. Res. Biogeosciences* 123, 1475–1485. doi:10.1029/2017JG004311.

Drake, T. W., Wickland, K. P., Spencer, R. G. M., McKnight, D. M., and Striegl, R. G. (2015). Ancient low–molecular-weight organic acids in permafrost fuel rapid carbon dioxide production upon thaw. *Proc. Natl. Acad. Sci.* 112, 13946–13951. doi:10.1073/pnas.1511705112.

Dutta, K., Schuur, E. A. G., Neff, J. C., and Zimov, S. A. (2006). Potential carbon release from permafrost soils of Northeastern Siberia: CARBON RELEASE FROM SIBERIAN PERMAFROST SOILS. *Glob. Change Biol.* 12, 2336–2351. doi:10.1111/j.1365-2486.2006.01259.x.

Garnett, M. H., and Murray, C. (2013). Processing of CO2 Samples Collected Using Zeolite Molecular Sieve for 14C Analysis at the NERC Radiocarbon Facility (East Kilbride, UK). *Radiocarbon* 55, 410–415. doi:10.1017/S0033822200057532.

Gentsch, N., Mikutta, R., Shibistova, O., Wild, B., Schnecker, J., Richter, A., et al. (2015). Properties and bioavailability of particulate and mineral-associated organic matter in Arctic permafrost soils, Lower Kolyma Region, Russia: Organic matter stabilization in permafrost soils. *Eur. J. Soil Sci.* 66, 722–734. doi:10.1111/ejss.12269.

Girkin, N. T., Turner, B. L., Ostle, N., Craigon, J., and Sjögersten, S. (2018). Root exudate analogues accelerate CO2 and CH4 production in tropical peat. *Soil Biol. Biochem.* 117, 48–55. doi:10.1016/j.soilbio.2017.11.008.

Griffith, D. R., McNichol, A. P., Xu, L., McLaughlin, F. A., Macdonald, R. W., Brown, K. A., et al. (2012). Carbon dynamics in the western Arctic Ocean: insights from full-depth carbon isotope profiles of DIC, DOC, and POC. *Biogeosciences* 9, 1217–1224. doi:10.5194/bg-9-1217-2012.

Hardie, S. M. L., Garnett, M. H., Fallick, A. E., Rowland, A. P., and Ostle, N. J. (2005). Carbon Dioxide Capture Using a Zeolite Molecular Sieve Sampling System for Isotopic Studies (13C and 14C) of Respiration. *Radiocarbon* 47, 441–451. doi:10.1017/S0033822200035220.

Knoblauch, C., Beer, C., Sosnin, A., Wagner, D., and Pfeiffer, E.-M. (2013). Predicting long-term carbon mineralization and trace gas production from thawing permafrost of Northeast Siberia. *Glob. Change Biol.* 19, 1160–1172. doi:10.1111/gcb.12116.

Koven, C. D., Schuur, E. A. G., Schädel, C., Bohn, T. J., Burke, E. J., Chen, G., et al. (2015). A simplified, data-constrained approach to estimate the permafrost carbon–climate feedback. *Philos. Trans. R. Soc. Math. Phys. Eng. Sci.* 373, 20140423. doi:10.1098/rsta.2014.0423.

Lenton, T. M. (2012). Arctic Climate Tipping Points. *AMBIO* 41, 10–22. doi:10.1007/s13280-011-0221-x.

Natali, S. M., Schuur, E. A. G., Mauritz, M., Schade, J. D., Celis, G., Crummer, K. G., et al. (2015). Permafrost thaw and soil moisture driving CO2 and CH4 release from upland tundra. *J. Geophys. Res. Biogeosciences* 120, 525–537. doi:10.1002/2014JG002872.

Pack, M. A., Xu, X., Lupascu, M., Kessler, J. D., and Czimczik, C. I. (2015). A rapid method for preparing low volume CH4 and CO2 gas samples for 14C AMS analysis. *Org. Geochem.* 78, 89–98. doi:10.1016/j.orggeochem.2014.10.010.

Palonen, V., Uusitalo, J., Seppälä, E., and Oinonen, M. (2017). A portable methane sampling system for radiocarbon-based bioportion measurements and environmental CH4 sourcing studies. *Rev. Sci. Instrum.* 88, 075102. doi:10.1063/1.4993920.

Pegoraro, E., Mauritz, M., Bracho, R., Ebert, C., Dijkstra, P., Hungate, B. A., et al. (2019). Glucose addition increases the magnitude and decreases the age of soil respired carbon in a long-term permafrost incubation study. *Soil Biol. Biochem.* 129, 201–211. doi:10.1016/j.soilbio.2018.10.009.

Pries, C. E. H., Schuur, E. A. G., Natali, S. M., and Crummer, K. G. (2016). Old soil carbon losses increase with ecosystem respiration in experimentally thawed tundra. *Nat. Clim. Change* 6, 214–218. doi:10.1038/nclimate2830.

Rethemeyer, J., Gierga, M., Heinze, S., Stolz, A., Wotte, A., Wischhöfer, P., et al. (2019). Current Sample Preparation and Analytical Capabilities of the Radiocarbon Laboratory at CologneAMS. *Radiocarbon* 61, 1449–1460. doi:10.1017/RDC.2019.16.

Santos, G. M., Southon, J. R., Drenzek, N. J., Ziolkowski, L. A., Druffel, E., Xu, X., et al. (2010). Blank Assessment for Ultra-Small Radiocarbon Samples: Chemical Extraction and Separation Versus AMS. *Radiocarbon* 52, 1322–1335. doi:10.1017/S0033822200046415.

Santos, G. M., and Xu, X. (2017). Bag of Tricks: A Set of Techniques and other Resources to Help 14C Laboratory Setup, Sample Processing, and Beyond. *Radiocarbon* 59, 785–801. doi:10.1017/RDC.2016.43.

Schädel, C., Beem-Miller, J., Aziz Rad, M., Crow, S. E., Hicks Pries, C. E., Ernakovich, J., et al. (2020). Decomposability of soil organic matter over time: the Soil Incubation Database (SIDb, version 1.0) and guidance for incubation procedures. *Earth Syst. Sci. Data* 12, 1511–1524. doi:10.5194/essd-12-1511-2020.

Schädel, C., Schuur, E. A. G., Bracho, R., Elberling, B., Knoblauch, C., Lee, H., et al. (2014). Circumpolar assessment of permafrost C quality and its vulnerability over time using long-term incubation data. *Glob. Change Biol.* 20, 641–652. doi:10.1111/gcb.12417.

Schaefer, K., Lantuit, H., Romanovsky, V. E., Schuur, E. A. G., and Witt, R. (2014). The impact of the permafrost carbon feedback on global climate. *Environ. Res. Lett.* 9, 085003. doi:10.1088/1748-9326/9/8/085003.

Schirrmeister, L., Dietze, E., Matthes, H., Grosse, G., Strauss, J., Laboor, S., et al. (2020). The genesis of Yedoma Ice Complex permafrost – grain-size endmember modeling analysis from Siberia and Alaska. *EG Quat. Sci. J.* 69, 33–53. doi:10.5194/egqsj-69-33-2020.

Schneider von Deimling, T., Grosse, G., Strauss, J., Schirrmeister, L., Morgenstern, A., Schaphoff, S., et al. (2015). Observation-based modelling of permafrost carbon fluxes

with accounting for deep carbon deposits and thermokarst activity. *Biogeosciences* 12, 3469–3488. doi:10.5194/bg-12-3469-2015.

Schuur, E. A. G., Vogel, J. G., Crummer, K. G., Lee, H., Sickman, J. O., and Osterkamp, T. E. (2009). The effect of permafrost thaw on old carbon release and net carbon exchange from tundra. *Nature* 459, 556–559. doi:10.1038/nature08031.

Strauss, J., Schirrmeister, L., Grosse, G., Fortier, D., Hugelius, G., Knoblauch, C., et al. (2017). Deep Yedoma permafrost: A synthesis of depositional characteristics and carbon vulnerability. *Earth-Sci. Rev.* 172, 75–86. doi:10.1016/j.earscirev.2017.07.007.

Strauss, J., Schirrmeister, L., Mangelsdorf, K., Eichhorn, L., Wetterich, S., and Herzschuh, U. (2015). Organic-matter quality of deep permafrost carbon – a study from Arctic Siberia. *Biogeosciences* 12, 2227–2245. doi:10.5194/bg-12-2227-2015.

Treat, C. C., Natali, S. M., Ernakovich, J., Iversen, C. M., Lupascu, M., McGuire, A. D., et al. (2015). A pan-Arctic synthesis of CH4 and CO2 production from anoxic soil incubations. *Glob. Change Biol.* 21, 2787–2803. doi:10.1111/gcb.12875.

Walz, J., Knoblauch, C., Tigges, R., Opel, T., Schirrmeister, L., and Pfeiffer, E.-M. (2018). Greenhouse gas production in degrading ice-rich permafrost deposits in northeastern Siberia. *Biogeosciences* 15, 5423–5436. doi:10.5194/bg-15-5423-2018.

Wetterich, S., Kuzmina, S., Andreev, A. A., Kienast, F., Meyer, H., Schirrmeister, L., et al. (2008). Palaeoenvironmental dynamics inferred from late Quaternary permafrost deposits on Kurungnakh Island, Lena Delta, Northeast Siberia, Russia. *Quat. Sci. Rev.* 27, 1523–1540. doi:10.1016/j.quascirev.2008.04.007.

Wild, B., Gentsch, N., Čapek, P., Diáková, K., Alves, R. J. E., Bárta, J., et al. (2016). Plant-derived compounds stimulate the decomposition of organic matter in arctic permafrost soils. *Sci. Rep.* 6, 25607. doi:10.1038/srep25607.

Wotte, A., Wischhöfer, P., Wacker, L., and Rethemeyer, J. (2017a). 14CO2 analysis of soil gas: Evaluation of sample size limits and sampling devices. *Nucl. Instrum. Methods Phys. Res. Sect. B Beam Interact. Mater. At.* 413, 51–56. doi:10.1016/j.nimb.2017.10.009.

Wotte, A., Wordell-Dietrich, P., Wacker, L., Don, A., and Rethemeyer, J. (2017b). 14CO2 processing using an improved and robust molecular sieve cartridge. *Nucl. Instrum. Methods Phys. Res. Sect. B Beam Interact. Mater. At.* 400, 65–73. doi:10.1016/j.nimb.2017.04.019.

Zolkos, S., Tank, S. E., and Kokelj, S. V. (2018). Mineral Weathering and the Permafrost Carbon-Climate Feedback. *Geophys. Res. Lett.* 45, 9623–9632. doi:10.1029/2018GL078748.

Acknowledgements

First and foremost, I would like to thank my supervisor, Prof. Dr. Janet Rethemeyer for giving me the opportunity to pursue and finish my thesis, as well as for giving me a lot of guidance and support in finishing publications. I would also like to say thank you for giving me the rare opportunity to participating in expeditions to the Arctic, which some people envy me for.

I would like to thank Prof. Dr. Martin Melles and Prof. Dr. Christina Bogner for joining the examination committee.

I am grateful for the support I got from Philipp Wischhöfer, who put a lot of effort into compiling data, proof reading, discussing results many times over as well as teaching me how to maintain all the equipment that is necessary for our expeditions. I am further grateful for the support and the introduction into the field of ^{14}C analysis that I got from Anja Wotte. Thank you, Gabriel Norén, for the worries we shared and the laughs we had together. I want to acknowledge the support I got from Merle Gierga regarding evaluation of data, improving results as well as taking the time for reading everything I wrote.

During the last years I met a lot of students working in our group, whom I would like to thank a lot for finishing all the small tasks, that piled up over and over again: Thank you Elisabeth, Reaz, Thorsten, Tim, Vera and Olga. I further appreciate the help and support, besides coffee and sweets, I received from our technical staff, thank you Svetlana, Bianca, Ulrike and Daniela. Without you and our students, this thesis would have hardly been possible.

Lastly, I would like to acknowledge Christian Knoblauch, for the fruitful discussions we had either in video calls, on the phone or by mail and the AWI Bremerhaven and Potsdam for making our research possible by handling logistics and organization for expeditions to the Arctic.